Technical Report 1350

On Directional Selectivity in Vertebrate Retina: An Experimental and Computational Study

Lyle J. Borg-Graham

MIT Artificial Intelligence Laboratory

This blank page was inserted to preserve pagination.

MASSACHUSETTS INSTITUTE OF TECHNOLOGY
ARTIFICIAL INTELLIGENCE LABORATORY

A.I. Technical Report No. 1350 January 1992

ON DIRECTIONAL SELECTIVITY IN VERTEBRATE RETINA: AN EXPERIMENTAL AND COMPUTATIONAL STUDY

Lyle J. Borg-Graham

This report describes research done at the Artificial Intelligence Laboratory and the Center for Biological Information Processing in the Department of Brain and Cognitive Sciences of the Massachusetts Institute of Technology. Support for the laboratory's artificial intelligence research is provided in part by the Advanced Research Projects Agency of the Department of Defense under Office of Naval Research contract N00014-85-K-0124. Research at the Center for Biological Information Processing is sponsored by the grant BNS-8809528 from the National Science Foundation; by a grant from the Office of Naval Research, Cognitive and Neural Sciences Division; by the Alfred P. Sloan Foundation; by a grant from the National Science Foundation under contract IRI-8719394. Tomaso Poggio is supported by the Uncas and Helen Whitaker Chair at the Massachusetts Institute of Technology, Whitaker College.

This empty page was substituted for a blank page in the original document.

Abstract

The retina is a good candidate for exploring the relationship between neural computation and circuit, in particular given its physically *peripheral* location and its physiologically *central* status. One example of a spatial–temporal computation in the retina is directional selectivity. This computation may rely on interactions within the dendritic tree which are incrementally more complex than the basic "point integration" and fire neuronal response.

In this Thesis I use experimental and theoretical techniques to characterize the direction selectivity circuit in vertebrate retina. For the experimental side I have developed *a)* an isolated intact turtle retina preparation and *b)* a whole-cell patch recording protocol of directionally selective ganglion cells, the combination of which is well-suited for characterizing complicated retinal receptive fields. I will show evidence that when the inhibitory synaptic input is markedly reduced the excitatory input to directionally selective ganglion cells in turtle is itself directionally selective. This reduction was accomplished by *a)* voltage clamping to the reversal potential of inhibitory currents and *b)* by removing ATP from the electrodes which, in turn, blocks the inhibitory input over time.

This finding implies that the necessary and sufficient conditions for the computation of directional selectivity occurs pre-synaptic to the ganglion cell. For the theoretical side of the Thesis, and consistent with the above constraint, I present a model for the direction selective circuit that relies on directionally selective distal outputs from functionally independent oriented amacrine cell dendrites. I postulate that these dendrite cables receive symmetric, evenly distributed, but temporally distinct excitatory and inhibitory inputs along their length. Performance of the model (tested with a biophysically and morphometricly detailed neuron simulator program, SURF-HIPPO) is consistent with the data, and generates testable predictions.

I shall also discuss how this model may work in a developmental context and, finally, implications for more general non-linear spatio-temporal filtering within dendritic trees.

This empty page was substituted for a blank page in the original document.

ACKNOWLEDGMENTS

First, my career at MIT and HST could not have happened without the inspiration and support of Ernie Cravalho, who decided to take a gamble.

My development as a scientist has been fundamentally guided by Tomaso Poggio, my advisor and advocate during my tenure at the Center for Biological Information Processing, and by Norberto Grzywacz, who has been my collaborator and teacher. I hope that the quality of my work may emulate the standards set by theirs.

During my stay at CBIP I was fortunate to mix with an eclectic and gregarious bunch that passed through over the years; thanks to Tommy, and Ellen Hildreth, co-directors of CBIP, and Elizabeth Willey, who runs the whole show, for making CBIP a Great Resource. Having Anya Hurlbert for an office-mate was icing, and to the honorary CBIP member Davi Geiger, thanks for the sanity checks. Discussions and debates with Christof Koch, Randy Smith, Heinrich Bülthoff, Jeff Sutton, Shimon Edelman, Daphna Weinshall, Gadi Geiger, Manfred Fahle, Michael Prince (honorary member from The Academy), Thomas Vetter, Jenny McFarland and Jim Smith always ended up illuminating the issue at hand. Thanks to Randy as well for his help and enthusiasm in the lab, and to Polly McGahan and Marcia Ross for all their help, especially since I was always late.

I was fortunate to be a part of the HST-MEMP program: my experience as a part-time med student, in particular alongside Mehmet Tomer, is greatly valued. The consistent and warm support from Keiko Oh at HST has been much appreciated during my time here. I would also like to acknowledge the support of the Department of Brain and Cognitive Sciences, including that from Jan Ellertsen. I also thank Mohymen Sadeek, Thomas Olsen, all my 'buds from California, and, especially, the poet David English for their friendship and good humour through the years.

I thank the rest of my thesis committee for their help and useful critiques: Ray Dacheux, John Wyatt, and, especially, Richard Anderson.

Finally, I would like to thank my mother, Kathy Graham, for her support in both word and deed, and, more importantly, for her passing onto me from her parents lessons of perseverance and quality. And to my brother Chris, who never let me down and always helped keep my chin up.

This Thesis is dedicated to Josette, whose spirit and creativity I honor.

This empty page was substituted for a blank page in the original document.

Contents

List of Figures

Chapter 1

Introduction

In this Thesis we investigate the generation of directionally selective responses in the vertebrate retina (Chapter 2). Our perspective will be both experimental and theoretical. We shall use the turtle retina (and to a lesser degree, rabbit retina) as a model system for both vertebrate retinal processing in particular and neural computation in general. The major results are as follows:

On the experimental side (Chapter 3), we shall show that at least some directionally selective ganglion cells in the turtle retina receive directionally selective excitatory input ([13]). This interpretation is supported by both voltage clamp recordings at holding potentials near inhibitory synaptic reversal potentials, and evidence that inhibitory input onto recorded cells is attenuated under our recording conditions. An important implication of this finding is a constraint placing the location for the computational elements necessary for direction selectivity onto cells presynaptic to ganglion cells.

On the theoretical side (Chapter 4), we shall present a model for the preganglionic computation of direction selectivity in vertebrate retina ([12]). This model is consistent with known properties of the retina and the aforementioned results, and requires reasonable assumptions/constraints on what is not known. Computer simulations of biophysically and morphometricly detailed models of amacrine cells demonstrate the performance of the model, and suggest that the model is robust for realistic variations in model parameters.

This model is based on the sequence-dependent output of a dendritic cable resulting from non-linear interactions between the cable's excitatory and inhibitory synaptic inputs. We suggest that the biophysical substrate

for this model might be found in extra-retinal systems (Chapter 5), and we discuss the possibility of such computations (non-linear spatial-temporal input filtering) in other contexts. We also discuss advantages that this particular model has for solving the developmental problem of the breaking of symmetry, and what this model suggests about ganglion cell function in general.

Finally, this project included the development of two new experimental protocols - isolation and recording from intact turtle retina ([11]), and whole cell patch recording from intact turtle retina([13]). These techniques are discussed in Appendix A and B. This project also included the development of a circuit simulator program, SURF-HIPPO, that facilitated our theoretical investigations. SURF-HIPPO is discussed in Appendix C.

Chapter 2

Directional Selectivity in the Visual System

2.1 A Definition of Directional Selectivity

What is directional selectivity (DS) in the visual system? In this thesis the definition is: The response of some visual pathway to a moving stimulus is DS when some linear measurement taken over the entire response (e.g. the integral) is significantly asymmetric with respect to stimulus direction. An example, and perhaps the classical definition, would be that a cell is DS if it consistently fires *more spikes* for a specific (preferred) stimulus trajectory as compared to the (null) stimulus trajectory that differs only in sign.[1] On the other hand, for a non-spiking cell, an EPSP with a significantly larger area for a specific motion direction is defined as DS. A common thread for our definition is that a DS system requires the breaking of symmetry over the receptive field of that system.

Behaviorly, of course, the most important DS signals are carried by spikes (we leave aside the possibility of subthreshold signaling within a subsystem, e.g. an intra-retinal DS channel). Certainly the motivation for studying DS starts with spike–based systems, but in this Thesis we are ultimately interested in dissecting the mechanisms underlying a specific computation. Strictly speaking, this may be done independent of considering the functionality of the specific computation. In the case of retinal DS, this means that all DS somatic ganglion cell responses are relevant, since it is straightforward

[1] Preferred or null may refer to either the stimulus or the system/cell response, as appropriate.

to apply known mechanisms to, for example, DS EPSPs to yield the classical signals. Thus in this Thesis we may consider motion asymmetries which may either account directly for the classical DS responses, or, in principle, be used by the brain for directional information.

2.1.1 Directional Selectivity *versus* Difference

In fact, for our analysis of DS we will also consider a broader *directional difference* (DD) response distinction, one which also requires a fundamental asymmetry: a system or cell output is DD if there is *any* consistent preferred/null (P/N) difference that is independent of any relative time shift of the two waveforms. For example, P/N output waveforms with equivalent averages but different shapes or amplitudes would constitute a DD, but not DS, response. As described by Poggio and Reichardt ([55]), DS responses also require a *nonlinearity* in the circuit.

2.1.2 Consistency of Directional Properties Over the Receptive Field

In either case, in this Thesis *consistency* means that a single P/N axis is dominant over the entire receptive field of the cell. This constraint is motivated by both the classical work on DS (e.g. [8]), and by the notion of breaking of symmetry mentioned earlier. Recently, center/surround DS antagonistic receptive fields have been reported in turtle retina ([22]), but in principle these cells would be considered DS since they still break symmetry. As a counter-example, a cell with a classical excitatory center/inhibitory surround may give a centrifugal "DS" response for movement across the receptive field edge (see Section 3.1). However, since the observed P/N axis rotates as a function of stimulus location, the cell would not be classified as either DS or DD.

2.1.3 Directionally Selective Responses Emerge at Different Levels for Different Species

Directionally selective visual responses emerge at different levels of the visual pathway in different species - in general, complicated receptive fields tend to appear at higher levels with higher species. For example, directionally selective responses are common in turtle optic nerve fibers (ranging between 20% to 40% [27], [20]), whereas in primate, similar responses appear in

relative abundance first in V1 (however, a small percentage of primate retina DS responses have been reported [57] [21]).

2.1.4 Structure of, and Directional Response in the Retina

The "sensory membrane of the eyeball" is a good candidate for study given its physically *peripheral* location and its physiologically *central* status ([24]). The vertebrate retina is organized in several layers of cell bodies and their interacting processes. Signal flow is both direct (perpendicular to the image) and lateral (parallel to the image) at all levels. Light is transduced at the photoreceptor layer, which outputs to bipolar and horizontal cells within the outer plexiform layer. Bipolar cell output impinges on the mesh of amacrine and ganglion cell dendrites within the inner plexiform layer (IPL). Finally, ganglion cell axons form the optic nerve. Each major cell type in the retina has several subtypes, classified either anatomically (e.g. according to dendritic tree shape), neurochemically (e.g. cholinergic, GABAergic), or physiologically (e.g. ON/OFF, DS, red/green opponent).

In turtle, motion dependent responses have been reported at all retinal layers [23]. The focus of this Thesis is to analyze the circuitry responsible for DS responses at the output layer – the ganglion cells – of the vertebrate retina, using turtle retina as an experimental model and turtle and rabbit retina as the primary basis for a theoretical circuit model.

2.2 Theoretical Requirements for Directional Selectivity and Difference

Motion detection is a computation on *spatially separated* inputs *over time.* Detection of motion *direction* (DD) requires a spatial *asymmetry* in the circuit. Finally, as mentioned earlier, a non-linearity is necessary to transform a DD signal to DS. Note that it is also possible to have a DS system in which there is no DD signal.

It is useful at this point to define two broad classes of retinal DS models: *ganglionic* models, where the crucial nonlinear interaction occurs in the ganglion cell, and *pre-ganglionic* models, where the interaction occurs prior to the ganglion cell (see review in [39]; in this paper *post-synaptic* means ganglionic, and *pre-synaptic* means pre-ganglionic).

Thus, the specific questions we are trying to answer here are:

- What is the anatomy and connectivity of the DS pathway?

- What is the crucial nonlinearity of the DS pathway?
- Where on the DS pathway is the nonlinearity, e.g. is it pre–ganglionic or ganglionic?

The experimental portion of this Thesis deals with the last point most directly, while the first two points are more pertinent to the theoretical portion.

2.3 Experimental Work on Retinal Directional Selectivity

Over the past thirty years there has been a large body of work investigating retinal DS with a variety of preparations. DS retinal output was first described in amphibian (frog, Maturana, Lettvin, McCulloch, and Pitts [50]) and eventually characterized in insect (fly, e.g. Hausen [34]), reptile (turtle, e.g. Lipetz and Hill [44]), bird (pigeon, Maturana [49]), and mammal (e.g. rabbit, Barlow and Hill [7]). We shall now overview some of the key findings in rabbit and turtle that are pertinent to this Thesis.

2.3.1 Extracellular Electrophysiology

The classical extracellular rabbit experiments of Barlow and Levick ([8]) described several phenomena related to the DS response. Using both moving slits and apparent motion[2] protocols they showed:

- DS subunits: Small non-overlapping stimulus regions within the slit–mapped receptive field which were DS consistent with the response to full field stimuli.
- Inhibitory Mechanisms: Stimulus at a given point in the receptive field inhibited later responses to stimuli in the null direction.

The first finding suggested that the DS circuit elements for a given ganglion cell were replicated many times for that cell. Historically, the most explored interpretation of the second finding was that the DS computation relied on an asymmetric inhibitory pathway. However, these data cannot

[2]Apparent motion stimuli are sequences of flashed spots in adjacent locations, similar to the lights in a movie marquee.

rule out a model in which excitation is asymmetric and inhibition is symmetric (e.g. from an antagonistic center/surround). Such a possibility is supported by the following finding.

Apparent asymmetric inhibition was not the only phenomena observed in DS; Barlow and Levick ([8]) also showed (and later Grzywacz and Amthor [30]):

- Facilitatory Mechanisms: A stimulus at a given point in the receptive field facilitates later responses to stimuli in the preferred direction.

Note that null direction inhibition and preferred direction facilitation may be accounted for by an asymmetry in *either* an excitatory (more precisely, facilitatory) *and/or* an inhibitory pathway.

Additional spatial and temporal parameters for the DS network may be inferred by the velocity tuning and size of DS receptive fields (e.g. Wyatt and Daw [69]; Grzywacz and Amthor [30]; Granda and Fulbrook [28]). For instance, the minimum length (measured on the retinal surface) of the lateral path in the DS circuit, near the visual streak, is 100 to 300 μm, as derived from apparent motion protocols.

Sequence–dependent responses may be resolved for very short separations, less than 10 μm (Amthor and Grzywacz, unpublished data). This short distance places a constraint vis-á-vis the electrotonic properties of the DS pathway: passive cable properties, specifically electrotonic length constants of hundreds of microns, are not well-suited for such fine distance discrimination. Thus, this result suggests that non-linearities in the path are important.

The velocity of effective DS stimuli ranges from approximately 0.01 to 10 μm/ms (0.1 to 100°/s in the visual field). These results add constraints on the synaptic kinetics in the DS circuit.

2.3.2 Intracellular Electrophysiology

As mentioned earlier, motion dependent responses have been recorded from all cell types in turtle retina ([23]). These recordings suggest that the crucial elements for DS are found throughout the retina, but two important caveats must be kept in mind. First, the existence of somatic DS signals prior to the ganglion cell layer does not provide, by itself, evidence that these signals are relevant to DS ganglion cell properties. Second, and most important, what constititutes a "true" DS response is open to interpretation, as we discussed earlier in this chapter (see also Section 3.1)

The classical paper of Marchiafava [47] explored ganglion cell input synapses in turtle, for example by examining the effects of injected current on DS responses (Figure 2.1). This paper analyzed the synaptic mechanisms underlying antagonistic center/surround responses, and the possible relevance of these mechanisms to directional selectivity. He concluded that:

- Inhibitory inputs to the ganglion cell with reversal potential close to the resting potential contributed to the antagonism between stationary stimuli in the center and annulus of the receptive field.
- Moving spots activated inhibitory inputs with kinetics and reversal potential similar to those activated by stationary large spots.
- The difference in kinetics between inhibitory and excitatory inputs is sufficient for the reduced null direction response being accounted for by a correlation between inhibition and excitation.

In concordance with this last point, Marchiafava suggested that evidence of motion–evoked inhibition meant that some part of the inhibitory input did not require diffuse stimulation, as might be inferred by the stationary center/surround properties. Presumably, this interpretation was based on the assumption that the motion–evoked inhibition seen for the relatively long stimulus trajectory shown in the paper (991 μm, Figure 8) was present for relatively short trajectories, although this was not explicitly demonstrated. However, the ganglion cell motion responses shown in this paper may also be accounted for by a DS excitatory input that is concurrent with a non-DS inhibitory input. A simulation of such a mechanism that reproduces the salient features of Figure 8 in [47] is shown in Figure 2.2.

The experiments of Watanabe and Murakami in frog retina ([67]) also looked at the effect of intracellular current injection on DS ganglion cell responses. They showed:

- Motion stimuli-evoked IPSP's in ON/OFF, but not ON nor OFF DS ganglion cells, both with no injected current, and with depolarizing current.

They concluded that a directionally-dependent interaction between excitation and inhibition at the ganglion cell could account for the DS in ON/OFF cells, but that "The neural mechanism responsible for the difference in EPSP amplitude in ON- and OFF-type cells probably lies presynaptic to the ganglion cells."

2.3.3 Neurochemistry

The neurotransmitters involved in the DS circuit has been investigated by pharmacological protocols in rabbit (Caldwell, Daw and Wyatt [18], Ariel and Daw [6]) and in turtle (Ariel and Adolph [5]). From this work we can conclude the following:

- Inhibitory Mechanisms: Blockage of GABAergic pathways reduces or eliminates DS.

As before, this result would seem to support the class of DS models in which inhibition is asymmetric. But as we shall see in Chapter 4, this data is also consistent with models in which the inhibitory pathway is symmetric. Also, recent results (Smith, Grzywacz, and Borg-Graham ([59]) with GABAergic antagonists in turtle show:

- Inhibitory Mechanisms: For about 50% of all DS cells, DS is maintained or *reversed* when GABAergic pathways are blocked.

These experiments are demonstrated in Figures 2.3 and 2.4. This result is similar to that reported previously in fly (Bülthoff and Bülthoff, [16]). As we discuss later, existence of DS without inhibition places strong constraints on the DS circuit model.

2.3.4 Anatomy

Physiologically identified DS ganglion cells have been stained in rabbit (Amthor, Oyster, and Takahashi [4]) and turtle (Jensen and DeVoe [38]). A clear result of this work is that:

- DS Morphology: The dendritic trees of DS ganglion cells are not aligned with their P/N axes.

Thus the morphometric substrate for DS is not immediately obvious from the histology.

2.4 Theoretical Work on Retinal Directional Selectivity

Inspired in part by the correlation models of Hassenstein and Reichardt ([33]) for motion detection in fly, several models for retinal DS have been

proposed which describe the location and biophysical mechanisms for the necessary (Section 2.2) spatial asymmetry and time–dependent nonlinear interaction (Figure 2.5).

Barlow and Levick ([8]) considered both asymmetric lateral inhibitory and excitatory pathways in the outer plexiform layer, with a nonlinear interaction at bipolar cells between these pathways and direct excitatory pathways. Others, including Torre and Poggio ([63]) and Koch, Poggio and Torre ([39]), suggested that the lateral pathway might be mediated by amacrine cells, among other possibilities. They showed that the interaction between an asymmetric lateral synaptic inhibition and symmetric synaptic excitation, possibly on the ganglion cell membrane itself, could provide the necessary nonlinearity for DS. In particular, Torre and Poggio showed how the shunting action of inhibitory synaptic conductances interacts non-linearly with other inputs. These models do not explicitly define the mechanism of the delay, other than to point out that a mechanism which has a low–pass filter characteristic (as had been suggested in fly DS literature), or slower inhibitory synaptic kinetics, might suffice.

We note that in these circuit architectures the only directional signal available is strictly DS, under any circumstances. This is because the interaction between the asymmetric and symmetric pathways is immediately nonlinear. If the nonlinearity is blocked (e.g. blocking inhibition for the inhibitory model), then no interaction can take place: there will be no DD signal at all. This property is directly relevant to the finding of DS with blocked inhibition that was mentioned in Section 2.3.3.

Koch, Poggio and Torre ([41]) (also O'Donnell, Koch and Poggio [53]) examined the electrotonic structure of a cat ganglion cell and a putative DS rabbit ganglion cell ([4]), respectively, in detail. They showed that the dendritic tree of the ganglion cell was well suited for local interactions within the tree between an excitatory input and an inhibitory input that has a strong shunting component (large conductance change with synaptic reversal potential near rest). The conclusion was that the computational substrate for subunit response was possible within the tree, e.g. supporting a ganglionic model.

2.4.1 Implications of Ganglionic Directionally Selective Interactions

Although not explored in the work cited above, a ganglionic DS model also predicts the arrangement of DS subunits with respect to the ganglion cell

dendritic tree, and the relative response to preferred direction motion which traverses the entire receptive field, given certain constraints. Assuming that DS interactions occurr at random locations in a radially symmetric ganglion cell dendritic tree, then preferred direction inhibition is predicted, despite the locality of the interactions (see Figure 2.6). For long distance motion, this arises because the distal tree on the preferred direction side is activated last. In order to get to the soma, the excitation from this area must traverse dendritic regions in which the locally non-correlated delayed inhibition remains activated. This phenomena would be expected to limit the spatial and temporal bandwidth of effective preferred direction stimuli. Likewise, subunits on the preferred side of the receptive field would be expected to have a smaller preferred response than that from subunits on the null side.

Barlow and Levick ([8]) compared subunit responses to the (stationary) spot-mapped receptive field. If we assume that that the latter mapping is congruent with the dendritic tree, then their results (Figure 4 in [8]) do not support the prediction of preferred direction inhibition. In this figure, for example, the preferred direction response for subunits $d \leftrightarrow e$, $i \leftrightarrow j$, and $n \leftrightarrow o$ (all on the preferred side) are similar to that for $a \leftrightarrow b$, $f \leftrightarrow g$, and $k \leftrightarrow l$ (all on the null side), respectively. On the other hand, there was a significant null direction response within the three null side subunits (anomalous response, see Section 4.3.4). Further work will be necessary to determine whether these observations are significant.

Correlation models also predict velocity tuning as a function of the delay and length of the asymmetric pathway, Δt and l, and for ganglionic model versions there is an inherent tradeoff between bandwidth of null direction motion and the above preferred direction inhibition. Consider the simple version shown in Figure 2.5 (B), where l refers to the spacing between the inhibitory and excitatory pathways. If we assume that the synaptic temporal transfer functions are given by $\delta(t)$, then for a moving spot the only null stimulus is motion towards the left with velocity:

$$v_{null} = l/\Delta t$$

All other velocities, even towards the left, will pass. To increase the rejection bandwidth we can add some width τ to the inhibition impulse response. Now the rejected null direction velocities are in the following range:

$$l/(\Delta t + \tau) \leq v_{null} \leq l/\Delta t$$

However, since the structure in which the interactions takes place is symmet-

ric, letting $\tau > 0$ allows the preferred direction inhibition described above (see Section 4.3.5).

2.4.2 Starburst Amacrine Cell Models for DS

Recently, Vaney and co–workers ([66] [64]) have expanded on ideas from Masland, Mills, and Cassidy ([48]) and suggested a specific cell type in rabbit, the starburst cholinergic/GABAergic amacrine cell, as providing an asymmetric excitatory pathway for the DS circuit. They further suggested that starburst dendrites also mediate a lateral inhibitory pathway in the DS circuit, since these cells contain GABA and the tips of adjacent starburst cells are in close proximity. In their "co–transmission" model (the same cell releases both GABA and acetylcholine), inhibitory connectivity from starburst cells is symmetrical, in contrast to the asymmetric excitation. On the other hand, the locus and biophysical mechanisms for the computation of DS are not specified in this model, although they mention both ganglionic and pre–ganglionic alternatives.

2.5 Summary

We have described a working definition of the DS (and DD) visual response and summarized the specific goals of this Thesis. We have also given an overview of both experimental and theoretical work in visual system DS, especially as regards to the vertebrate retina.

It is important to be precise with respect to the visual system phenomena under scrutiny, since quite different hypotheses may derive from subtle differences in experimental or theoretical conditions. For example, the retinal DS model described in Chapter 4 includes predictions for (at least) DD signals within the circuit that underly the DS output. These DD signals will identify where in the retina the specific computation of DS first appears. Such a DD finding may be used, in principle, to rule out experimentally models which predict that a strictly DD signal will *not* be found elsewhere in the circuit, under any conditions. While the sloppyness of real neural circuitry would generate some degree of asymmetric responses in general, the appropriate experimental protocol should be able to determine the presence or absence of a significant DD response that is relevant to these alternate models.

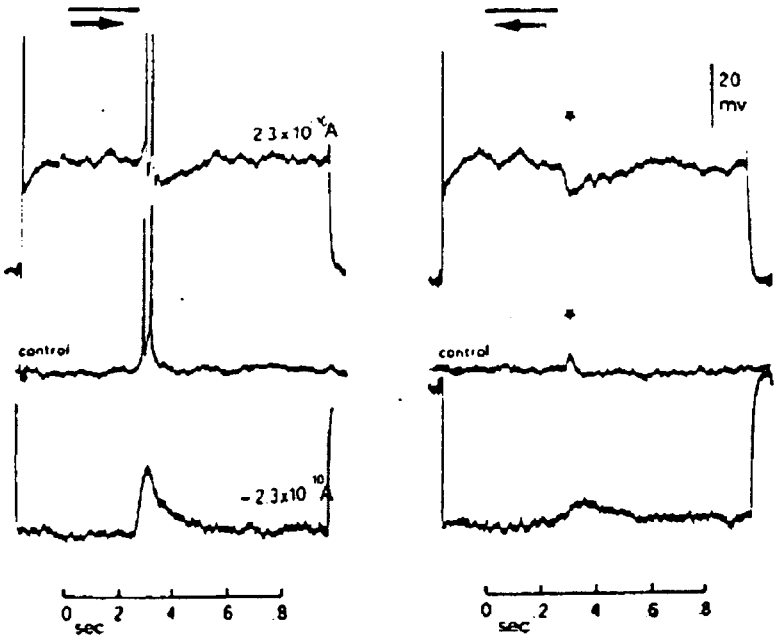

Fig 8. The effect of intracellular current injection upon the photoresponses to a moving spot. The trajectory of the spot (991 μm at 3.5 μ/msec) was along the preferred–null axis. The responses to movement in the preferred and null directions (marked by a star) are shown at the left and the right side of figure, respectively. At the top, the duration and the direction of movement are indicated. *Control* indicates responses recorded at resting potential. Upper and lower records show the photoresponses during artificial polarization of the cell membrane obtained with the current intensity indicated by the numbers above the records on the left. Zero time coincides with the onset of the spot movement.

Figure 2.1: Protocol by Marchiafava (Figure 8 from [47]) investigating the effect of current injection on DS responses in turtle retinal ganglion cells. An important feature of this protocol is that for both directions of the stimulus, the hyperpolarizing current is sufficient for the synaptic potentials to stay below the resting potential. The small EPSP for the null stimulus under hyperpolarization implies that a null-direction correlation of inhibition and excitation *does not* underly DS in this cell.

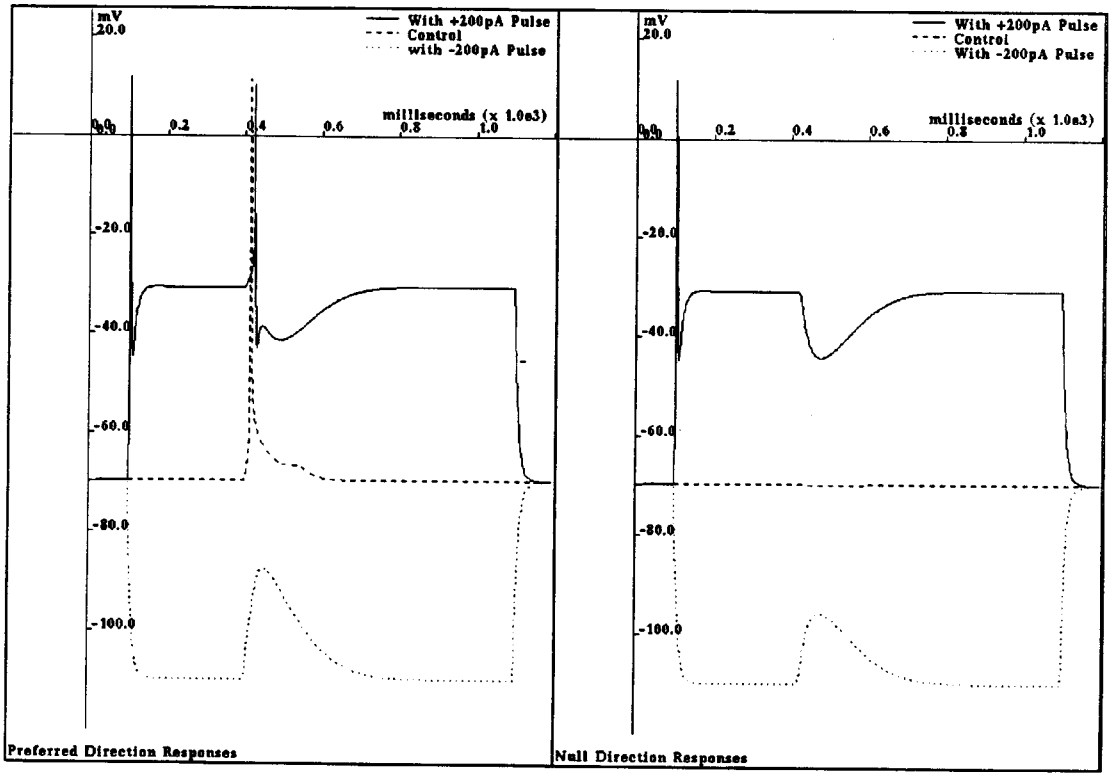

Figure 2.2: Simulation of lumped cell with DS excitatory input and non-DS inhibitory input. Cell parameters, including τ_0, R_{in}, synaptic conductances' kinetics, sizes, and reversal potentials, and voltage-dependent channels underlying the spike were chosen to recapitulate data from [47] reproduced in Figure 2.1. Note that when the cell is hyperpolarized below the reversal potential of the inhibitory synapse (set here at E_{rest}), the activation of both the excitatory and inhibitory synapses in the preferred direction combine to produce an "EPSP" that is higher than that produced by the inhibitory synapse alone in the null direction, as seen in Figure 2.1. Also, this choice for the inhibitory reversal potential means that the membrane must be away from E_{rest} in order to see the activation of the "silent" inhibition. In order to account for the distinct spike thresholds (e.g. high threshold spikes for preferred stimulus when cell is depolarized), two putative Na^+ channels are included with midpoints of activation set to -60 mV and -25 mV, respectively. These channels may account for the multiple spike heights reported in DS ganglion cells in turtle by Jensen and DeVoe ([38]), e.g. differential activation of more than one type of Na^+ channel. Such diversity of Na^+ channels has been reported in other neurons and has been predicted by modelling studies ([9]).

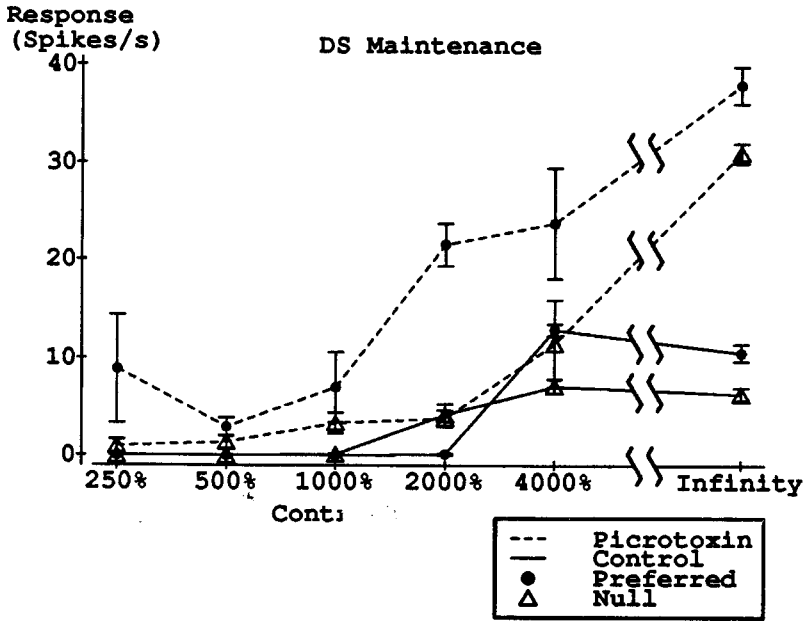

Figure 2.3: Smith et. al. ([59]) tested the sensitivity of DS to picrotoxin (a GABAergic antagonist) in isolated intact turtle retina, using the extracellular preparation described in Appendix A. In some cells DS was maintained despite saturating levels of picrotoxin in the superfusate (50 to 200 μM), as demonstrated in the example cell above. Motion stimulus: 200μm X 600μm bar at various angles, speed ranging from 1 to 5 $\mu m/ms$, centered on the spot-mapped receptive field. In this figure, contrast is defined as $(f-b)/b$, where f is the foreground light intensity, and b is the background light intensity.

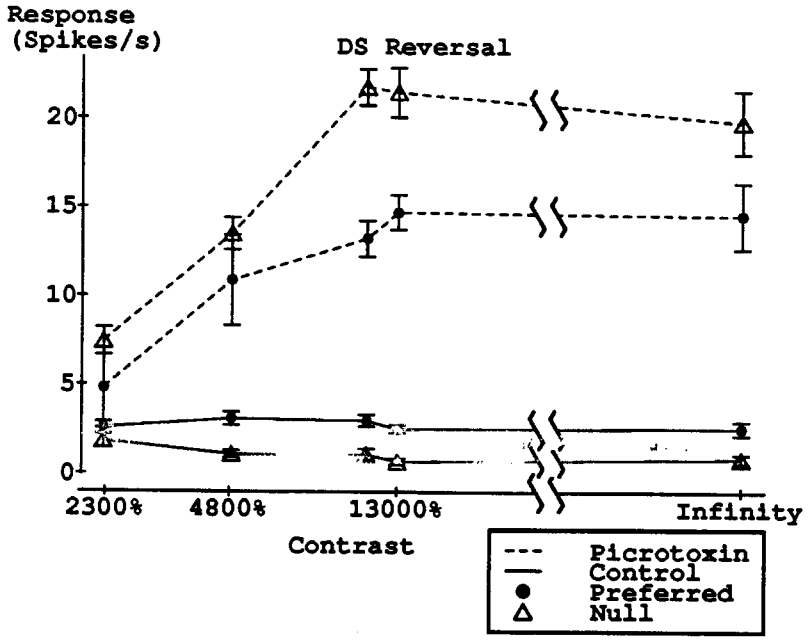

Figure 2.4: Smith et. al. also reported that in some cells, blockage of GABAergic pathways resulted in a reversal of the DS P/N axis along with the expected increase in overall response. Experimental and stimulus conditions similar to that in Figure 2.3.

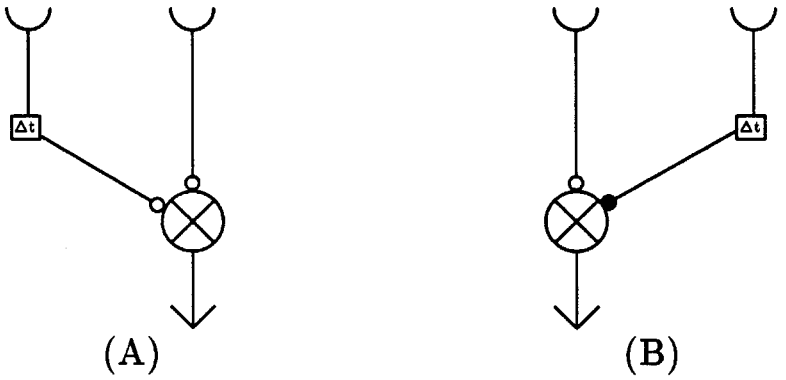

Figure 2.5: Correlation-type models for the computation of DS are typified by that proposed for the fly and vertebrate retina. Versions of this model have considered both an all-excitatory interaction (A) or an excitatory/inhibitory interaction (B) (e.g. asymmetric-veto or AND-NOT models). In the diagram the nonlinear interaction between the direct and asymmetric delayed inputs is expressed as a multiplication, but this particular nonlinearity is not crucial to the model. In all figures open and closed circles are excitatory and inhibitory inputs, respectively. Note that a position-dependent delay is applied before the nonlinearity. For both (A) and (B) the preferred response is for motion to the right. For rightward motion in (A), the delayed lefthand input is correlated with the un-delayed righthand input; for leftward motion the delay amplifies the temporal separation at the nonlinearity. For rightward motion in (B), the delayed righthand input is correlated with the un-delayed lefthand input, and the inversion of the righthand input cancels out the lefthand input; for leftward motion again the delay amplifies the temporal separation at the nonlinearity, in this case allowing passage of the lefthand input (assuming that the nonlinearity is not strictly multiplicative).

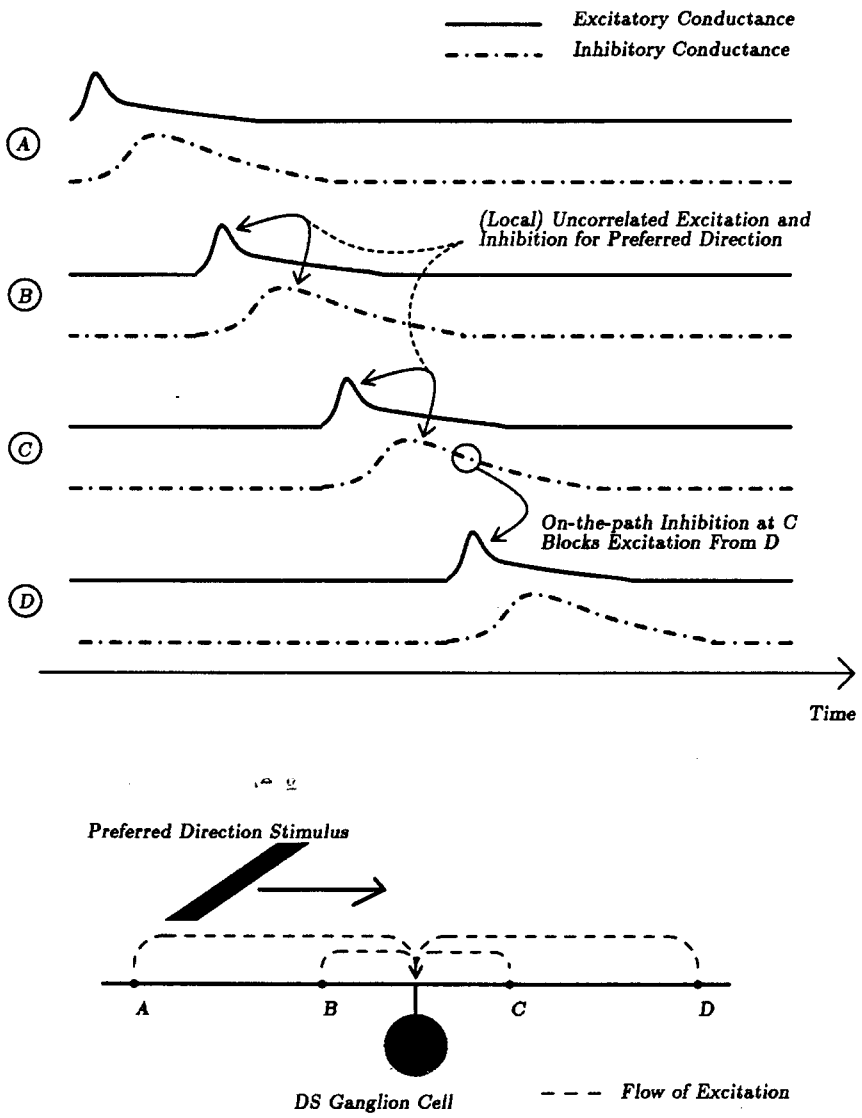

Figure 2.6: DS models in which the ganglion cell dendritic tree is the site for DS excitatory-inhibitory interactions (correlation of local inputs in the null direction) predict inhibition of the late phase of long distance preferred direction motion and subunit preferred response that depends on location, assuming that inputs occur throughout the tree. This inhibition is from previously activated inhibition (e.g. at C) that is non-correlated with local excitation, but that is nonetheless both on-the-path *and* correlated for the later excitation (e.g. at D).

Chapter 3

Directionally Selective Ganglion Cells in Turtle: Experimental Results

We shall now present data from whole-cell patch (intracellular) recordings of ganglion cells in turtle retina. As we saw in the last chapter, various models for retinal directional selectivity have different predictions as to the properties of synaptic input onto directionally selective ganglion cells. The recordings presented here show that some ganglion cells receive DS excitatory input: therefore the necessary elements for the DS computation must occur in cells pre-synaptic to the ganglion cell.

Further, we present on-cell patch[1] (extracellular) and subsequent whole-cell patch recordings from the same cells in which extracellularly-determined DS properties are consistent with DS properties of the excitatory input. These recordings suggest that the whole-cell patch protocol does not introduce artifactual DS properties. Details on the tissue preparation, stimulus generation, and experiment control apparatus are described in Appendix A. Details of the whole-cell patch technique, and basic properties of cells recorded with this technique, are described in Appendix B.

[1] On-cell patch recordings are made with a patch electrode in a tight seal configuration onto the cell, with the cell membrane intact.

3.1 Stimuli for Characterizing Directional Selectivity

A variety of light stimuli with different motion components may be used to explore directional properties. Depending on the spatial and temporal properties of the stimulus, each type emphasizes different aspects of motion sensitivities.

3.1.1 Gratings Versus Bars, Temporal and Spatial Windowing

As mentioned in the last chapter, previous work investigating directional visual responses have used both aperiodic stimuli (e.g. moving bars or spots, apparent motion protocols) and quasi-periodic stimuli (e.g. spatially and temporally windowed gratings). Both classes of stimuli have strong (directional) motion components. Aperiodic stimuli, however, emphasize the transient (in time) and wide (in space) components of the DS circuit's transfer function, while the quasi-periodic stimuli tend to emphasize the steady-state and narrow (in space) components.[2]

In principle any realizable DS circuit will show a DS response to periodic stimuli. However, there are several candidates for inactivating or adaptive mechanisms along any neural pathway which tend to emphasize the transient response of the system, as shown in Figure 3.1. Examples include eithor inactivation or adaptation of phototransduction, synaptic release (e.g. transmitter depletion), synaptic receptors, and of voltage or Ca^{++}dependent channels (e.g. adaptation of repetitive firing, channel inactivation [36]). Inhibitory feedback may also be important in retinal function [68]. Also, in retina, inhibitory feedforward pathways are relatively slower than their excitatory counterparts.

The inhibitory pathways in the retina are not only relatively slower than the parallel excitatory pathways, but they tend to have wider spatial range as well. To the extent that a DS circuit depends on inhibitory input, these properties would tend to generate a more asymmetric response to stimuli with larger size (e.g. in terms os moving spot path length or moving grating aperture).

[2] In this Thesis, the "steady-state" response is defined similar to that used in electrical engineering practice, i.e. the response of a system at long times relative to the start of a periodic input.

Stimuli with a relatively smaller size have another disadvantage when it comes to characterizing receptive field asymmetries. We expect a DS cell to have a consistent asymmetry over its receptive field, as we discussed earlier. The classical antagonistic center-surround receptive field, while symmetric overall, includes *local* asymmetries (Figure 3.2) which could give DS responses to spatially-limited stimuli (assuming non-linear center-surround interactions). A harbinger of such a situation would be a strong DS sensitivity to aperture size (e.g. DS for apertures below some maximum size). A consistent DS receptive field would not show such a sensitivity to the *spatial* change in a larger stimuli (although a concomitant increase in temporal characteristics might reduce the DS of the complete response). Such mechanisms may explain some previous findings, e.g. spatially–limited DS cells prior to ganglion cells [23]. An alternate explanation for the spatial limitation may, however, be center/surround DS antagonistic receptive fields [22].

We have used both gratings and bar stimuli in the experiments presented here. Although DS responses were found using both types of stimuli, preliminary results suggest that the most effective DS stimuli under the recording conditions described in Appendices A and B are spots (e.g. 100 to 200μm in diameter) with a long path ($>$ 500μm, drifting from 0.5 to 5 μm/ms). Long moving bars (e.g. 1000 $\times$ 200μm) do not seem to be as effective, possibly because of activation of the inhibitory surround.

Moving grating stimuli were presented within a square aperture (100 to400μm sides, oriented along the motion axis). Gratings were exposed for 2 second "burst" windows from a dark background; depending on the temporal frequency of the grating, each burst included 1 to 10 cycles of the grating. The spatial phase of the gratings was set such that at the start of each temporal window an ON edge appeared at one side of the aperture. The spatial period of all gratings was at least 800 μm, so the aperture was completely dark at the start of the temporal window. Responses from a series of windows at a given orientation were then averaged together, maintaining zero relative phase. This protocol provided both a transient response to the first ON edge drifting across the aperture, and the first cycles of the "steady-state" response. Although the rotating square aperture meant that slightly different areas of the retina were illuminated depending on orientation, the illuminated areas for motions of opposite directions (relevant to the DS determination) was identical.

As described in Appendix A, 100% contrast (point on monitor either full on or full off) stimuli were used in all experiments.

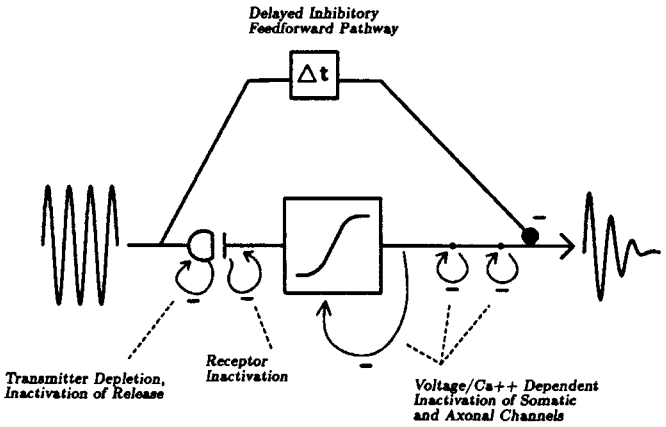

Figure 3.1: Mechanisms within neural pathways include many which are time-dependent. These dependencies may have both activating and inactivating components, but any inactivating link in a serial path will shut off the signal in the path, independent of any activating links. The net result will be to attenuate the system response to continued presentation of the input.

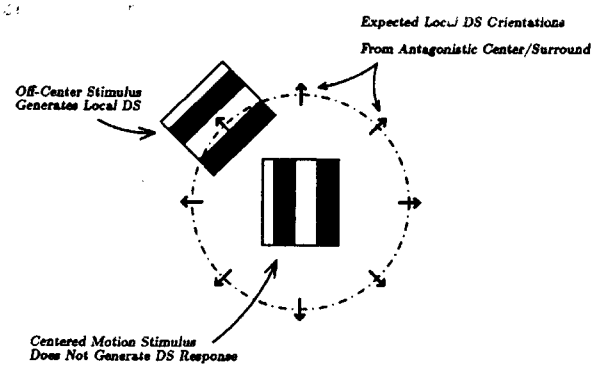

Figure 3.2: The relatively slower kinetics of feedforward inhibitory pathways result in local DS regions in an overall symmetric center/surround cell, assuming that the center-surround interaction is non-linear. The preferred direction of a region is centripetal with respect to the receptive field center, and thus is dependent on the location of the region.

3.2 Protocols for the Identification and Characterization of Directionally Selective Cells

3.2.1 Basic Protocols

In each the experiments described here, basic DS properties were determined as follows:

1. Single cell response were obtained with extracellular (spiking) on-cell patch recordings using flashing spots (typically 400 μm square) at 1 Hz, centered either at the electrode tip location or roughly midway between the electrode tip and the visual streak, when visible).

2. Receptive field spot map was then obtained extracellularly using (typically) 100 μm square spots flashing at 1 Hz, stepping over a 5 by 5 square grid (100 – 200 μm distance between grid points)(protocol type "RF"). The center of the resulting spot map was estimated by eye.

3. Using the center of the receptive field as the center of rotation, the extracellular responses to a series of moving gratings or spots, moving at either 8 or 16 directions, were collected. A DS cell was defined as one in which a chosen single-valued response parameter, summed over at most three (for 8 direction experiments) or five (for 16 direction experiments) adjacent directions over all trials, was significantly greater than the summed response to the complementary orientations (Student T test, $p < 0.05$). For example, for a 16 direction experiment, the (preferred) value

$$P = \sum_{i=-2}^{2} R(\theta_0 + (i \times 22.5°))$$

was compared with the (null) value

$$N = \sum_{i=-2}^{2} R(\theta_0 + (i \times 22.5°) + 180°)$$

for the 16 values of θ_0, where $R(\theta)$ is the response for direction θ. When P was statistically significantly greater than N, a direction index

$$DI_{sum} = (P - N)/(P + N)$$

was then computed (see Section 4.3.2). The preferred direction of the cell, θ_P, was defined as the value of θ_0 which gave the maximum statistically significant value of DI_{sum}. The degrees of freedom for the Student T test was defined as the number of trials (2 to 8) multiplied by the number of grouped orientations (1 to 5). These protocols, which also generate an orientation tuning for the cell, are defined as type "WF".

4. Whole cell (intracellular) access was then obtained and WF protocols were used to determine if extracellular DS properties (DS or not DS, preferred direction and DS tuning) were maintained over time, under both current and voltage clamp conditions.

Single-valued response parameters used for DS determination ($R(\theta)$) included spike count, integral of membrane potential minus E_{rest} (for current clamp protocols), and integral of the holding current minus the total clamp current (for voltage clamp protocols; note that negative clamp current implied an excitatory event).

Ideally, extracelluar recordings were stable enough to perform the DS determination, but in many cases either whole-cell access was obtained prior to completion of the DS protocol, or the extracellular recordings were too noisy for evaluation in the limited time available. Likewise, in the ideal case whole-cell access provided clear and stable spikes so that recapitulated protocols (using spike count as the response parameter) could be more directly compared with the previous extracellular protocols. However, in some cells spikes disappeared within minutes, and either synaptic potentials (via current clamp) and/or synaptic conductances (via voltage clamp) were evaluated for DS properties. In this case, either the DS properties of the waveforms were obvious to the eye, or a similar student-T test as above was applied using the appropriate waveform integral as the dependent variable.

3.2.2 Advanced Protocols

For many identified DS cells, particularly when the recordings were sufficiently stable, more specific DS measurements were made. These included the following:

- In order to replicate the data of Marchiafava directly (Figure 2.1) and thus highlight ganglion cell inhibition, preferred/null runs using spots or gratings under various current clamp conditions were run as soon

as possible and after at least 30 minutes of whole-cell access (protocol type "PN"). These included a control run (current clamp at 0 pA), and runs with a constant depolarizing or hyperpolarizing currents (typically to about ± 10 to 30 mV around rest, i.e. ± 10 to 30 pA). Ideally, if extracellular DS was determined then the first set of these runs was done immediately after whole-cell access in order to avoid IPSP attenuation. Otherwise, a WF protocol was done immediately after whole-cell access and then (if the cell was DS) the first run of this protocol was done.

- In order to explore velocity tuning and/or spatial dependence, various WF protocols were used with different temporal and spatial parameters, e.g. various spot speeds or grating temporal frequencies, or spot path lengths or grating aperture sizes.

- In order to evaluate DS edge effects of symmetrical receptive field properties, and to measure DS subunit properties, a series of 5 P/N runs with gratings or spots of limited extent were used, with stimulus centers spaced on typically 100 μm centers along the P/N axis and the entire series centered on the receptive field center.

- In order to map DS subunit properties more fully, WF protocols using spatially limited moving spots or gratings were used over a 3 by 3 grid (100 – 200 μm distance between grid points), with the entire grid centered on the spot-mapped receptive field center.

- In some cases, RF protocols were repeated at various intervals to check the stability of the spot-mapped receptive field.

For some cells, simple size dependence for flashing spots was determined using 50 to 1600 μm square spots, centered on the spot-mapped receptive field. This protocol, called type "SP", was especially useful for observing the evolution of inhibitory post synaptic potentials (IPSPs) during whole-cell access. Because of its importance in the interpretation of intracellular DS recordings, we shall discuss this phenomenon now.

3.3 Elimination of IPSPs With Maintenance of Antagonistic Center Surround Excitatory Input

In Section 2.4 we discussed ganglionic models in which the interaction between (non-DS) excitatory and inhibitory input onto the ganglion cell underlie the cell's DS response. Also, interpretation of ganglion cell membrane potentials may be complicated by inhibitory input onto the cell which might not have a direct link to the directional properties (Section 2.3.2).

For this reason we have recorded from ganglion cells using whole cell patch electrodes in which the electrode solution is free of ATP (in some cases without Mg^{2+} as well) (Appendix B). Given the large bore of the electrode (1-2 μm), it is likely that the cell contents are dialyzed by the electrode solution within several minutes after the start of recording. It has been reported in hippocampus that such conditions block the response of $GABA_A$ receptors ([60]); thus this technique offers a method for selectively blocking an inhibitory component of the recorded cell's synaptic input, without disturbing the rest of the network.

Using this technique we have recorded from ganglion cells which show clear light-evoked IPSPs and EPSPs at normal resting potential at the onset of whole-cell access. However, in almost all these cells, within typically ten to twenty minutes after whole-cell access, light-evoked IPSPs disappear while EPSPs are maintained, suggesting the block described above. This apparent removal of direct inhibitory input to these cells was verified by depolarizing the cells: negative synaptic potentials were not observed despite large depolarizations (30 mV above the resting potential). Hyperpolarizing phases of spike repolarizations were observed, however, suggesting preservation of voltage-dependent hyperpolarizing mechanisms.

Figures B.6 through B.12 in Appendix B demonstrate the reduction of IPSPs to flashing spots over time. In this chapter we shall show DS recordings of these same cells or cells recorded under the same conditions. To recapitulate, DS ganglion cell responses without measurable inhibitory input, especially with P/N distinctions that are stable with respect to hyperpolarizing or depolarizing current, suggest that some turtle ganglion cells receive excitatory input which is already DS.

3.4 Directionally Selective Responses

We shall now present DS recordings from several ganglion cells taken with a variety of protocols. We shall describe the basic findings under current clamp and voltage clamp, and then present example recordings in Figure 3.3 through 3.25. These recordings are listed in Table 3.1 for quick reference.

DS data is presented in several formats. Polar plots of single-valued response parameters are presented with standard deviations when the parameter was computed for each trial, and then averaged over several trials. Response waveforms are presented both in the standard fashion and in perspective plots (moving gratings only). Each perspective plot is composed of a series of averaged current or voltage clamp waveforms in response to motion stimuli at 16 orientations (WF protocol). The responses shown in these plots are passed through a low pass filter ($f_c = 20hz$) before averaging. As mentioned earlier in the description of moving grating burst averaging, each averaged waveform shows both the transient response and the (beginning of the) steady state (grating) response. The waveform data is replicated once by concatenating 2 full cycles of the 360° sweep of the stimuli direction, in order to more clearly show any directional component.

For some cells, we also show spot-mapped receptive fields overlaid with the cells' DS axis.

3.4.1 Directionally Selective Responses Under Current Clamp

DS EPSPs and spike responses have been obtained with the whole-cell patch technique under the conditions which reduce or eliminate IPSPs. The DS of the responses are stable with respect to holding current, which was adjusted to move the resting potential within ± 30 mv from the control E_{rest}.

3.4.2 Directionally Selective Responses Under Voltage Clamp

DS responses were also recorded under voltage clamp. In the perspective plots of these responses clamp current polarity has been reversed for clarity; thus positive current implies an *excitatory* synaptic event. The DS of the response are stable with respect to holding potential, which ranged from -90 to -35 mV.

For example, in cell A56 (Figure 3.8) the dependence is striking (best at about 157°), and is independent of the holding potential (Figure 3.10). For comparison, cell A81 (Figure 3.13) shows little dependence of the voltage

clamp waveforms on stimulus direction.

Although the degree in which the dendritic tree of these cells is actually clamped during the voltage clamp protocol is not know directly, the observation of DS inward currents at low (somatic) holding potentials is further evidence for at least a component of the excitatory synaptic input being DS, independent of any local blockage of IPSPs.

Cell	Type	Figure	Recording Method	Stimulus Protocol	Plot Type
A47	±	3.3	CC	WF3	Conventional
		3.4	CC	-WF3	Polar
		3.5	VC	WF15	Conventional
		3.6	CC	WF15	Polar
A56	+	3.7	EC	WF2	Polar
		3.8	VC	WF4	Perspective
		3.9	VC	WF4	Polar
		3.10	VC	WF6	Perspective
		3.11	VC	WF6	Polar
		3.12	CC	RF1-2	RF w/DS axis
A81	±	3.13	VC	WF6	Non-DS Persp.
A84	±	3.14	EC	WF2	Polar
		3.15	CC	WF3	Conventional
		3.16	VC	WF5	Perspective
		3.17	VC	WF5	Polar
A105	±	3.19	CC	WF?	Polar
		3.20	CC	PN2-4	Conventional
		3.21	CC	RF2	RF w/DS axis
A115	+	3.22	EC	WF4	Polar
		3.23	CC	PN1-3	Conventional
		3.24	CC	WF5	Polar
		3.25	CC	PN4-8	Conventional
		3.26	CC	RF2	RF w/DS axis

Table 3.1: Reference to figures of DS recordings. Cell type: ± = ON/OFF, + = ON. Recording Method: CC = current clamp, VC = voltage clamp, EC = extracellular. Stimulus Protocol: WF = wide field DS test and tuning, RF = receptive field map with spots, PN = preferred/null motion runs. Numbers after stimulus protocol designations refer to specific experiments.

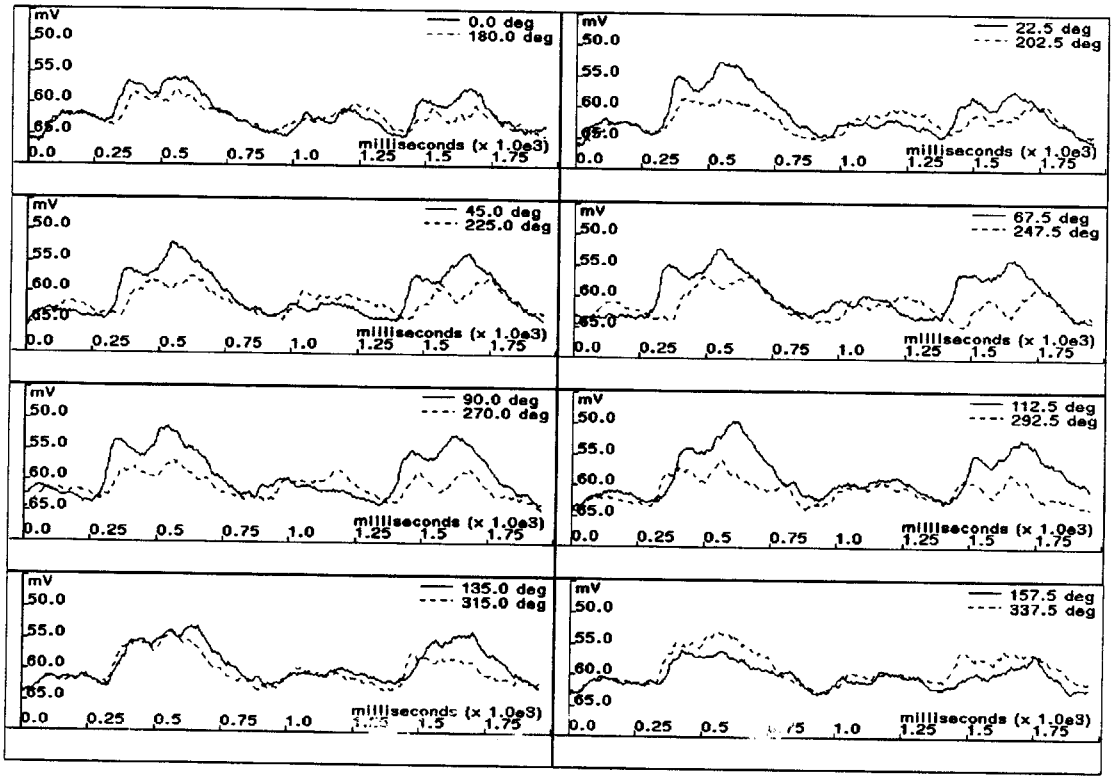

Figure 3.3: DS responses to moving gratings under current clamp for ON/OFF ganglion cell A47 (protocol A47WF3). Each waveform is the average of 4 trials. The grating had a 200 μm square aperture, a temporal frequency of 1 hz and a spatial period of 800μm. In this protocol, $\theta_P = 67.5°$, $DI_{sum} = 0.2$ ($p < 0.05$) (integral of $V - E_{rest}$). This recording was made 17 minutes after whole-cell access (there was no extracellular response recorded). Although this cell responded to both ON and OFF edges of stationary spots, the expected 2nd harmonic of the motion response is small. Small IPSPs were observed within 5 minutes of whole-cell access during receptive field stationary spot mapping.

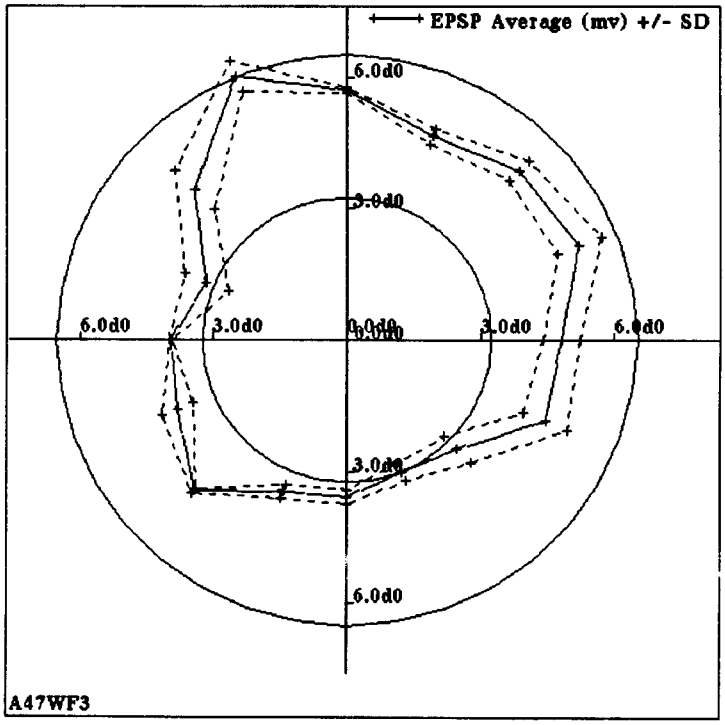

Figure 3.4: Polar plot of average $(V - E_{rest}) \pm SD\ (mV)$ for waveforms whose averages and DS statistics are shown in Figure 3.3 (A47WF3).

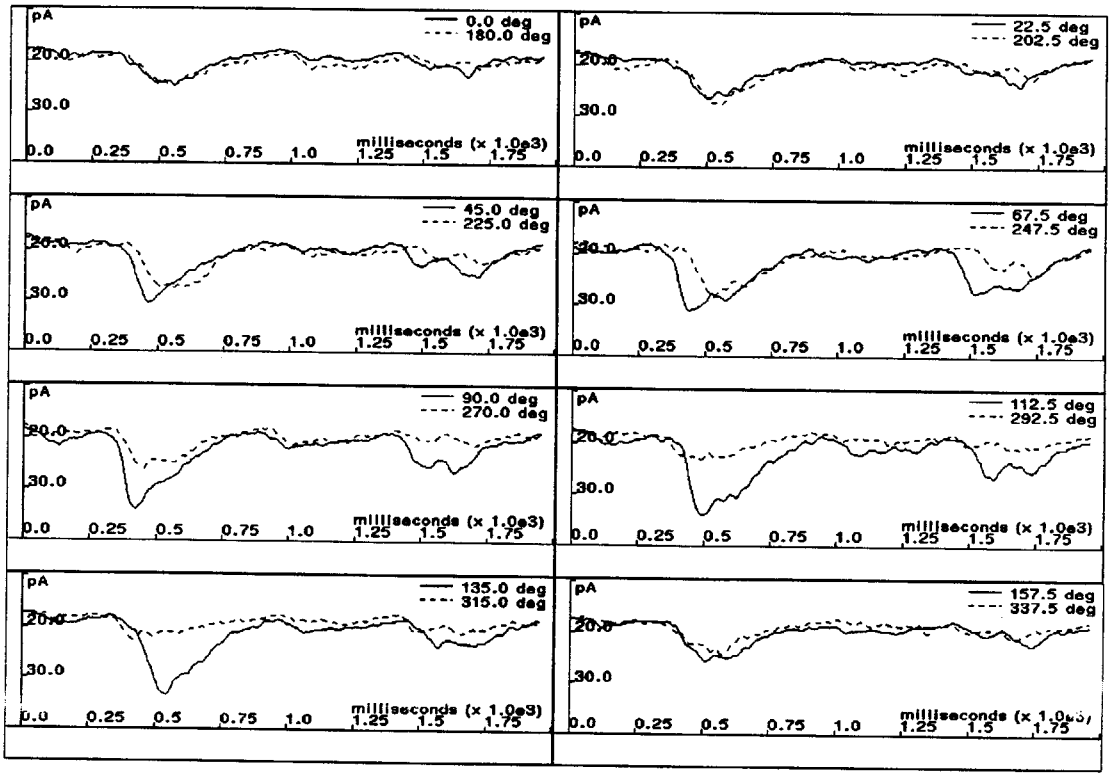

Figure 3.5: DS responses to moving grating under voltage clamp for cell A47 (protocol A47WF15), taken 2 hours after the responses in Figure 3.3. Holding potential = -80mV, average of 4 trials. Stimuli are identical to those used for Figure 3.3. Using the integral of $(I_{holding} - I_{clamp})$ as the response variable, the DS statistics are $\theta_P = 112.5°$, $DI_{sum} = 0.3$ $(p < 0.05)$. The preferred direction has apparently shifted from the previous protocol (though the statistical significance of this was not evaluated), but remains consistent with the original axis of asymmetry.

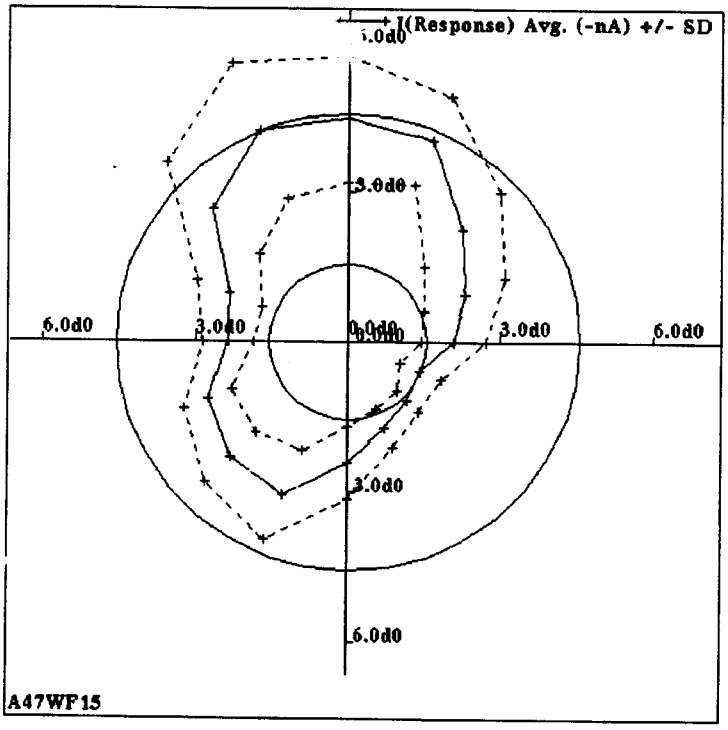

Figure 3.6: Polar plot of average $(I_{holding} - I_{clamp}) \pm SD$ (pA) for waveforms whose averages are shown in in Figure 3.5 (A47WF15).

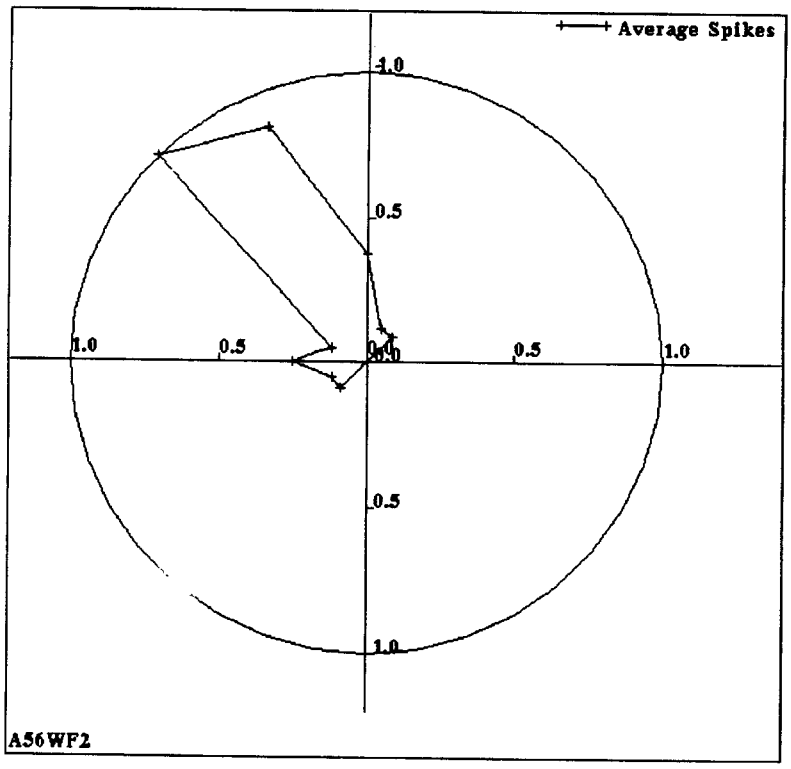

Figure 3.7: Polar plot of DS extracellular spike response of ON cell A56 to a moving grating (average of 8 trials per orientation, 16 orientations). Grating aperture was 200μm square, with a temporal frequency of 1 hz and spatial period of 800μm. For this protocol $\theta_P = 135°$, $DI_{sum} = 1.0$ ($p < 0.05$). The standard deviation for this protocol was not available.

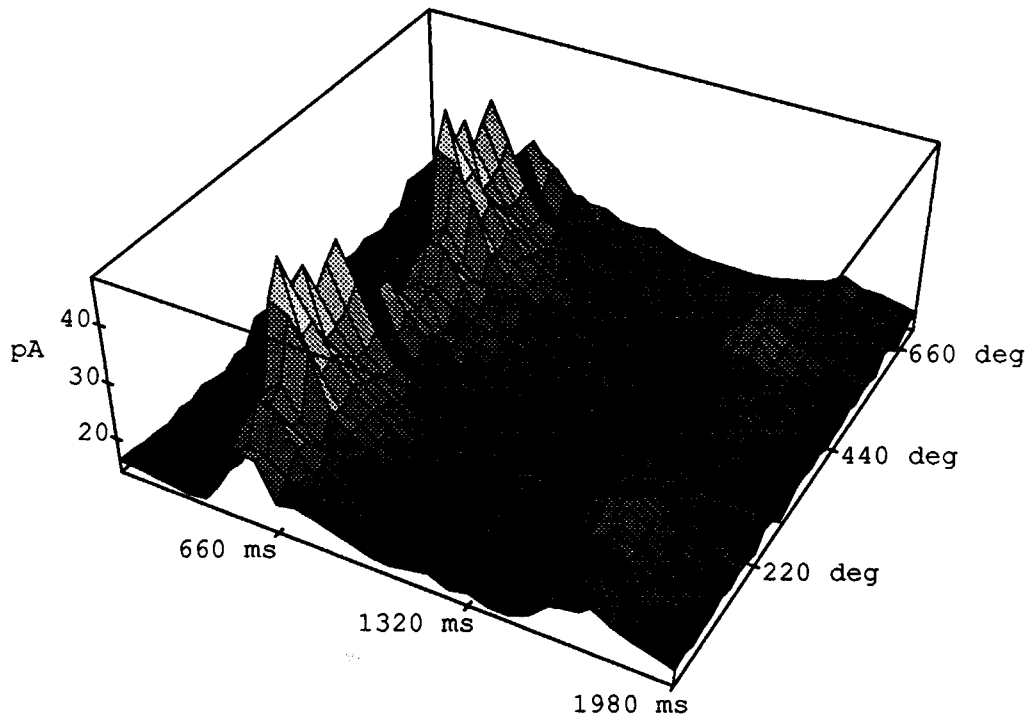

Figure 3.8: Perspective plot of DS responses to moving grating under voltage clamp for cell A56, taken 14 minutes after whole-cell access (average of 2 trials). The response to the initial ON edge has a delay of about 400ms, and a very slight response to the first OFF edge is seen around 1300ms. The holding potential $= -80$mV strongly attenuates any inhibitory synaptic current, even if the dendritic tree is not fully clamped. Thus, this response suggests that excitatory input to this cell has a large DS component. Grating aperture was 100μm square, with temporal frequency of 1 hz and spatial period of 800μm.

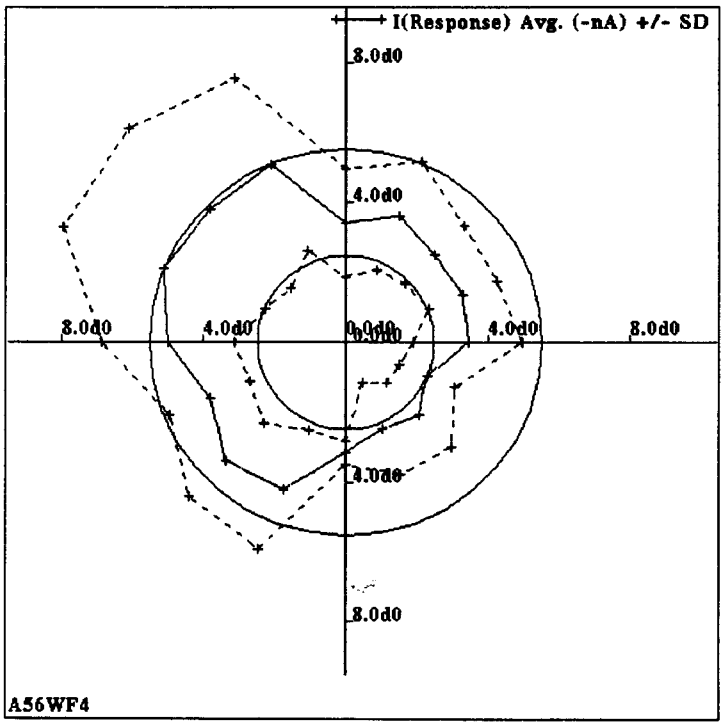

Figure 3.9: Polar plot of average $(I_{holding} - I_{clamp}) \pm SD$ (pA) for waveforms whose averages are shown in in Figure 3.8 (A56WF4). For this protocol, $\theta_P = 157.5°$, but there is no statistically significant DS based on this parameter alone (presumably because of the low number of trials).

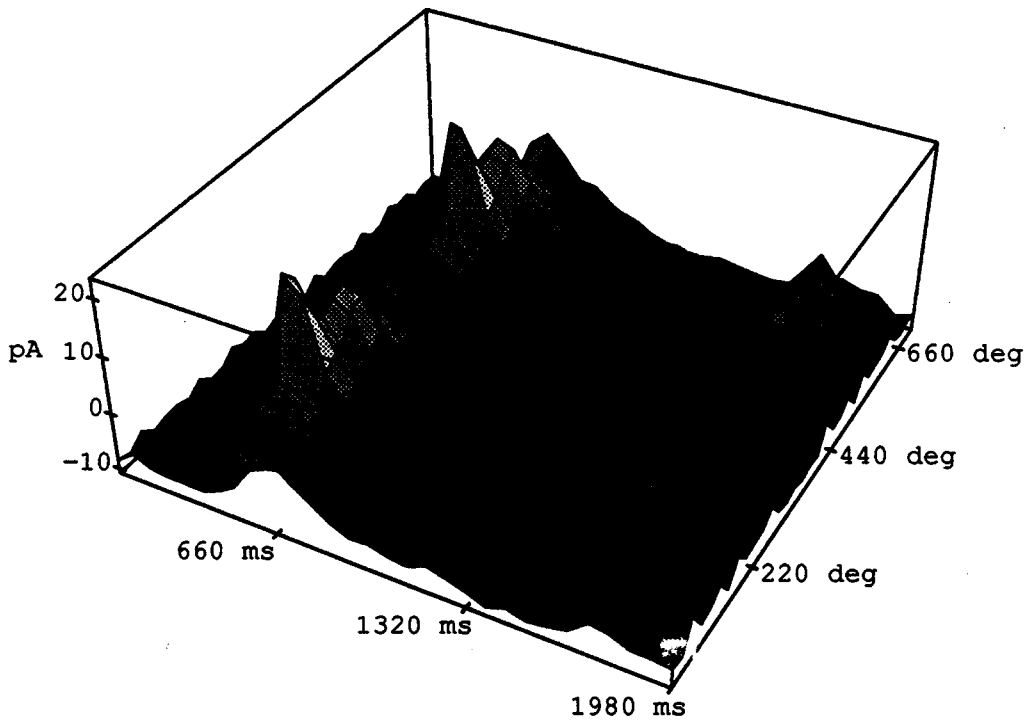

Figure 3.10: Perspective plot of DS responses to moving grating under voltage clamp for cell A56, taken 48 minutes after whole-cell access (average of 2 trials). Stimulus parameters identical to those used for Figure 3.8. Holding potential = −35mV. The lack of a negative phase (relative to the holding current) in this plot of the inverted clamp current suggests that any inhibition activated by the gratings occur in phase with the excitation, independent of orientation. This observation, along with the the fact that the total clamp current is DS suggests that either excitation or inhibition or both types of synaptic input is already DS.

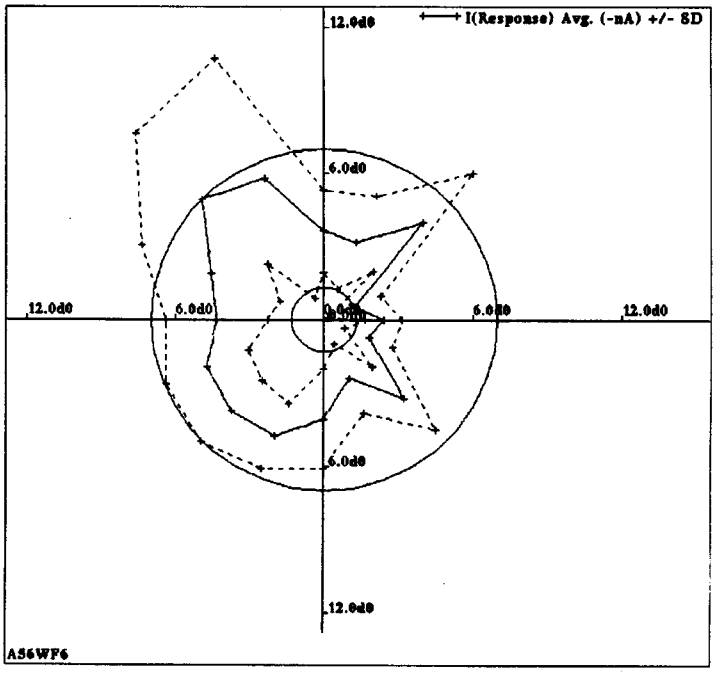

Figure 3.11: Polar plot of average $(I_{holding} - I_{clamp}) \pm SD$ (pA) for waveforms whose averages are shown in in Figure 3.10 (A56WF6). As for the A56WF4 data shown in Figure 3.8, $\theta_P = 157.5°$, but there is no statistically significant DS based on this parameter alone (presumably because of the low number of trials).

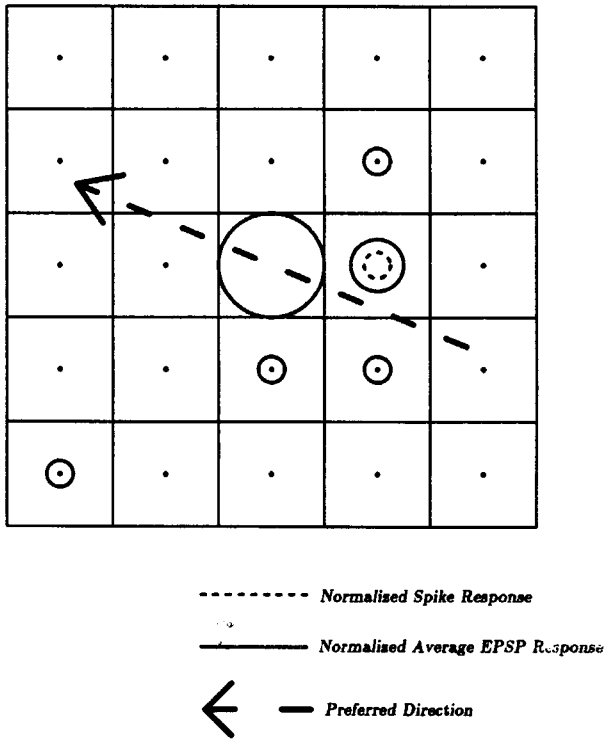

Figure 3.12: Spot mapped receptive field for cell A56 (protocols A56RF1 and A56RF2). Grid is 1000 by 1000 μm (centered on electrode tip), spot size 200 μm square, flashing at 1 hz. Spike results obtained extracellularly; EPSP results obtained within 5 minutes of whole-cell access. DS orientation from A56WF protocols presented in earlier figures. Circle diameters are proportional to normalized responses. Both spike and EPSP response was maximum at the center of the grid. Note that the DS orientation is orthogonal to the somewhat elongated RF, similar to results reported by [28]. Also, the EPSP receptive field is larger than the spike receptive field, as would be expected from a thresholding spike mechanism.

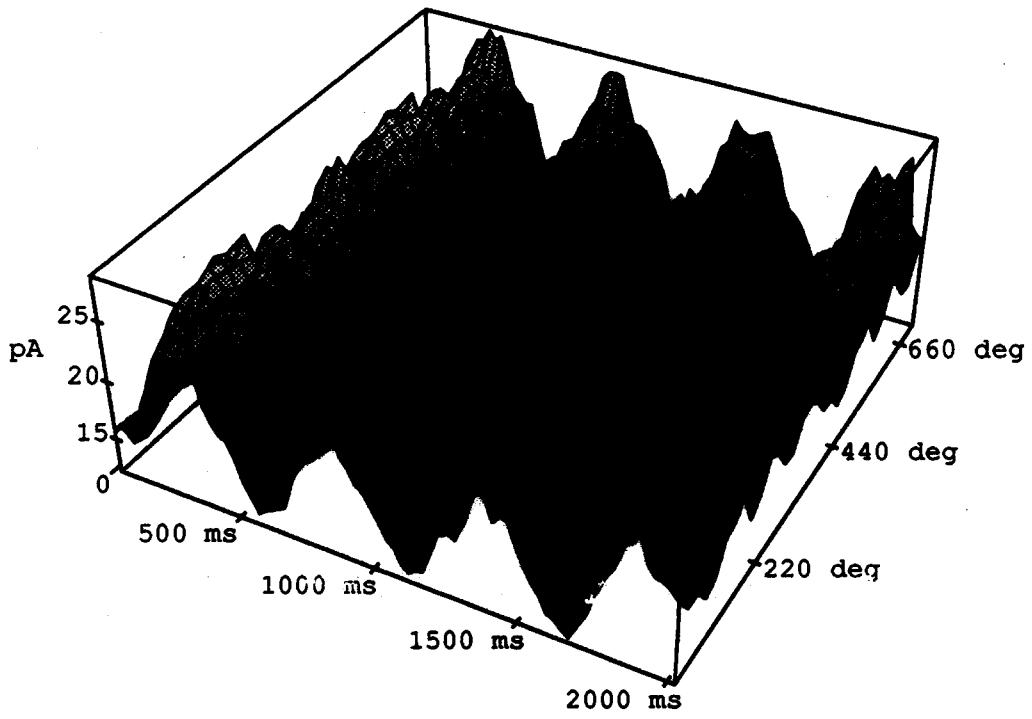

Figure 3.13: Perspective plot of non-DS responses to moving grating for comparison with DS perspective plots. Voltage clamp protocol for cell A81 (average of 4 trials), holding potential = −80mV. Grating aperture was 400 μm square, temporal frequency of 2 hz. This cell shows no dependence on the stimulus direction.

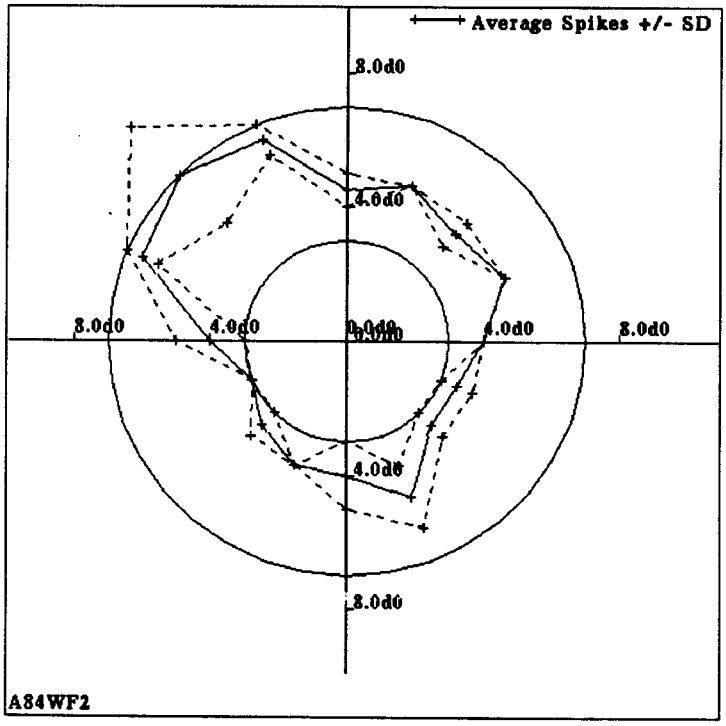

Figure 3.14: Polar plot of DS extracellular spike responses of ON/OFF ganglion cell A84 to a moving grating (average of 2 trials per orientation, 16 orientations). Grating aperture was 300μm square, temporal frequency of 2 hz. DS statistics of average spike response was $\theta_P = 112.5°$, $DI_{sum} = 0.2$ ($p < 0.05$).

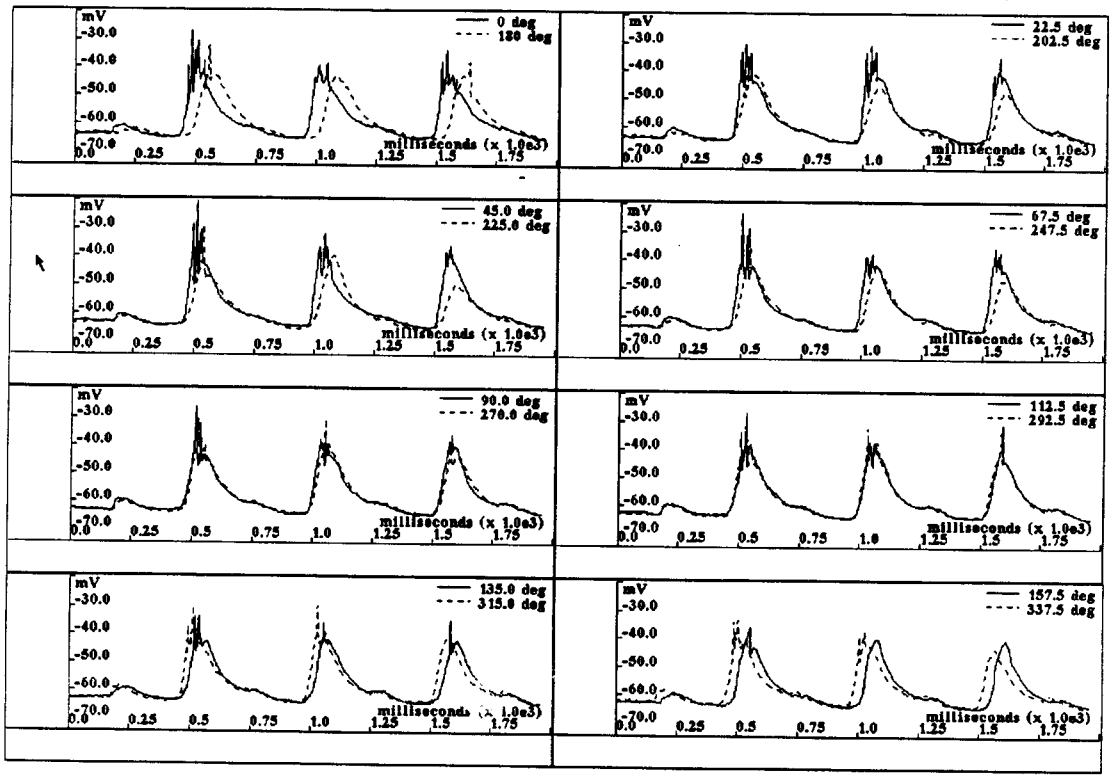

Figure 3.15: DS responses to moving gratings under current clamp for ON/OFF ganglion cell A84 (protocol A84WF3). Each waveform is the average of 4 trials. The grating had a 200 μm square aperture, a temporal frequency of 2 hz and a spatial period of 800μm. In this protocol, $\theta_P = 45°$, $DI_{sum} = 0.7$ ($p < 0.05$) (spike count). This recording was made 9 minutes after whole-cell access. Note that the ON response is much weaker than the OFF response under current clamp, but that the ON EPSP is still slightly directional.

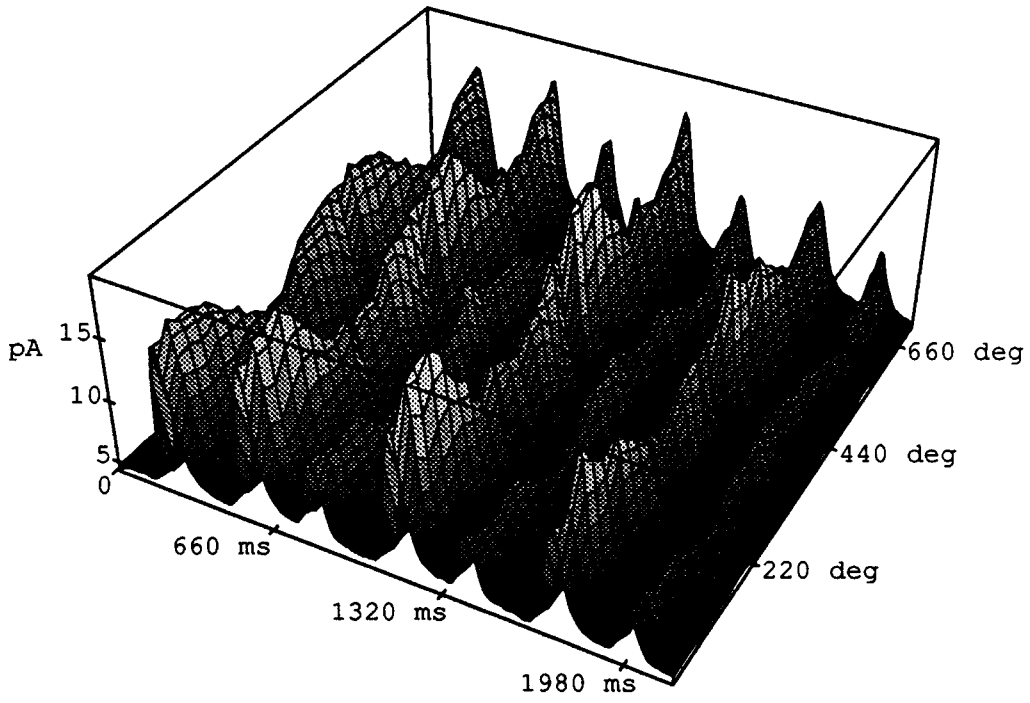

Figure 3.16: Perspective plot of response to moving grating under voltage clamp for cell A84, taken 30 minutes after whole-cell access. Holding potential = −80mV (average of 4 trials), suggesting that excitatory input to this cell has a large DS component. Grating aperture was 200μm square, temporal frequency of 2 hz. The 2nd harmonic from the ON/OFF cell is clearly seen in this motion response, and the ON response is relatively larger than that seen in Figure 3.15, possibly because the voltage clamp reduces the contribution of inhibition, and the inhibition may be more blocked by the lack of ATP at this later recording time. Also, the ON response adapts more than the OFF response, which in turn has a stronger directional dependence over time. The shift in preferred direction between this figure and Figure 3.14 (here, $\theta_P = 22.5°$, $DI_{sum} = 0.12$ ($p < 0.05$)) might be accounted for by a shift in the aperture location (see Figure 3.18), although the statistics of a broad directional tuning may also account for an apparent shift.

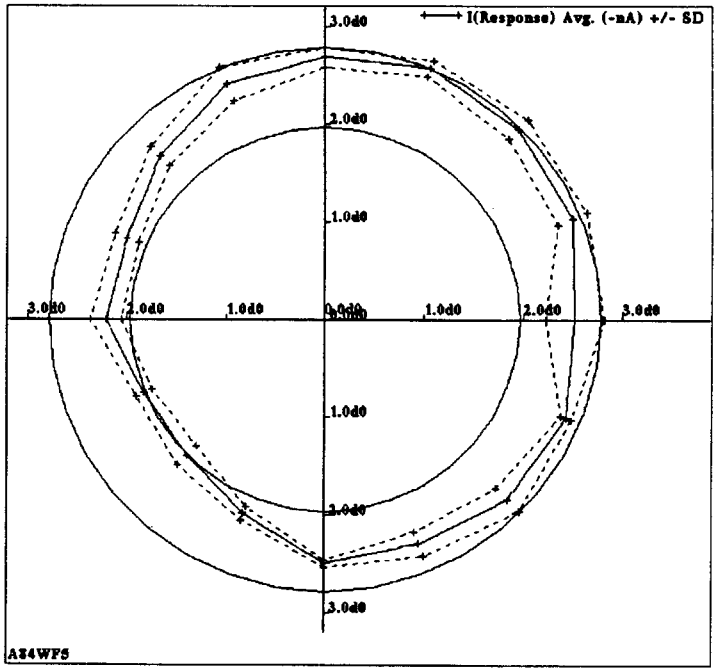

Figure 3.17: Polar plot of average $(I_{holding} - I_{clamp}) \pm SD$ (pA) for waveforms whose averages are shown in in Figure 3.16 (A84WF5).

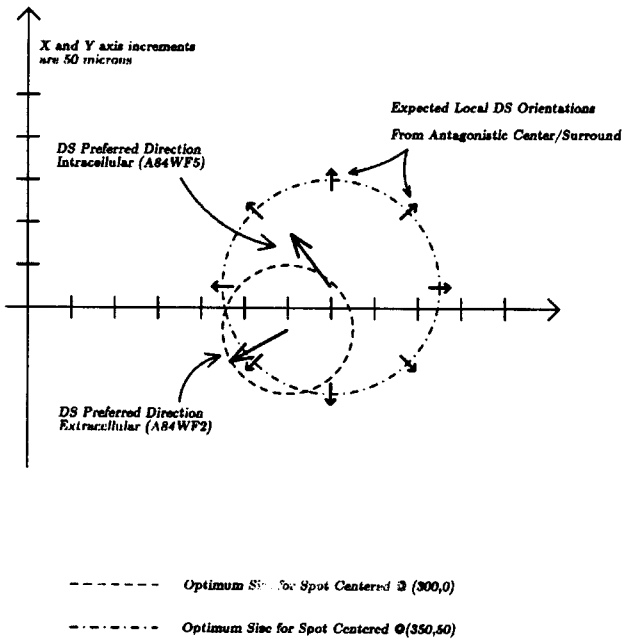

Figure 3.18: Extracellular determination of DS properties for cell A84 were done with reference to an initial estimate (by eye) of the receptive field center of (x =300,y =0), units in μm, relative to the electrode tip. Subsequent and more careful intracellular receptive field measurements moved the receptive field center to (x =350,y =50). A contribution of asymmetric activation of the symmetric inhibitory surround in the extracellular DS measurements, with the DS properties of correctly centered stimuli can account for the shift in θ_P between protocols for this cell. However, since the extracellular θ_P is close to that predicted by the center/surround DS artifact, it is possible that this DS is purely due to center/surround mechanisms.

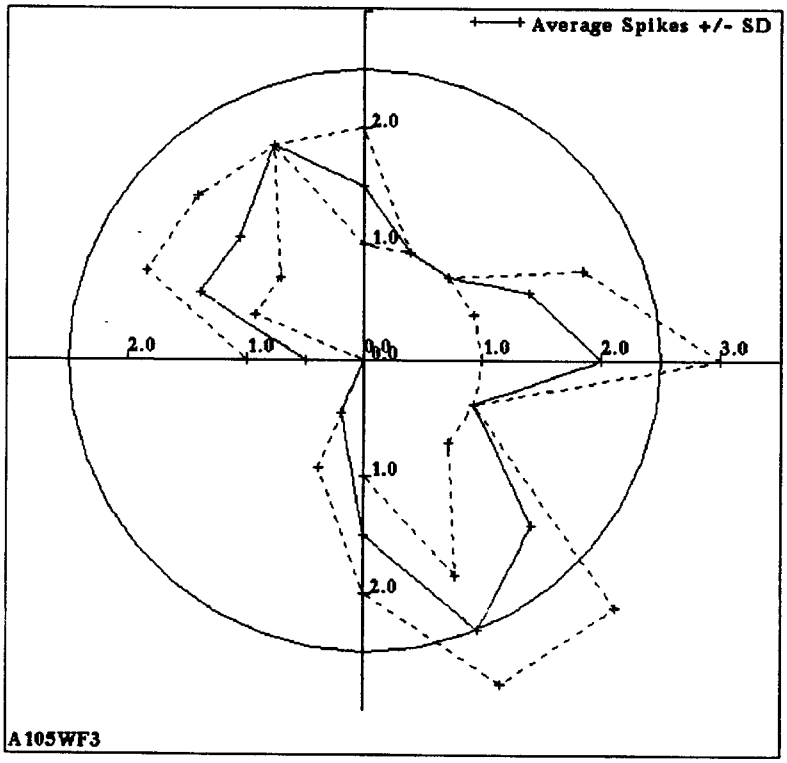

Figure 3.19: Polar plot of DS intracellular spike response (with SD) of ON/OFF cell A105 to a moving spot taken after 5 minutes of whole-cell access. Spot is 200 μm square, moving at 4 μm/msec, with a path length of 1200μm. Average of 2 trials per orientation, 16 orientations. The DS statistics on this protocol give $\theta_P = 45°$, $DI_{sum} = 0.47$ ($p < 0.05$). Although the strongest responses are along the 112.5/292.5° axis (showing a strong orientation selectivity), the most statistically significant radial asymmetry is towards 45 degrees.

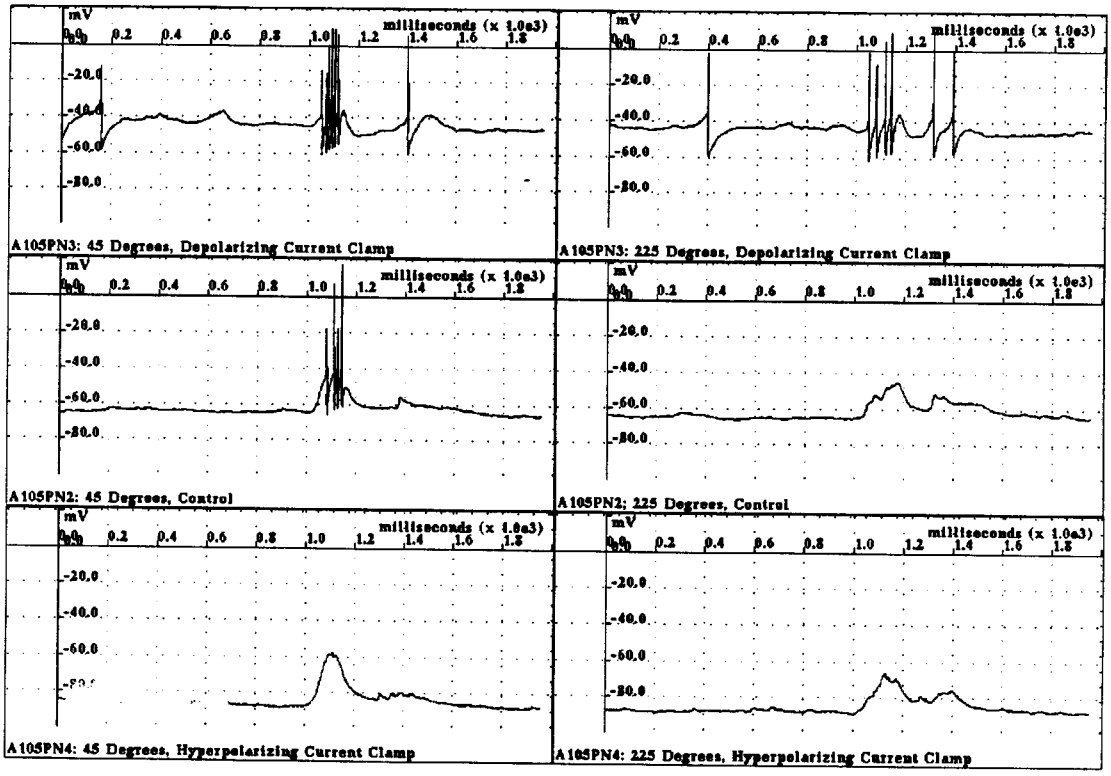

Figure 3.20: Single trial DS responses of cell A105 to moving spots, 7 minutes after whole-cell access, with positive, 0, and negative holding currents (protocols A105PN2-4). Spot stimulus is same as Figure 3.19, except that orientation is restricted along the 45/225° axis. Spot motion is timed so that the spot passes over the center of the receptive field at about 1000ms. In this cell the preferred orientation of 45° is independent of the holding current. Also, there is little evidence for IPSPs in these traces, suggesting that the directionality does not depend on ganglion cell inhibition.

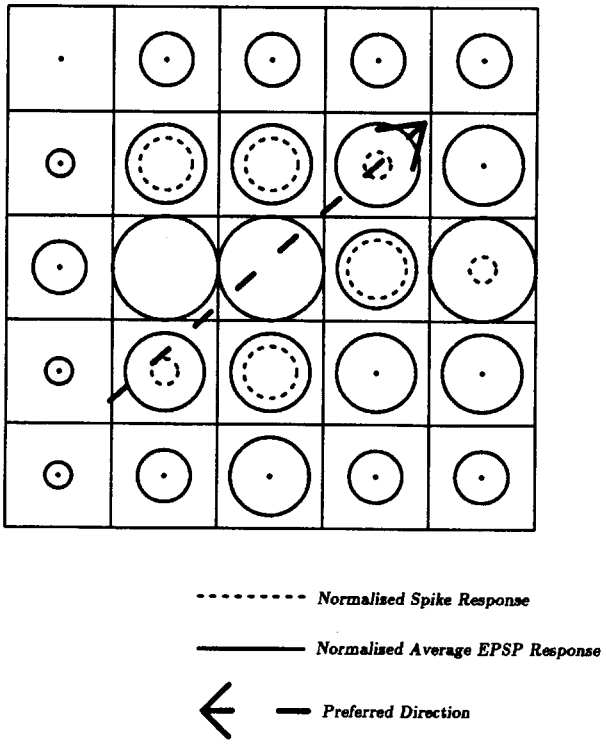

Figure 3.21: Spot mapped receptive field for cell A105 (protocol A105RF2). Grid is 500 by 500 μm (center at (-100 μm, 300 μm) relative to electrode tip), spot size 200 μm square, flashing at 1 hz, responses recorded 17 minutes after whole-cell access. DS orientation from A105WF protocols presented in earlier figures.

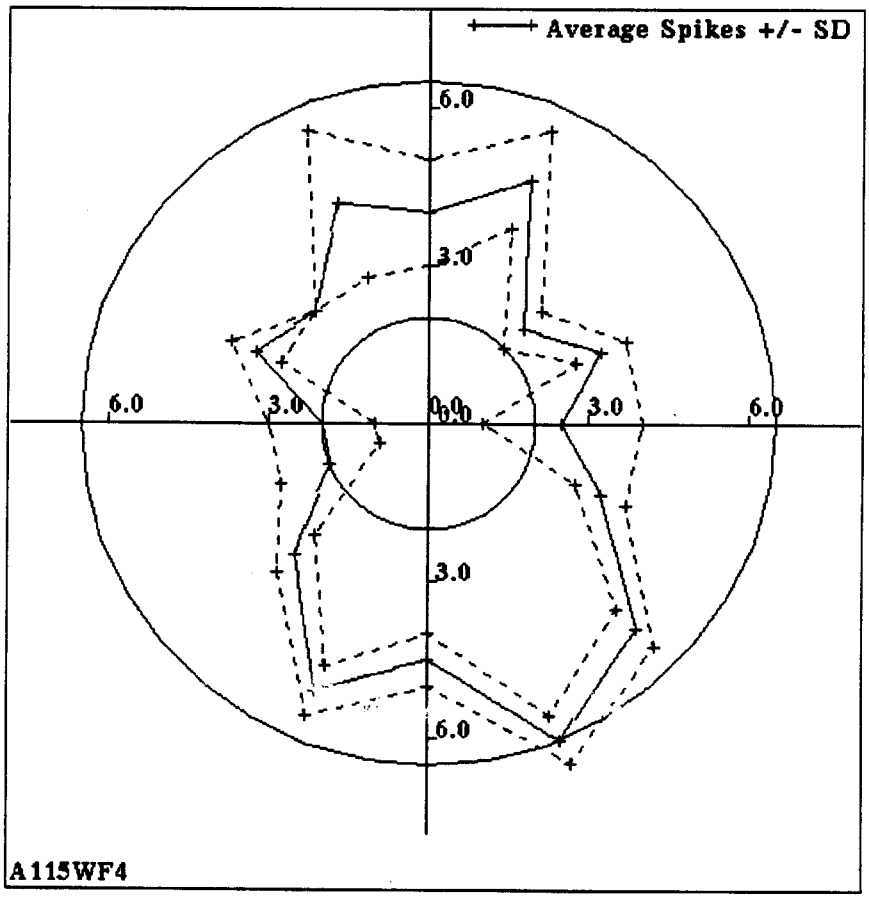

Figure 3.22: Polar plot of DS extracellular spike response (with SD) of ON cell A115 to a moving spot. Spot is 200μm square, moving at 2 μm/msec, with a path length of 1000μm. Average of 2 trials per orientation, 16 orientations. DS statistics give $\theta_P = 270°$, $DI_{sum} = 0.15$ ($p < 0.05$).

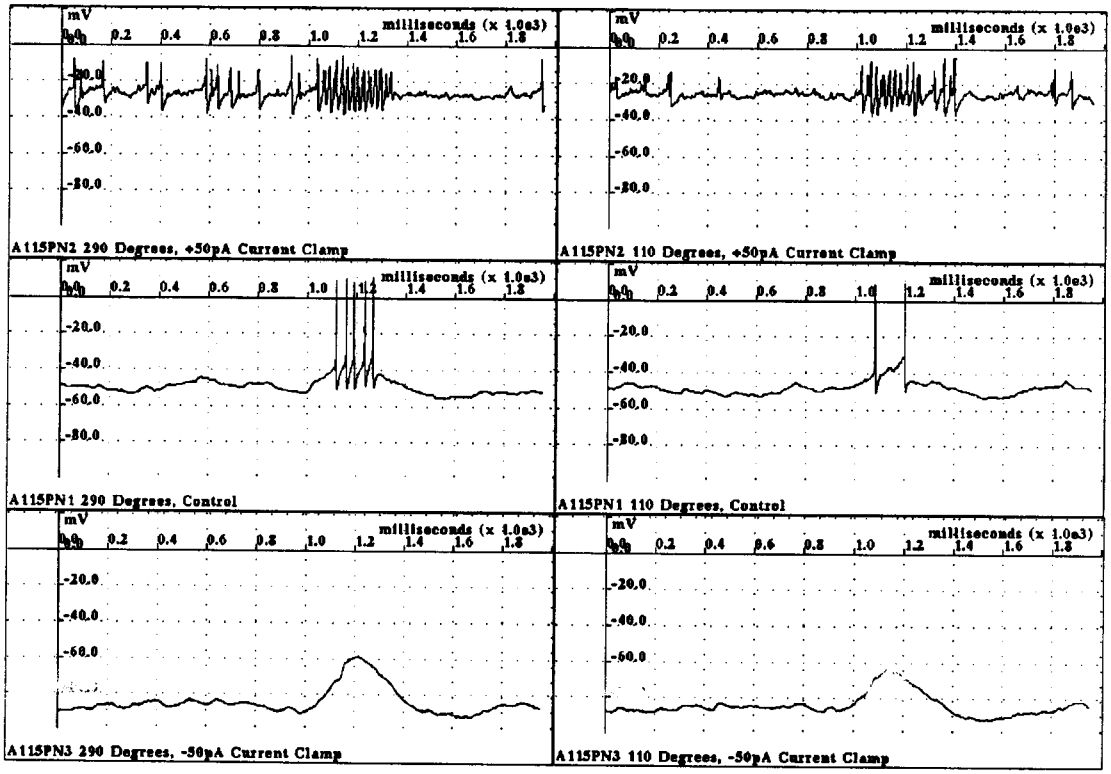

Figure 3.23: Single trial DS responses of cell A115 to moving spots, immediately after whole-cell access, with positive, 0, and negative holding currents (protocols A115PN1-3). Spot stimulus is same as Figure 3.22, except that orientation is restricted along the 290/110° axis (timing as in Figure 3.20). Similar to cell A105, the preferred orientation of 290° is independent of the holding current, and there is little evidence for IPSPs involvement in the DS response.

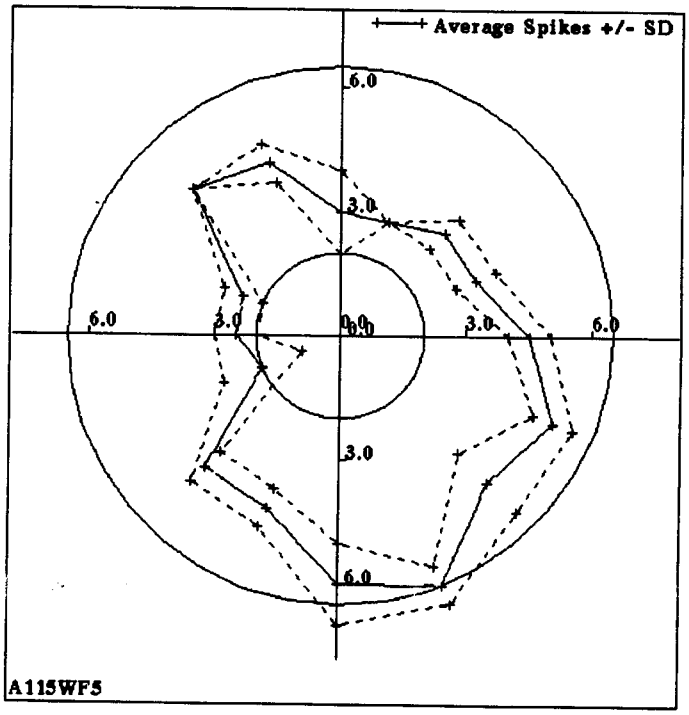

Figure 3.24: Polar plot of DS intracellular spike response ($\pm SD$) of cell A115 for same protocol as Figure 3.22 (A115WF5). This protocol was taken immediately after the P/N runs shown in Figure 3.23 (within 10 minutes from start of whole-cell access). The DS statistics for this protocol give $\theta_P = 315°$, $DI_{sum} = 0.22$ ($p < 0.05$).

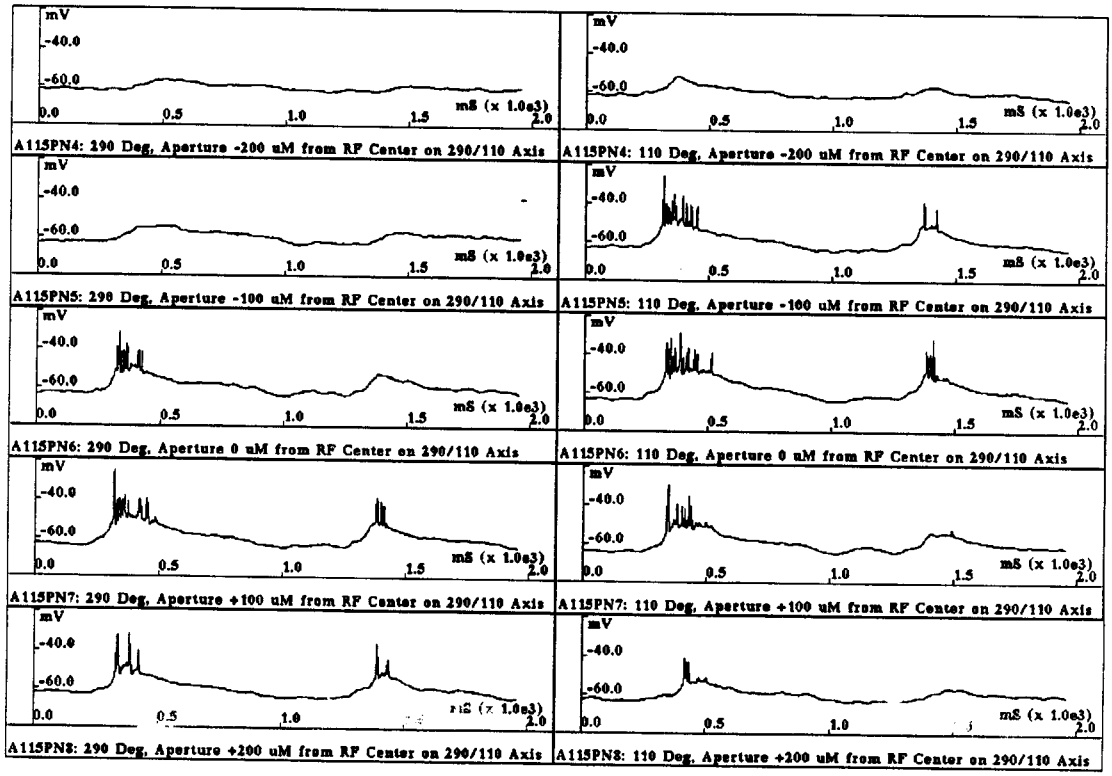

Figure 3.25: Responses of cell A115 to moving gratings, 31 minutes after whole-cell access, to investigate subunit properties. Each waveform is the average of 2 trials, with each trial consisting of 2 full cycles of the grating. Grating apertures are 200μm square, temporal frequency 1 hz, and orientation of the gratings was restricted along the 290/110° axis. Aperture centers were placed at 100μm steps along the 290/110° axis, as noted in the figure. In this series local DS center/surround responses are seen, but the DS response to long trajectory stimuli (such as in Figure 3.23) cannot be predicted from the localized responses, e.g. there is no consistent DS subunit response.

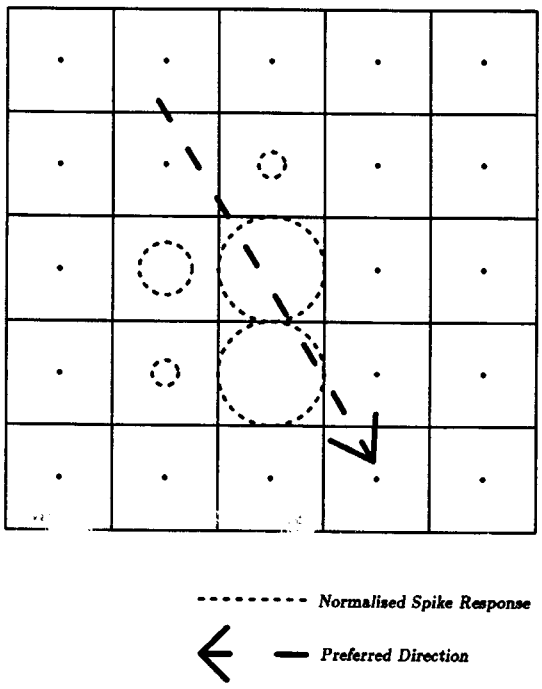

Figure 3.26: Spot mapped receptive field for cell A115 (protocol A115RF1). Grid is 500 by 500 μm (center at (100 μm, -100 μm) relative to electrode tip), spot size 100 μm square, flashing at 1 hz, extracellular spike response. DS orientation from A115WF protocols presented in earlier figures.

Chapter 4

A Model of Retinal Directional Selectivity

Models for retinal directional selectivity have proposed various locations for the asymmetric path, delay elements, and non-linear interactions required for this computation, as we discussed in Chapter 2. The experimental results of the previous chapter add some constraints, namely that all these elements must occur prior to the DS ganglion cell, which, in turn, apparently receives DS excitatory input.

We now present a pre-ganglionic model for DS which is morphometricly similar to Vaney's ([66], [64]) in that the lateral pathway is via individual branches of amacrine cells with tip outputs [12]. We find as well that given a plausible set of constraints on *a)* the distribution and biophysics of synaptic input and output on the branches and *b)* the intrinsic cable properties, the outputs of this pathway are at least DD and normally are DS. Thus, both the lateral path and the non-linear interaction underlying the DS computation occur on the same substrate.

4.1 Oriented Amacrine Cell Branches with Directionally Selective Outputs

The crucial DS element in this circuit is shown in Figure 4.1, and the anatomy of the asymmetric pathways and the target DS ganglion cell is shown in Figures 4.2 and 4.3. We suggest, as Vaney, that DS subunits arise from multiple oriented amacrine cell dendritic tips connecting to the DS ganglion cell. In the context of retinal DS, the directional properties of a

cable with distributed synaptic conductance input has also been described by Grzywacz and Amthor ([29]). Likewise, Koch, Poggio and Torre ([40], Figure 9a) suggested a similar (ganglionic) arrangement of locally symmetric excitatory and delayed inhibitory inputs along the branch of a putative asymmetric DS ganglion cell.

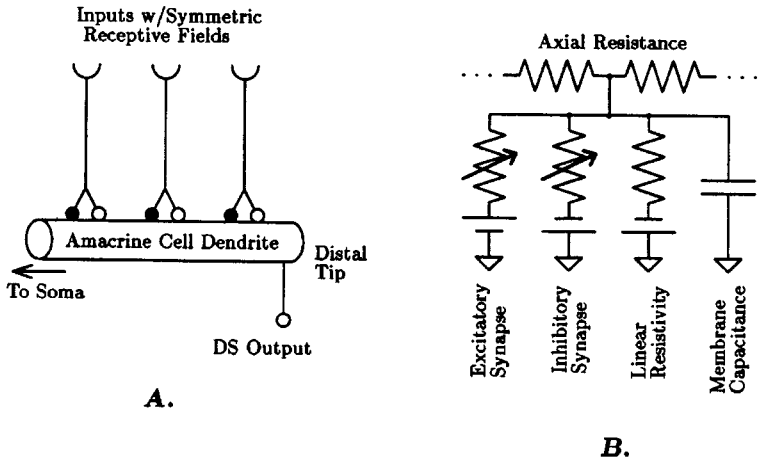

Figure 4.1: (A) Structure of cable model discussed here. In this model the time element necessary for DS is provided by the inherent kinetics of the input synapses (most importantly by the slower time course of the inhibition), and the nonlinearity also necessary for DS by the distributed inhibitory synaptic conductance. Under certain conditions the location-dependent delay (phase shift) provided by the cable membrane time constant (τ_m), and an output nonlinearity, may also be relevant (Sections 4.2.4 and 4.3.2). The preferred response of the tip output above is for motion to the right, for the model version analyzed in this chapter. (B) Equivalent circuit for a section of the dendrite cable, including the axial resistance, the linear resting membrane resistance and capacitance, and the synaptic inputs. Directionality of the distal tip output arises because in the null direction the slower inhibition shunts subsequent excitatory input as the stimulus moves away from the tip. In the preferred direction the inhibition is much less effective at attenuating the excitation, due to the on-the-path condition (see text).

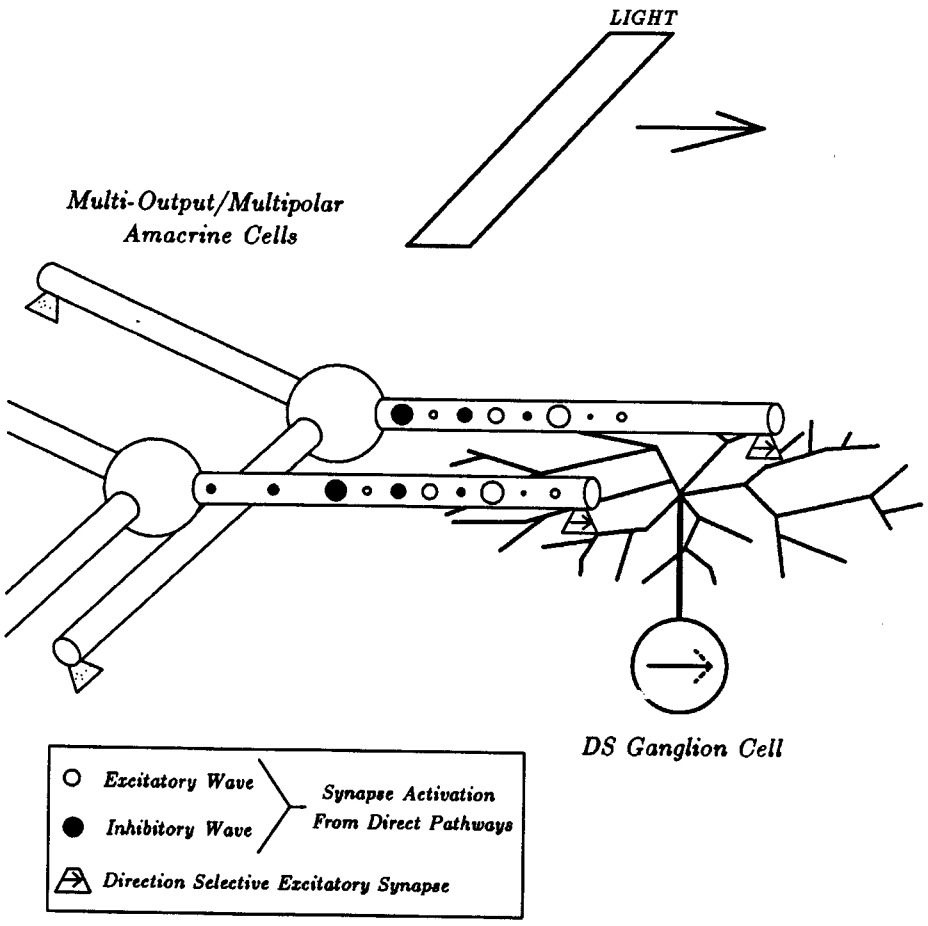

Figure 4.2: Relationship between the asymmetric pathways in the cable model and the target DS ganglion cell, and pattern of activation for light moving in the preferred direction. Input onto the asymmetric amacrine cell dendritic paths are from symmetric (direct) pathways (either via bipolar cells or amacrine cells). The DS ganglion cell also receives direct input from bipolar and amacrine cells (not shown). Note that the wave of inhibition lags behind the wave of excitation. Other tips of the amacrine cell with different orientations may connect to other DS ganglion cells, since the tip responses are essentially independent of one another.

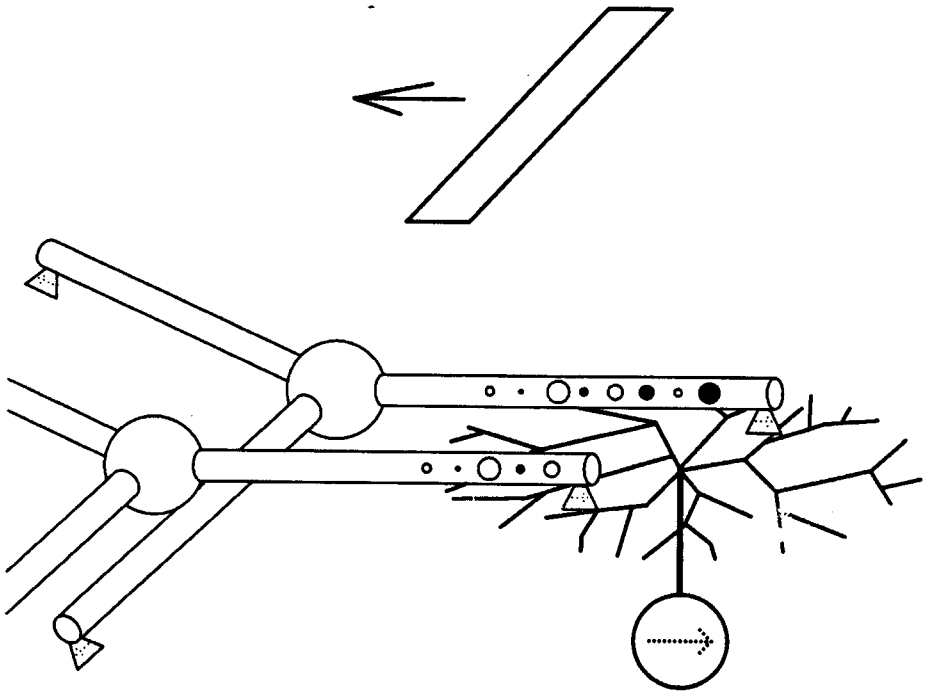

Figure 4.3: Pattern of activation for light moving in the null direction. In this case, after the light has passed over the amacrine cell dendrite tips there is a zone of activated inhibition between the tips and the activated excitation.

4.1.1 Start by Finding the Asymmetry

Histological data from retina does not immediately suggest the spatial asymmetry required for directional selectivity, as mentioned in Chapter 2. However, if we consider putative outputs on the dendritic tips of amacrine cells, the IPL becomes full of asymmetries, since for a large number of amacrine cells the tips are displaced with respect to the entire tree (see Section 5.7). This interpretation deviates from the assumption of classical neuronal polarity: input onto the dendritic tree, conducted proximally and integrated by the soma membrane, cell output via the somatic axon. Some retinal neurons challenge this dogma, and the distinction of dendrite versus axon becomes blurred. Many retinal cells do not have an axon at all *per se*, and single cell processes may have both input and output.

As Vaney pointed out, detailed studies of starburst amacrine cell dendrites support this potential asymmetry for the rabbit retina ([26], [25], [65], [62]). Small swellings in the outer third of the dendritic tree have been described, and electron micrographs show that synapses with ganglion cells occur in the swellings' zone [14]. In contrast, the general distribution of synaptic inputs along the dendrites is apparently uniform[1].

It should be emphasized that the critical asymmetry in this model requires inputs all over the amacrine cell dendrite branch and outputs near the tip. There is no restriction on outputs elsewhere on the branch, however, and the most general version of the model would have uniform inputs and outputs over the entire amacrine cell dendritic tree. On the other hand, only a subset of those outputs will have strong DS properties, and an assumption of the model is that a given target DS ganglion cell will receive at least some of the outputs from this subset. This problem will be addressed in Section 5.5.

4.1.2 Add Location Dependence

The morphometric asymmetry is necessary for directional selectivity, but not sufficient. If the dendrite branch is isopotential then there is no location

[1]It should be pointed out that there is conflicting support for the starburst amacrine cell specifically in the DS circuit for rabbit. For example Linn and Massey [43] suggest that cholinergic release from starburst cells is not inhibited directly by GABA, which is contrary to the model prediction. However, other amacrine cells may have the necessary input/output relationship. Later we shall show simulations of a cell whose morphometry is based on the starburst cell; despite the evidence against the starburst cell specifically, we feel that the conclusions from this tree geometry are applicable to other amacrine cells.

dependence of branch input, precluding any sort of motion selectivity, much less directional selectivity. When we add the intracellular resistance of the cable, however, then location dependence results.

4.1.3 Directional Dependence for the Linear Case

Let us now examine the response of the cable tip to moving inputs. We begin with the simplest case: distributed excitatory synaptic input onto the (linear) cable. If the synapses are modelled as current sources, e.g. the excitatory synapse injects a depolarizing current, then the tip response can be obtained by the appropriate superposition of responses to individual inputs. The resulting waveforms for motion in the two directions will have different shapes, but, since the system is linear, equal areas.

As simulations by Rall demonstrated implicitly ([56]), we now have in the dendrite cable the prerequisites – location dependency and asymmetry – for DD (but not DS). Accentuating the difference is the location–dependent delay of the cable (due to the cable time constant). This delay tends to increase the output amplitude for motion towards the tip; the EPSPs arriving at the tip are more correlated since the cable delay (phase shift) counters the motion delay. Otherwise the two waveforms would simply be reversed in time. We shall return to this phenomena later in the simulations section (Section 4.3.2).

Now ... me that at each point on the cable there is a paired excitatory/inhibitory input, with the inhibitory kinetics slower than that of the excitation[2]. Again, if the inhibitory synapse is modelled as a hyperpolarizing current source the (linear) responses for the two directions will have equal area. The DD response holds, still without DS.

4.1.4 Synaptic Nonlinearities and Cable Directionality

Synaptic input, however, is more accurately modelled by a conductance change in series with a battery. The circuit is now a nonlinear one: the variable conductance of the inputs means that motion responses cannot be derived from the superposition of a sequence of point responses. As a result the integral of the response for the two directions is generally *not* conserved.

The effect of the inhibitory input is particularly important on the directionality of the cable tip response. Assuming that the reversal potential for

[2]Note that if the excitatory and inhibitory kinetics were identical, then synapses at the same location could be lumped together as one.

the inhibition is close to the cell's resting potential, then the main effect of the inhibition will be to *shunt* locally any excitatory current to the extracellular space. The effect of the shunt on the tip response strongly depends on the relative location of the excitatory and inhibitory inputs with respect to the output. As Rall ([56]) and Koch et al. ([41]) showed, inhibition is most effective when it is *on the path*, that is interposed between excitation and the output. Conversely, if the excitation is closer to the output, then the inhibitory shunting is much less effective (Figure 4.4).

The inhibitory shunting now supplies the necessary nonlinearity for the DS response. This prediction is in concert with the experimental evidence as to the importance of inhibitory mechanisms for DS, and with the evidence that inhibitory shunting might mediate DS in rabbit ([3]). We also note that while the efficacy of the inhibitory synapse with respect to DS is mainly due to its shunting component, it is also true that the precise value for the inhibition E_{rev} is not crucial (as long as the E_{rev} is in the neighborhood of E_{rest}). Locality of synaptic interaction is strongest when the inhibitory $E_{rev} = E_{rest}$ (silent inhibition), but this is not relevant for the geometry of the model presented here.

4.1.5 Considering Tip Output Nonlinearity, Facilitation, and the Sign of the Output

Inhibition onto the ca... suffices to make the towards-tip response larger than the opposite direction, so a linear output function at the tip would preserve the distinction. It is more likely, though, that the output synapse has a threshold. However, the resulting supralinear region will only amplify the DS distinction. Saturation of the output, on the other hand, may have other consequences (Section 4.2.4).

At first glance, the experimental evidence of preferred–direction facilitation data mentioned earlier supports placing a facilitatory mechanism on the DS pathway, as opposed to only a symmetric location (e.g. intrinsic to the ganglion cell spike mechanism). Further evidence for a DS path location for the facilitatory mechanism in rabbit ON/OFF DS cells has been reported by Grzywacz and Amthor ([31]), including ON and OFF segregation of facilitation, no correlation between facilitation strength and response strength as a function of receptive field position, and no correlation between time courses of facilitation and response. These results could be accounted for by various mechanisms located at the amacrine cell tip. For example, facilitatory mechanisms intrinsic to the synaptic output might suffice. Likewise, we may

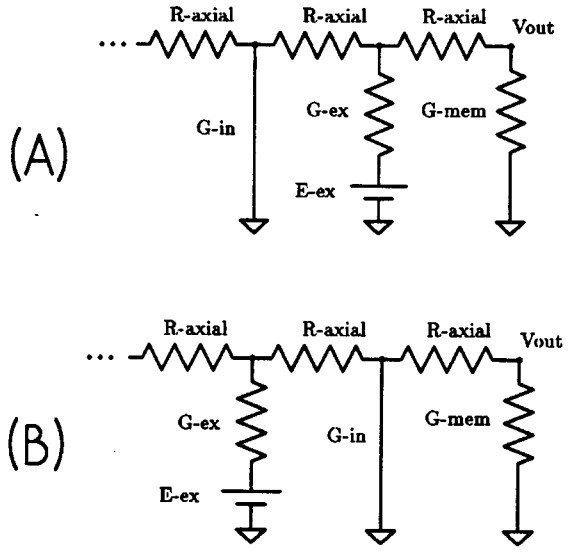

Figure 4.4: The effect of inhibition on tip output is dependent on the relative positions of the excitation and inhibition with respect to the output. To illustrate, we use an extreme case in which the inhibitory battery is equal to the resting potential, and the activated inhibitory conductance is infinite. In (A) the excitatory input is closer to the tip than the inhibitory input. Although the membrane potential at the site of inhibition is clamped to the resting potential (short-circuited), the axial resistance of the cable partially isolates the excitatory location, and the tip (V_{out}) is depolarized. In (B) the interposed inhibitory input clamps the cable between the excitatory input and the output to the resting potential, so that the output stays at rest. Adding membrane capacitance, a finite conductance to the activated inhibitory synapse, or making the inhibitory reversal potential not exactly equal to the resting potential does not change the basic interaction. However, a non-zero R_{axial} *is* crucial.

consider a voltage and time–dependent K^+ channel at the tip which is normally open at rest but slowly inactivates with depolarization, similar to the I_D channel identified in hippocampal pyramidal cells (see review by Storm [61]). The characteristics of this channel would cause the tip output to be "primed" by distant cable input, such that subsequent excitation near the tip (for motion in the preferred direction) would be unopposed by the now–inactivated K^+ shunt. In Section 4.3.3 we show simulations of an apparent motion protocol that demonstrates this particular facilitatory mechanism.

Two versions of this model include either that the amacrine DS output forms an excitatory connection with a DS ganglion cell, or the connection is inhibitory. It is also possible to include plausible voltage and time dependent nonlinearities in the cable so that the preferred direction for the branch output is *away* from the tip. Also, the tip output may pass through sign–inverting bipolar cells or amacrine cells before the ganglion cell.

While any combination of the above polarities will yield a ganglion cell DS response, the fact that directional responses have been recorded in the absence of GABAergic inhibition (Section 2.3.1) suggests that the DS pathway has an excitatory component at every junction. Further, the data described in Chapter 3, in particular with local block of GABAergic inhibitory input, supports the excitatory connectivity version. Also, simulations of model cells with likely membrane parameters favor the preferred–towards–tip orientation for the cable output (Section 4.3 and unpublished data).

4.2 Predictions of the Model

We now consider testable predictions, namely that for somatic recordings of amacrine and target ganglion cells.

4.2.1 Directionally Selective Somatic Recordings?

With respect to amacrine cells, the model predicts that moving stimuli centered on the (somatic) receptive field would not elicit a directionality, assuming a symmetrical dendritic tree. If either the stimuli or the dendritic tree was asymmetric with respect to the soma, then a directional response would result, perhaps similar to the preganglionic DS/DD recordings of DeVoe et. al. ([23]). While this result supports the proposed mechanism for DS, it does not link the mechanism to an identified DS ganglion cell.

From the point of view of DS ganglion cell, the model predicts that the input waveforms to the cell are themselves DS; any ganglionic computational

mechanisms will be inherently symmetric and serve only to refine the P/N response properties. This result is in contrast with the ganglionic model class, in which the inputs are not DS by themselves.

4.2.2 Dependence of Directional Selectivity on Ganglion Cell Membrane Potential

Differences in P/N EPSPs are predicted by the ganglionic model, but since the differences arise from ganglionic interaction of conductances with different reversal potentials, this model predicts that the relationship between the preferred and null EPSPs will depend on the membrane potential.

For example, let us consider the ganglionic AND-NOT circuit: Null direction response reflects a temporal overlap of the excitatory input with inhibitory (mainly shunting) input at the ganglion cell. Since the inhibitory reversal potential might be near the rest potential, there would be little negative portions in either the preferred or null response. A negative portion would result if the membrane potential is artificially raised by injecting current. The "unmasked" IPSP would be expected to be more correlated with the control EPSP in the null direction as compared to the preferred direction (e.g. [47]). If the ganglion cell was hyperpolarized by the electrode, the "unmasked" inhibitory input would now contribute a component to the EPSP. With sufficient hyper/depolarization the *amplitude* of the null response could become greater than that of the preferred response (see Figures 2.1 and 2.2).

This result is in clear distinction to a pre–ganglionic model. The single reversal potential of the ganglion cell DS inputs imply that the ratio of the preferred and null EPSPs is *independent* of the membrane potential: Manipulating the membrane potential will not reverse the P/N axis.

4.2.3 Comparing Total Synaptic Input for the Preferred/Null Responses

The above result is related to measuring the somatic input conductance, $G_{In}(S,t)$, of the ganglion cell during a motion stimulus $S(x,t)$. For a lumped cell approximation and no voltage-dependent membrane, predictions about $G_{In}(S,t)$ are simple. In the ganglionic model, the only difference in the inputs for the preferred versus null responses is in their timing. Thus the model predicts:

$$\int G_{In}(S(x,t)) = \int G_{In}(S(-x,t))$$

where $S(x,t)$ and $S(-x,t)$ are stimuli moving in the preferred and null directions, respectively. On the other hand, for the pre–ganglionic model there is more synaptic input for one direction versus the other; therefore (assuming the lumped cell without voltage dependencies):

$$\int G_{In}(S(x,t)) > \int G_{In}(S(-x,t))$$

for a pre–ganglionic excitatory DS input model, and

$$\int G_{In}(S(x,t)) < \int G_{In}(S(-x,t))$$

for a pre–ganglionic inhibitory DS input model. An advantage of comparing the integrals of G_{In} for the preferred and null stimuli is that the effect of the membrane capacitance may be ignored. It can be shown that under some constraints on the ganglion cell and the experimental protocol, similar relationships are testable even with distributed inputs on dendritic trees and voltage dependent membrane.

4.2.4 Dynamic Range of Cable Mechanisms: Saturation and Reversal of Directional Selectivity

Real biophysical mechanisms saturate, e.g. a supralinear transfer function will not stay supralinear for unbounded inputs. We now consider possible implications of saturation on the performance of the model.

Saturation of an input synaptic conductance onto the cable will not change the basic distinctions between the preferred and null waveforms, since this saturation is independent of stimulus direction. Saturation (strictly speaking, a sublinear region) of the output nonlinearity can have quite different effects: for strong enough cable excitation the null waveform, with its greater temporal support (due to cable τ_m spreading out the synaptic potentials), will eventually yield a final output that is equal to the preferred output, despite the larger amplitude of the preferred waveform. Increasing excitation further could cause a *reversal* of the P/N orientation, after the output nonlinearity. This might be observed, for example, with a stimulus contrast that is normally DS, but under conditions in which inhibition is reduced or blocked (e.g. with pharmacological manipulations). Whether DS would be entirely eliminated or reversed would be dependent on circuit and stimulus parameters.

This result is unique to models in which the DS asymmetry includes distributed excitatory input with relative delays along the P/N axis. Such

models been explored theoretically for the interpretation of DS reversal in fly ([54]), and in Section 4.3.2 we show simulations which demonstrate this effect.

4.3 Simulations of Morphometricly and Biophysically Detailed Amacrine Cell Models

To investigate neuronal properties which are pertinent to the cable model, we have run simulations of amacrine cells. The model parameters are as constrained as possible; morphometry is obtained from histological data in the literature, and membrane properties are either inferred from experimental data and/or supported by theoretical studies of other cells ([9]).

An important aspect of these simulations is that dynamic retinotopic stimuli may be used as input to the model circuit. Since the simulator maintains the 3-dimensional structure of the cells, it is straightforward to interpret model response to realistic arbitrary stimuli (Appendix C).

4.3.1 Simulations of Asymmetric Responses from Symmetric Cells

In Figures 4.5 through 4.7 we show a simulation of an amacrine cell whose morphometry is taken from a rabbit starburst amacrine cell ([62]). All membrane and cable properties are uniform, including specific capacitance (C_m), membrane resistivity (R_m), intracellular resistivity (R_i), excitatory synaptic density (G_{ex}), and inhibitory synaptic density (G_{in}). R_m and R_i are fixed at $100K\Omega\text{cm}^2$ and $200\Omega\text{cm}$ ([58]), respectively. C_m is set to 1.0 $\mu\text{F/cm}^2$ (τ_m = 100mS), G_{in} is set to $100\text{pS}/\mu\text{m}^2$, and G_{ex} to $1\text{pS}/\mu\text{m}^2$. The resting potential for the cell is -70mV. The reversal potentials for the excitatory and inhibitory synapses are 50mV and -70mV, respectively. No voltage–dependent membrane is included.

The synaptic transfer functions are fixed. The excitatory input response is given by the half-wave rectified convolution of the light stimulus by the difference of two alpha functions, $\alpha_\tau(t)$,

$$\alpha_\tau(t) = \frac{t}{\tau^2} e^{-t/\tau}$$

the first with a τ of 10 mS and the second with a τ of 60 mS. This transient response is typical of retinal ON response to a flashing stimulus. The inhibitory response is the half–wave rectified convolution of the light stimulus

with a single alpha function of unit area and τ = 100 mS. This sustained ON response approximates the time course for inhibition to various stimuli [2]. Adding an OFF component to the transfer functions does not change the motion–dependent behavior. For simplicity the spatial impulse response for both synapse types is $\delta(x, y)$, although the receptive field of candidate bipolar or amacrine cell outputs are on the order of tens to hundreds of microns wide. Since spatial properties derive from the successive convolution of each circuit element, minimizing the intrinsic spatial spread of the amacrine input yields an upper bound on overall spatial resolution of the DS dendrite structure.

The large value for R_m is consistent with values measured in our lab and others in various neurons using the whole cell patch technique (e.g. [19]). Synaptic conductance densities and kinetics are less constrained as far as the literature is concerned; the range of values we have chosen produce synaptic potentials which are consistent with available data.

In Figure 4.6 we show the response of the soma and a distal node to a bar moving across the entire field of the cell. The soma response is almost identical for opposite motions, while the tip response is highly DS. In Figure 4.7 we have plotted the total response of each dendritic tip of the cell, scaled by stimulus speed, as a function of angle off the soma, for a slit traveling across the entire breadth of the cell. Despite the overall symmetry of the cell, this functional is highly directional.

4.3.2 Parametric Simulations of Cable Mechanisms

In this section we present a series of simulations on a simple cell model (chosen to allow rapid parametric simulations) to illustrate how the different mechanisms in the dendrite cable interact. The basic structure of this model is a 1-dimensional symmetrical cell with two opposing unbranched processes (Figure 4.8). Cell membrane and synaptic parameters are identical to the simulated cell in Figure 4.5, except as follows: We shall vary C_m (1.0 and 1.0^{-5} μF/cm^2, or τ_m = 100ms and 0.001 ms)[3], and G_{in} (100, 10, 1, 0.1, and 0 pS/μm^2). The goal here is to see how directionality depends on the inhibitory input versus the intrinsic cable delay properties.

As before, the stimulus is a moving slit, 50μm wide, now with velocities of 0.5, 1, 2, 4, 8, and 16 μm/msec. The response waveforms from the righthand distal tip for rightward and leftward motion will be compared.

[3] A C_m of 0 μF/cm^2 was not possible due to the integration technique of the simulator.

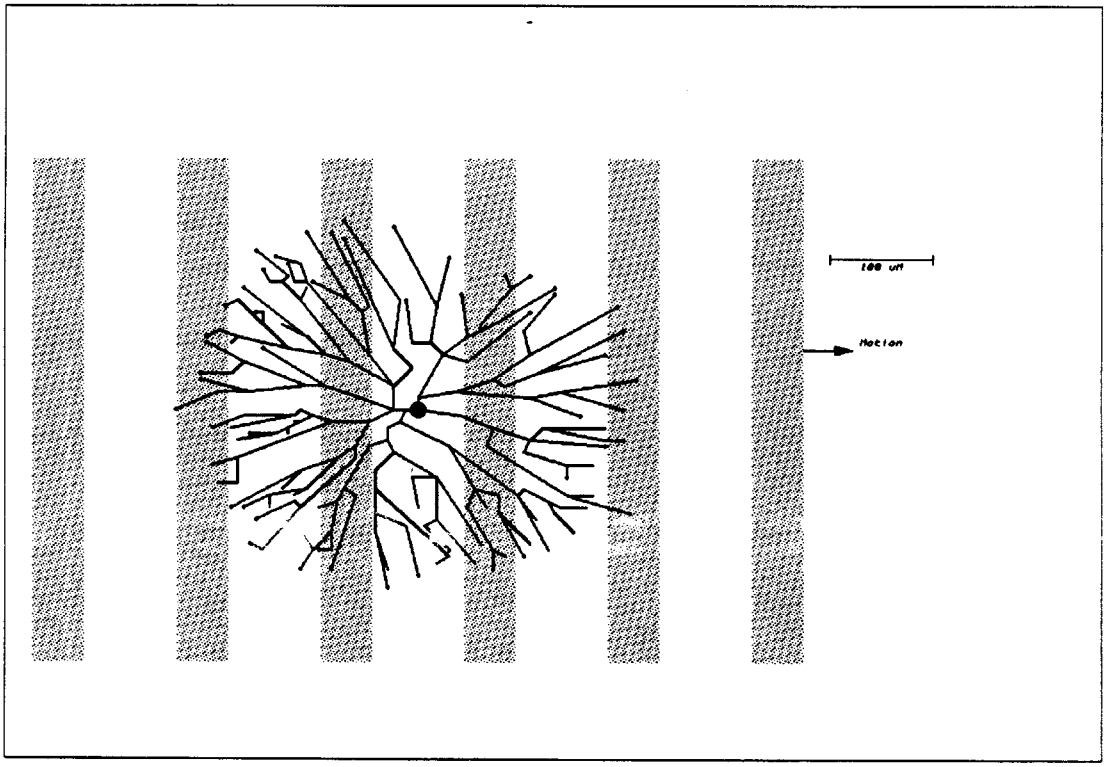

Figure 4.5: Simulations were done of a model cell based of the morphometry of a rabbit starburst amacrine cell, taken from Tauchi and Masland ([62]). Shown here is a flat mount view of cell, with snapshots of the stimulus slit trajectory. Node 32211 referred to in Figure 4.6 is the distal tip farthest to the right.

In particular, we shall compute a directional index (DI) (after [32]) for both the linear integral of the waveforms and the integral of the waveforms after being passed through a sigmoidal nonlinearity (representing synaptic transmission):

$$DI = \frac{\int f(V_P) - \int f(V_N)}{\int f(V_P) + \int f(V_N)}$$

$DI = -1$	$DI = 0$	$DI = 1$
Strongly Selective for V_N (Motion Away From Tip)	No Directionality	Strongly Selective for V_P (Motion Towards Tip)

where $f()$ is either the identity ($\Rightarrow DI(Average)$), or the sigmoidal nonlinearity shown in Figure 4.12 ($\Rightarrow DI(Sigmoid\ Average)$). V_P is the voltage waveform for the distal tip for light moving toward the tip, and V_N is the waveform for the opposite direction.

As shown in Figures 4.11 and 4.12, the "normal" directionality of the tip outputs ($DI > 0$) is strongly dependent on the presence of inhibition. However, if a nonlinear functional is applied to the tip waveform, the distributed nature of the cable *without* inhibition generates a directional response, although it is much weaker than the control case. In addition, the particular nonlinearity and other model parameters in Figure 4.12 causes a DI reversal when inhibition is blocked. As illustrated in Figures 4.9 and 4.12, the ability of a nonlinear integrator to make this distinction depends on the delay provided by the cable capacitance, since a time delay is a necessary condition for DS (or DD). This prediction is consistent with the experimental results cited earlier for turtle and fly.

4.3.3 Simulations of Facilitation by an Inactivating K^+ Channel

Apparent motion protocols consisting of two stimuli in the sequence $X \rightarrow Y$ can be used to evaluate how the relative position of X and Y affects the response to Y, compared to the response to Y alone. In a DS system, either X must reduce the Y response, when the sequence is in the null direction, and/or X must enhance the Y response for the preferred direction sequence. As mentioned in Chapter 2, both the former (null direction inhibition) and the latter (preferred direction facilitation) have been observed.

In Figures 4.13 and 4.14 we show a simulation of apparent motion for the starburst amacrine cell presented earlier. The cell parameters are identical to before, except that an inactivating K^+ channel (as mentioned in Section 4.1.5) was included in the distal portions of the tree. In Figure 4.14 the response of the second stimulus is strongly affected for motion in both directions.

4.3.4 Accounting for the Anomalous Area Response

As mentioned in Section 2.4 Barlow and Levick reported a subregion of the DS ganglion cell's spot receptive field in which preferred and null responses were similar. This subregion lay on the spot receptive field edge from which preferred motion originated. Since both directions give a response, the simplest explanation is that the receptive field of the DS sub-circuit also has an "anomalous area", which is recapitulated by the ganglion cell. For a reasonable set of parameters our model predicts such an area for a particular morphological class of amacrine cells: those amacrine cells whose individual branches have orthogonal mates (e.g. stellate and starburst morphological types).

Consider the response of a tip output of such a cell to the following stimulus: a moving bar whose length is greater than the threshold spot diameter for motion, and whose trajectory is over some fraction of the cell's dendritic field, along the preferred/ null axis of the tip. Movement over the distal third of the tree adjacent to the output gives the expected DS waveform. Movement over the distal third on the other side of the soma produces a much weaker, perhaps nil, response, due to the distance and the intervening somatic load. However, movement centered over the soma would produce a more nearly equivocal set of preferred and null responses. This is because the bar passes activates synapses on dendrites with a trajectory that is *orthogonal* to those dendrites' preferred/null axes. These branches get activated almost all at once as the bar sweeps over the soma. The resulting bolus of excitatory current might by strong enough to generate a tip response, despite the cable attenuation.

4.3.5 An Asymmetric Substrate for Non-Linear Interactions Avoids Preferred Direction Inhibition

As described in Section 2.4.1, putting a synaptic vetoing mechanism onto a symmetric ganglion cell dendritic tree has the problem of preferred direction

inhibition for motion over the side of the receptive field that lies towards the preferred direction. In these models there is a tradeoff that depends on the duration of the inhibitory response: the longer the response, the wider the null velocity bandwidth, but also the greater the preferred direction inhibition. The model described here does not have this tradeoff, since the integrating substrate (the single amacrine cell dendrite) is asymmetric. The important signal flow is always in one direction (towards the dendrite tip). For a single spot, there is *no* velocity *nor* duration of inhibitory kinetics such that preferred direction motion will elicit residual (interposed) inhibition that can interfere with excitation.

4.4 Summary

We have presented a model for directional selectivity in retina whose anatomical structure and simulated performance is consistent with the data. The crucial elements for directionality are as follows:

- Asymmetric input to output distribution on the DS amacrine cell dendrite pathway.
- Intracellular resistivity of the dendrite cable allowing on—the–path interactions which, in turn, depend on stimulus direction.
- Inhibitory nonlinear shunting of sufficient duration to mask subsequent proximal excitation of the distal tip output.

Further, we have showed that other cable mechanisms may generate testable predictions unique to this model.

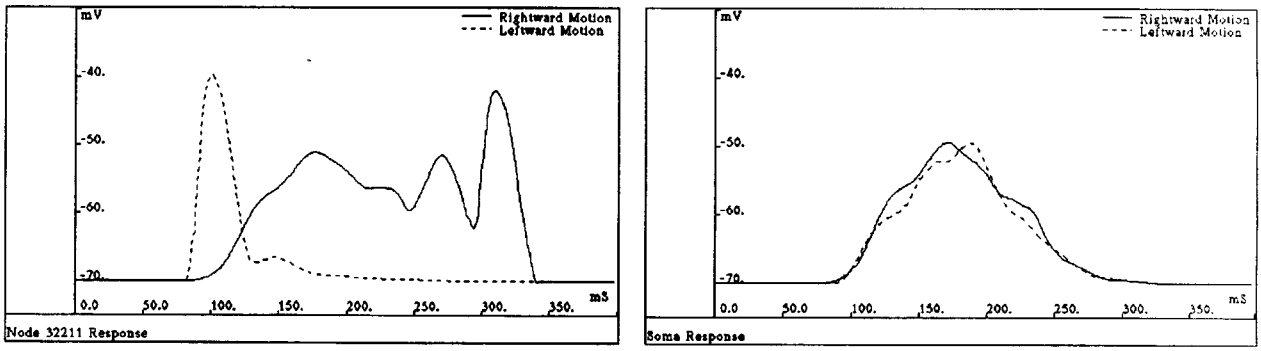

Figure 4.6: Responses of cell in Figure 4.5 to 50μm slit moving from left to right and back again at 2 μm/ms. The voltage at the rightmost distal tip in Figure 4.5 (Node 32211) is highly DS, whereas the soma response is barely DD. Model parameters are given in the text. Simulations also show that inclusion of a K^+ conductance which inactivates with depolarization can both facilitate the preferred-direction response and attenuate the null-direction response (see Sections 4.1.5 and 4.3.3).

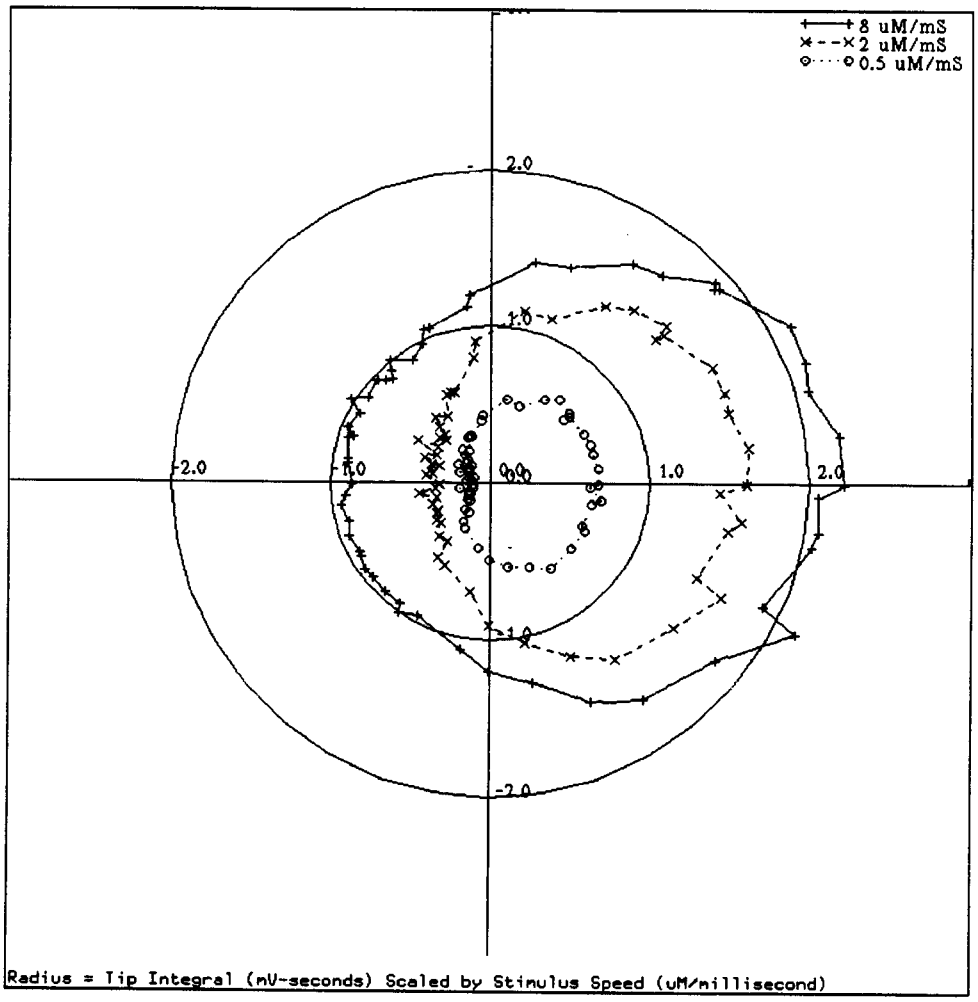

Figure 4.7: Polar plot of integral of distal tip voltages scaled by the stimulus speed versus angle of tip with respect to the soma, relative to the slit trajectory shown in Figure 4.5. Slit speeds include 0.5, 2, and 8 μm/ms. Despite the overall symmetry of the cell, the tip outputs respond asymmetrically to motion.

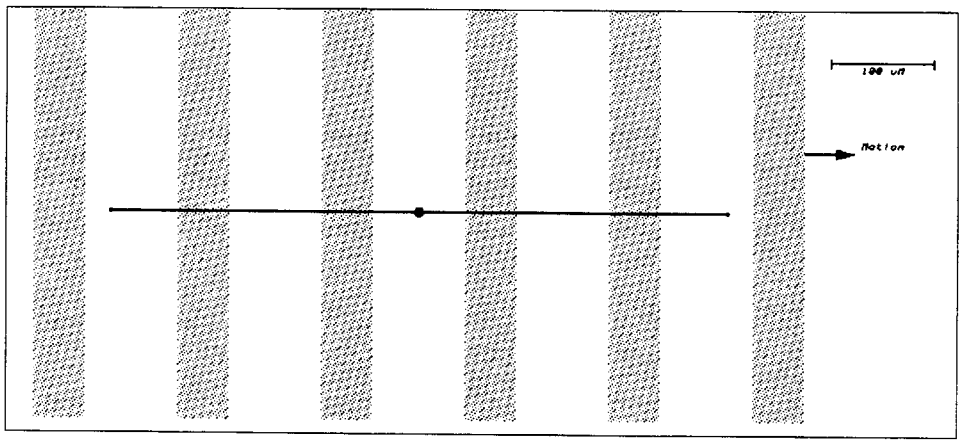

Figure 4.8: **Model cell with two opposing dendrites whose diameters taper linearly from 1.0 to 0.2 μm, (proximal to distal), with snapshots of the stimulus slit trajectory. The output used in the later figures is from the righthand distal tip.**

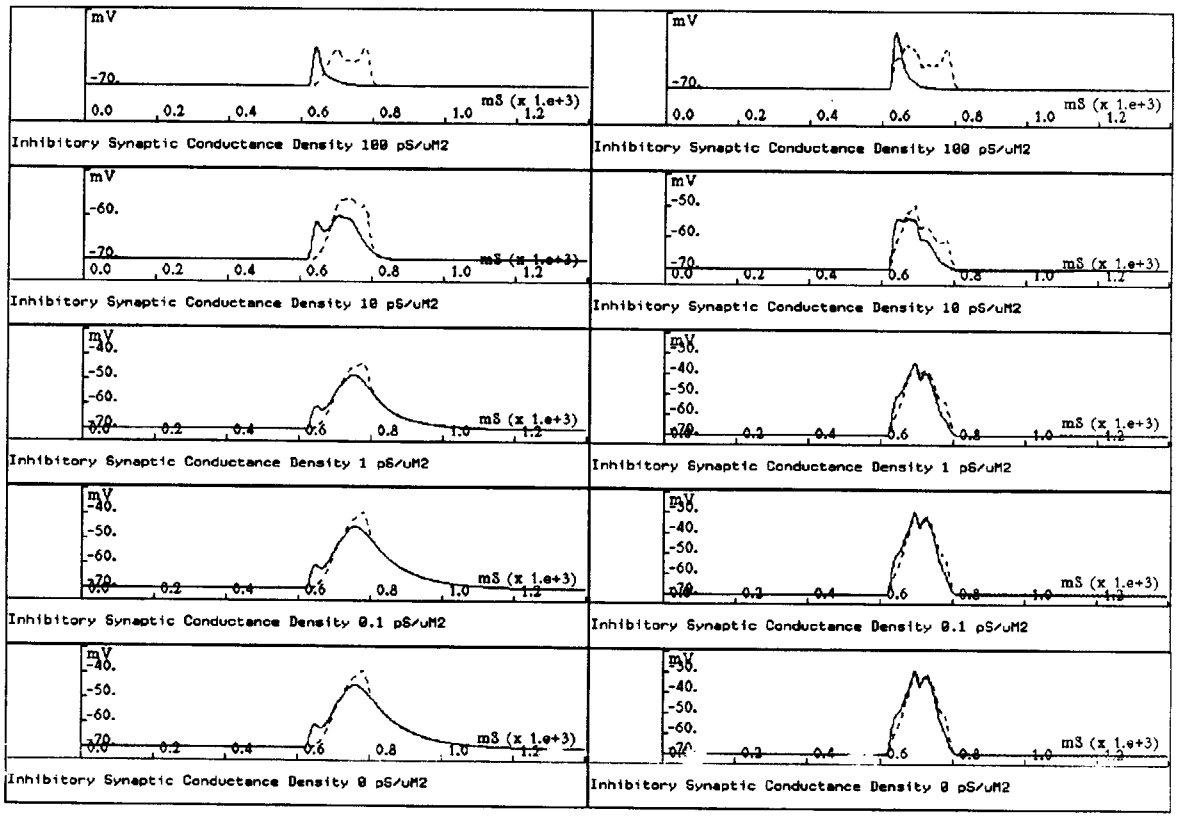

Figure 4.9: Example set of simulations for cell in Figure 4.8 for a stimulus moving at 4 $\mu m/msec$ at various values for G_{in} and C_m. On the left $C_m = 1.0\mu\mathrm{F/cm^2}$, and on the right $C_m = 1.0^{-5}\ \mu\mathrm{F/cm^2}$. Tip output is from the righthand distal tip in Figure 4.8, and the solid and dashed waveforms are for leftward and rightward motion, respectively. When inhibition is absent (bottom simulations) the cable capacitance distorts the equal area waveforms so that a nonlinear integrator may distinguish them (bottom left). If the nonlinearity saturates, then the "fatter" leftward response yields a larger total output than the higher amplitude rightward response (DS reversal). With no inhibition and very low capacitance (bottom right) the waveforms become mirror-symmetric.

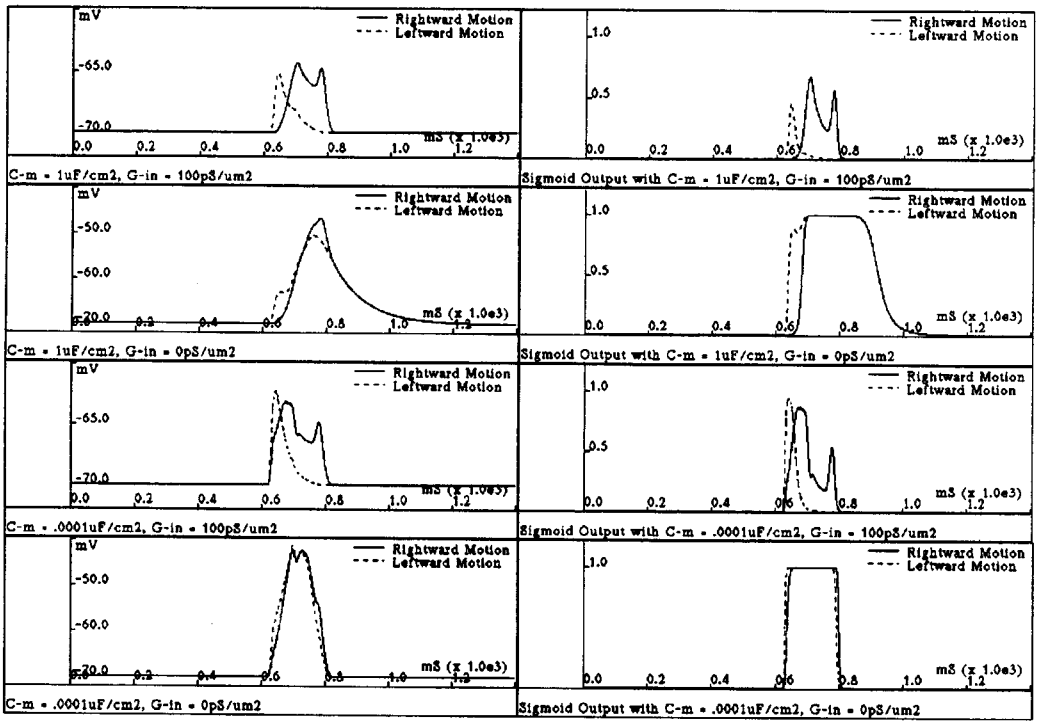

Figure 4.10: Selected simulations from previous figure, comparing tip voltage output before and after processing through an output non-linearity (sigmoid shown in Figure 4.12). Reversal of DS is seen for the simulation on the second row, in which the sigmoid generates a larger total output for the "fatter" leftward motion response. Under the same conditions, but with negligible capacitance (bottom row), the sigmoid merely preserves the mirror-symmetry of the voltage output.

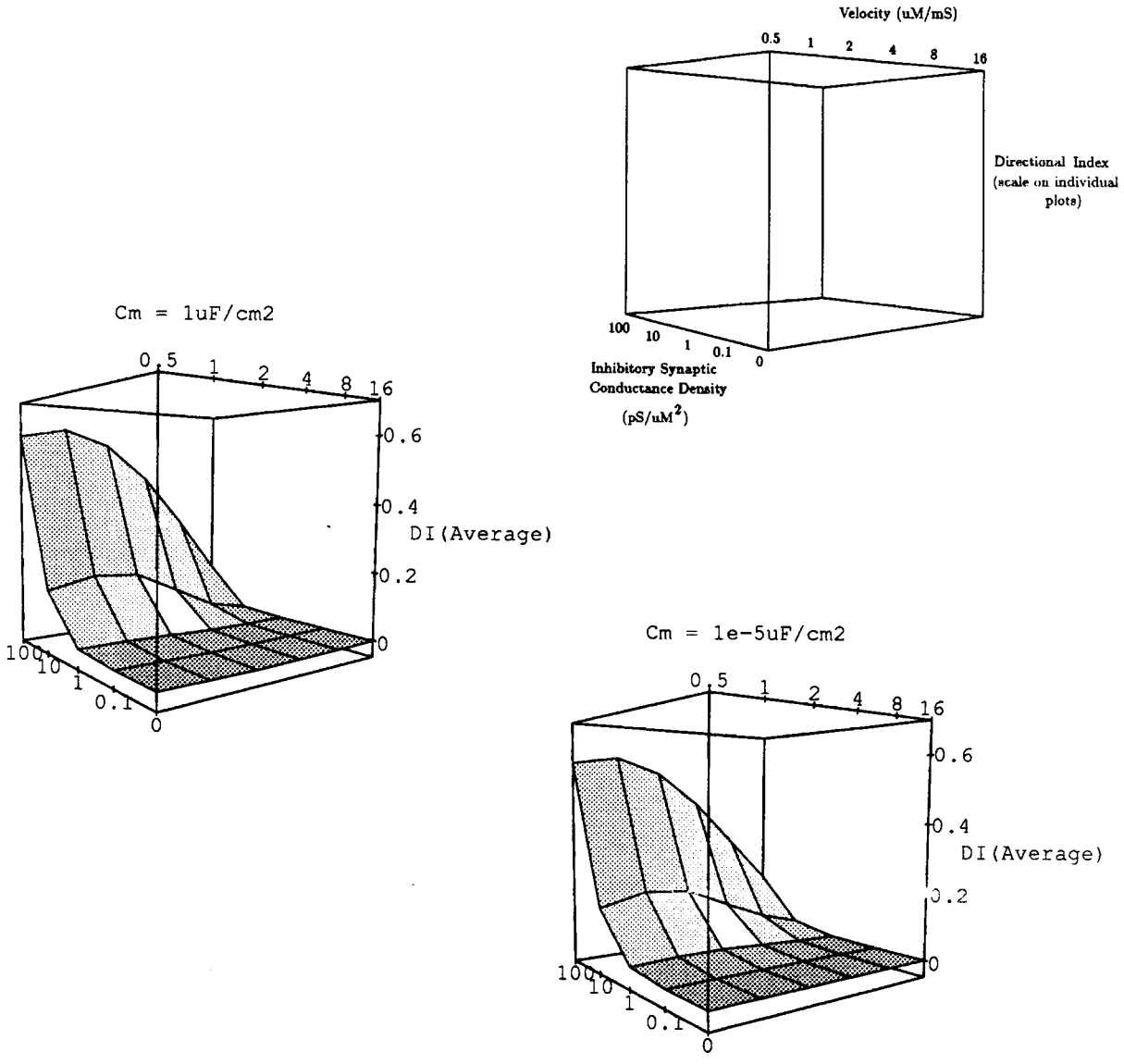

Figure 4.11: *DI* for the linear average of distal tip waveforms obtained from simulations of cell in Figure 4.8, over a range of inhibitory synaptic conductance densities and stimulus velocities, for $C_m = 1.0\mu\text{F/cm}^2$ (middle left) and $10^{-5}\mu\text{F/cm}^2$ (lower right). Axes are shown in the upper right. For this linear functional DS is eliminated as inhibition is lowered, independent of C_m. Furthermore, cable capacitance does not seem to have a significant effect on DS when inhibition is present.

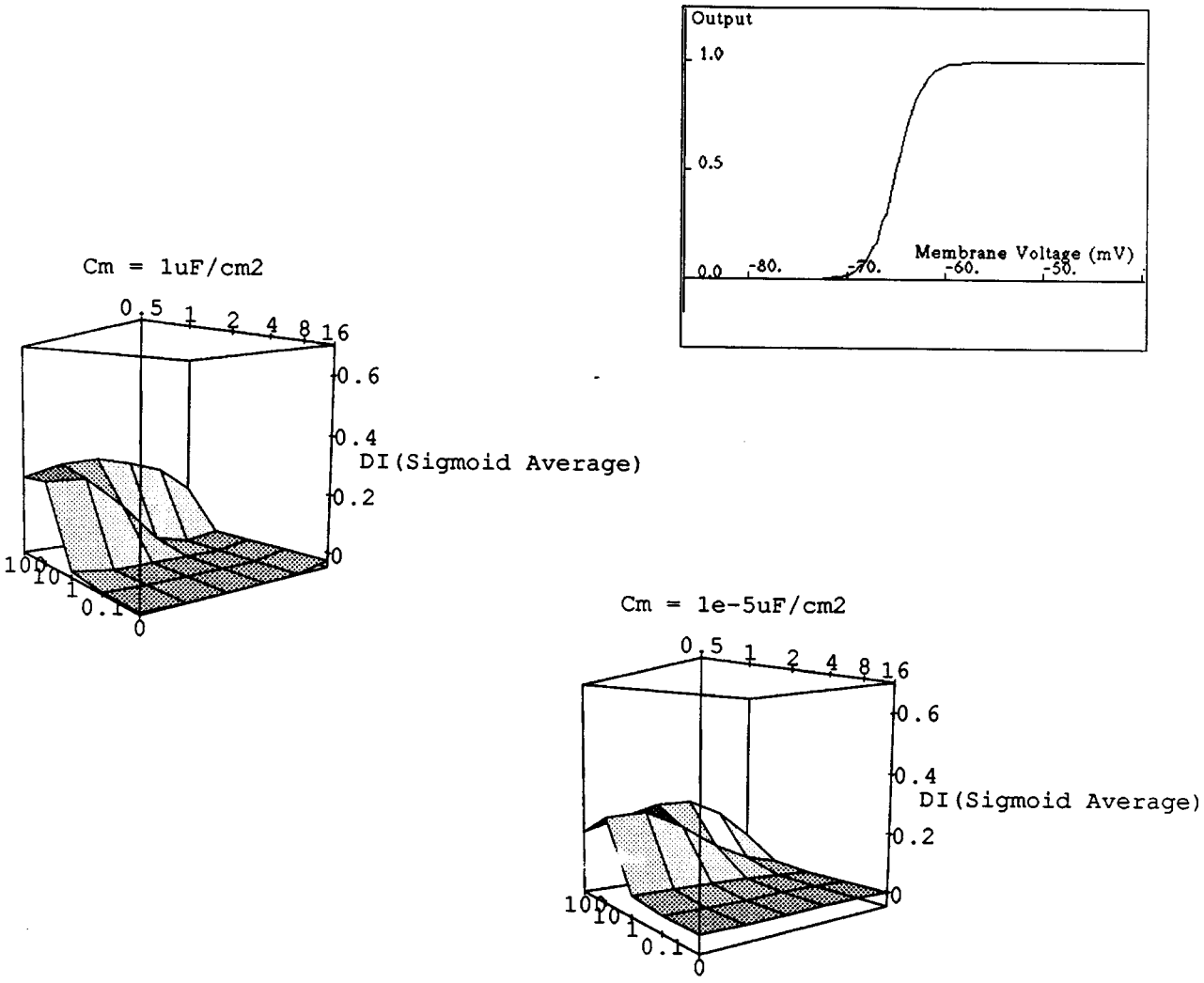

Figure 4.12: DI for the same simulations as Figure 4.11, but taken of the average of distal tip waveforms after being passed through the sigmoid shown in upper right. With normal C_m (middle left) the directionality *reverses* ($DI < 0$) as inhibition is lowered. When C_m and inhibition are both small (lower right) this reversal is dramatically reduced. Axes are as Figure 4.11. Although the strength of the DS reversal is rather small for the particular parameters in these simulations, subsequent non-linearities could in principal amplify the predicted negative DI.

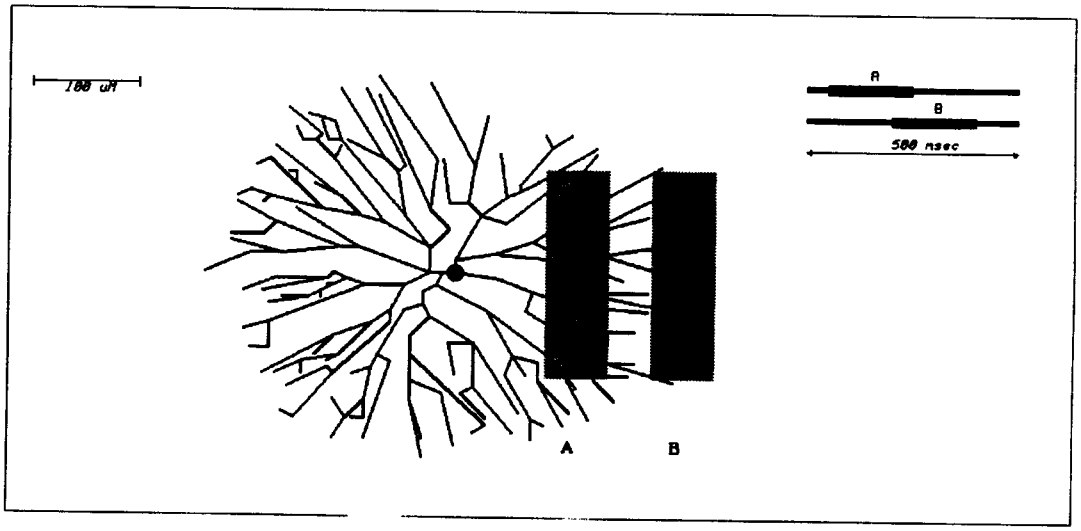

Figure 4.13: Geometry of apparent motion simulations using the starburst amacrine cell described earlier, with the addition of an inactivating K^+ channel at each of the distal portions of the tree. Inset shows the time course of the preferred direction apparent motion sequence. As before, the tip output of interest is the highlighted node at the right edge.

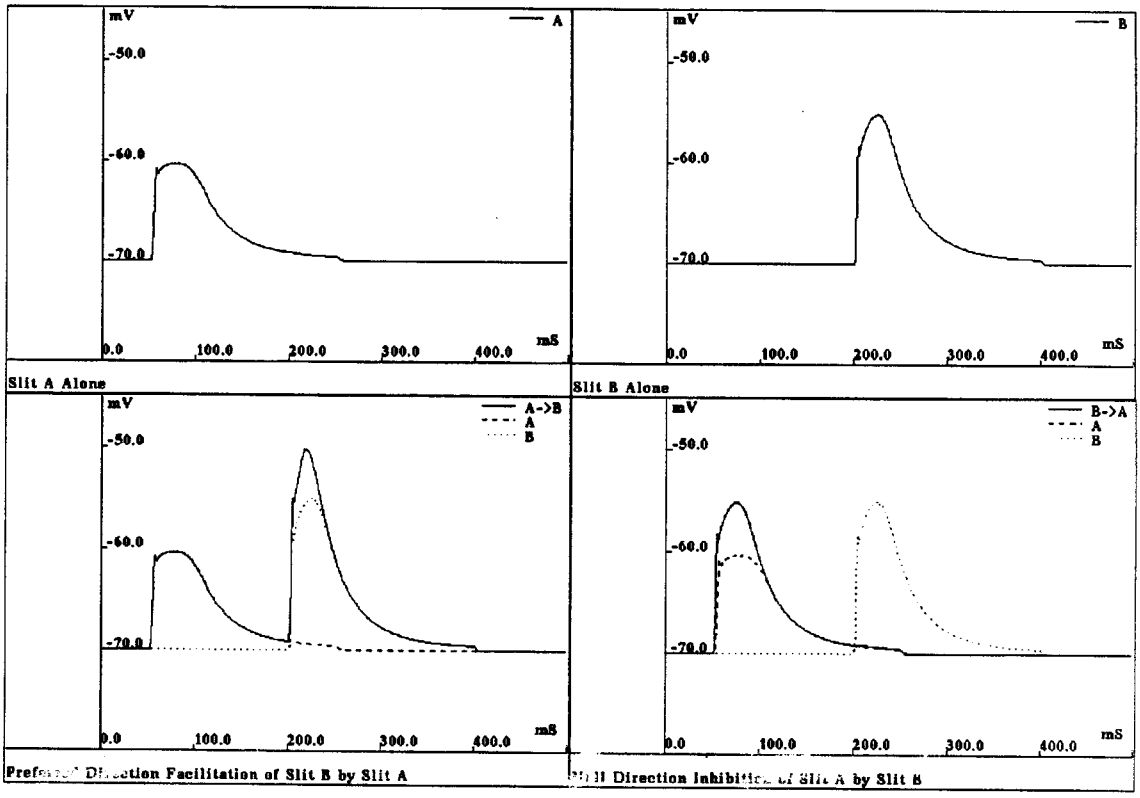

Figure 4.14: Voltage at the righthandmost distal tip in Figure 4.13, in response to slit A and B alone and in the preferred and null direction apparent motion sequences. Preferred direction facilitation, in which the amplitude of the response to B is enhanced by the prior stimulus A, is due to the voltage-dependent inactivation of a distal K^+ channel by A. Null direction inhibition, in which the amplitude of the response to A is *reduced* by the prior stimulus B, is due to the on-the-path shunting described in the text.

Chapter 5

Discussion

We shall now recapitulate and discuss the experimental and theoretical results, and discuss some related issues, including that of developmental considerations and the possible relevance of the model and data to other brain areas and computations.

5.1 Experimental Evidence of Pre-Synaptic Computation of Directional Selectivity and Possible Complications

Again, we interpret the recordings shown in Chapter 3 as evidence for excitatory synaptic input onto DS ganglion cells in turtle retina as being already DS. This finding pushes the computational elements for DS back onto amacrine cells or further. Thus, in Chapter 4 we have postulated a specific model for DS in which evenly distributed excitatory and (slower) inhibitory inputs onto individual amacrine cell dendrites generate DS excitatory outputs onto DS ganglion cells, the outputs being at or near the tips of the amacrine cell dendrites. The crucial asymmetry in this model is found in the receptive fields (the spatial extent of the input) of the distal tip output synapses: the input onto the amacrine cell, although evenly-distributed and with symmetric receptive fields, is displaced with respect to any tip output. This asymmetry must be maintained in the afferents onto any given DS ganglion cell, that is the ganglion cell must contact amacrine cell tips of a specific orientation (see Section 5.5). Also, the most important nonlinearity in the system arises from the interaction between the excitatory

and inhibitory synaptic conductance input onto the amacrine cell dendrites.

The observation that under our recording conditions IPSPs are reduced soon after whole-cell access supports the above interpretations, but we may ask whether this blockage is complete for distal inhibitory inputs and, if not, whether such inputs may preserve DS via a correlative null direction vetoing mechanism. If a synaptic event (such as distal inhibition) is able to influence somatic events, however, then in principle that event must be observable by somatic recordings (though not necessarily accurately measured). Since neither inhibitory voltages (under current clamp) nor currents (under voltage clamp) were observed in the motion responses, then we submit that the blocking of inhibitory input in our experiments is sufficient to support the DS excitatory input interpretation.

A similar argument may be used if we consider possible contributions from other DS ganglion cells which do not have their inhibition blocked but are able to transmit DS potentials via gap junctions to the recorded cell. In this case, as well, the electrical continuity of the gap junctions would mean that *any* inhibitory event that could eventually influence the soma voltage of the recorded cell must, in turn, be observable from that cell.

5.2 Anatomical Predictions of the Cable DS Model

The essence of the DS model presented in Chapter 4 is that amacrine cell output synapses that are asymmetric with respect to the dendritic tree of the amacrine cell will have directional responses which, under reasonable conditions, will be DS. We have focused on the distal tip synapses in particular since, assuming that the input to the tree is homogeneous, these locations have the most asymmetric input. Since a given DS ganglion cell would collect DS inputs of a given orientation, then the model predicts an overall spatial asymmetry in the amacrine cell connectivity onto the ganglion cell. For the model version discussed at length, the input cells would be shifted towards the null side of the ganglion cell receptive field (see Figure 5.1). It may also be that the amacrine cell DS outputs pass through bipolar cells before going to the ganglion cell: for the model version discussed here the amacrine cell asymmetry is still towards the null side for a sign-preserving bipolar connection, and towards the preferred side for a sign-inverting bipolar connection. DS facilitatory data (Section 4.1.5), however, argue against the latter possibility.

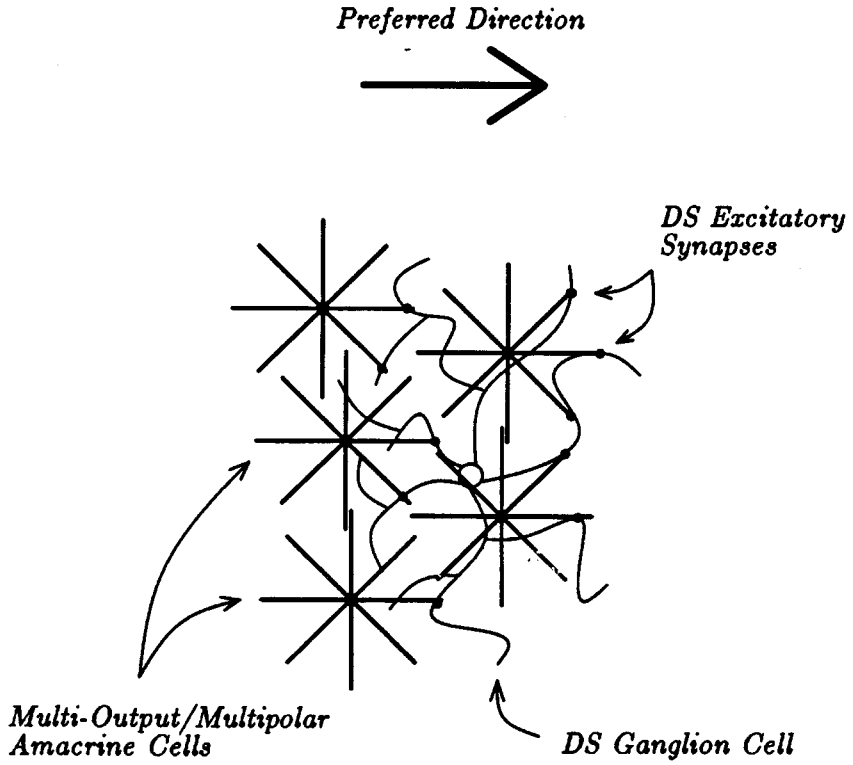

Figure 5.1: The model of DS amacrine cell tip excitatory outputs predicts that the dendritic fields of amacrine cells presynaptic to a given DS ganglion cell would be displaced towards the null direction, with respect to the ganglion cell's dendritic field (see also [66]).

5.2.1 Correlating Anatomy with Function

One experiment to test these predictions would be to inject a physiologically characterized DS ganglion cell with a retrograde tracer, such as Herpes Simplex virus [52], and then compare the distribution and orientation of stained dendritic afferents with the DS receptive field properties. The whole–cell technique described here may be well suited for this type of experiment because *a)* the wide bore of the patch electrode facilitates delivery of electrode contents to the cell and *b)* the stability of the method allows for detailed mapping of the receptive field.

5.3 Relative Frequency of Directional Selective Responses

At this stage of our work we have avoided characterizing the percentage of DS cells using this preparation, primarily because *a)* the protocols and recording techniques were evolving, *b)* the DS criteria described in Chapter 3 are probably weaker than that usually used (explicitly or implicitly) in the literature, and *c)* for many cells a DS response from a WF protocol was not stable over time. With respect to the second point, while our criteria does pick out statistically significant asymmetries, it does not consider the strength of the asymmetry (e.g. *DI*). With these points in mind, for the cohort of 89 cells described in Appendix B, $\approx 50\%$ showed DS responses at some point during the recording. The cells shown in Chapter 3 were chosen because they had particularly stable DS responses. As we have seen, all of these cells show evidence for DS synaptic input. On the other hand, we have found *no* cells in which an initial DS response disappeared over time (i.e. subsequent to removal of inhibition at the cell) without a concurrent degradation of the cell response in general. In other words, we found no evidence that ganglion cell DS in turtle depends on the presence of inhibition onto that cell.

5.4 Comparison to Results of Watanabe and Murakami: Directionally Selective Responses in ON, OFF, and ON/OFF Cells

Our experimental results are similar to that of Watanabe and Murakami ([67]). However, in addition we have observed evidence for DS input into DS ON/OFF ganglion cells, as well as into ON and OFF (not shown) DS ganglion cells. These results do not necessarily contradict Watanabe and Murakamis' observations, since in their paper they simply did not observe IPSPs at all in either ON nor OFF cells. It is quite possible that if they were either able to selectively block inhibitory input to the ganglion cell, or if they voltage clamped their cells, as we have done here, then they may have concluded that the observed IPSPs for motion responses in ON/OFF cells were not necessary for DS.

5.5 Development of Direction Selectivity: The Problem of Coordination of Asymmetries

A problem for any model of DS is how to break symmetry on a scale significantly larger than that predicted by random distributions of local asymmetries. In the retina the DS response is correlated over multiple subunits, and several directions are represented. For the model presented here, this translates into determining how a ganglion cell could selectively connect to amacrine dendrite tips of similar orientation. One solution that seems natural for this model is to postulate a Hebbian–type correlational process ([35]) similar to long-term potentiation in the hippocampus (see review by Brown, Kairiss, and Keenan [15]). A Hebbian–type process strengthens active synapses when the pre and postsynaptic cells fire simultaneously and weakens synapses when activity is not correlated (see Figure 5.2).

The initial symmetry in the retina may then be broken as follows: Assume that at an early stage of synaptogenesis initial DS amacrine connections to a proto-DS ganglion cell have a range of orientations, but overall there is a slight orientation bias. If this bias is strong enough, then a Hebbian mechanism could reinforce it. The connectivity of subsequent synapses would then become stronger or weaker depending on their dendrite's alignment relative to the initial (weak) orientation.

A Hebbian mechanism, at least in this simple form, is suited for a pre–

ganglionic DS model because the mechanism requires signals which can be correlated; the postsynaptic cell tends to collect correlatable inputs. Ganglionic computation of DS loses this advantage, since there is no motion asymmetry intrinsic in the ganglion cell afferents.

This scheme requires the proper IPL input, that is motion stimuli, to work. Thus it will be important to determine when DS properties emerge relative to visual experience in any given species. It is possible, though, that prenatal DS properties may be formed in response to *motion-simulating* stimuli onto the IPL, for example spontaneous retinal waves [51] (see Section 5.7).

5.6 Retinal Directional Selectivity: Exemplar of a Canonical Computational Mechanism?

Thus far we have discussed the directional properties that may arise intrinsically whenever dendrites have distributed excitatory and inhibitory input, at least in terms of the waveforms at the dendrite end. The key to this property is the asymmetric distribution of the inputs with respect to the output, and we have demonstrated how this sort of asymmetry may be especially effective when the output synapse is on the dendrite tip. Since in retina the salient stimuli features are retinotopic, it is very important to consider the exact geometry of the amacrine cells' dendritic trees.

5.6.1 For Generic Central Neurons: Trees of Dendrite Filters

However, in the more general case, we may consider the cascade of inputs along a dendritic branch of a generic central neuron. The performance of the retinal DS model suggests that a similar directionality will exist under some conditions for non–retinal neurons, with respect to the afferents along each branch. We suggest that with plausible biophysical parameters the soma of a more general cell, which is asymmetric with respect to the dendritic input, will see a "directional" response from each of its branch inputs. Specifically (at least with the version of the model discussed here), for a given set of inputs over time along a branch, the soma EPSP will be greatest when the temporal order of the inputs is from distal to proximal, i.e. stepping in time toward the soma. Conversely, the same set of inputs, only reversed in time, may be much less effective in depolarizing the soma.

With the conventional neuron's dendrite-to-soma signal flow, the polarity of the filter is reversed from that of the retinal version: the relevant output

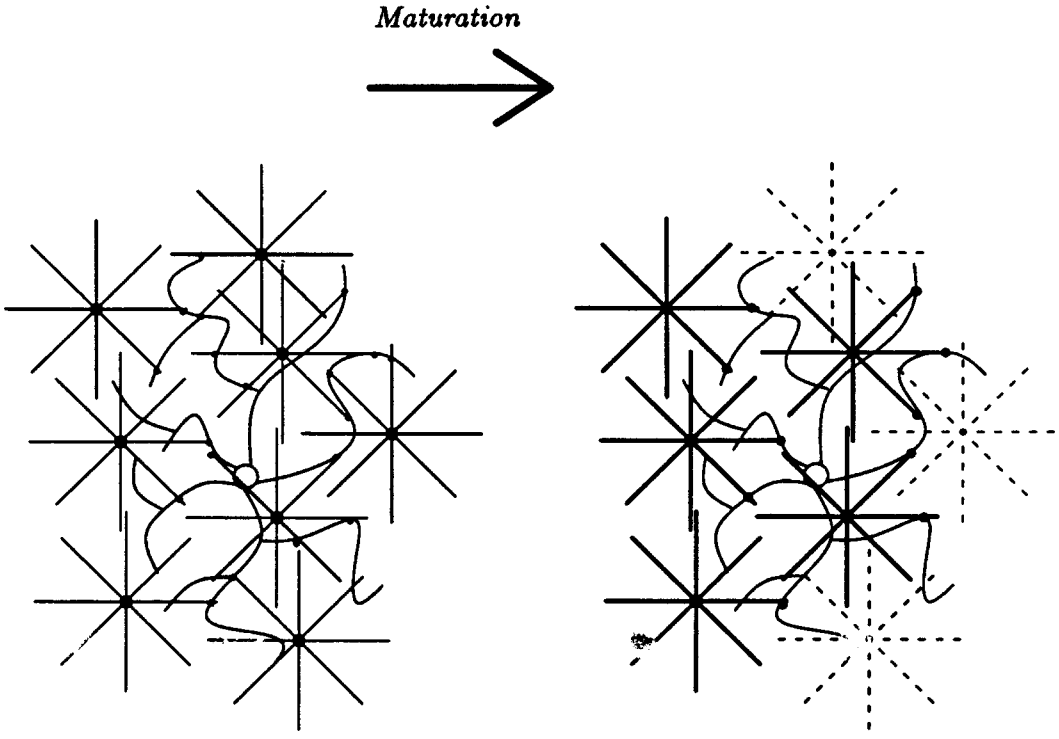

Figure 5.2: According to the model presented here, Hebbian mechanisms may be used during development to reinforce an initial slight directional bias between random amacrine cell DS tip connections and a proto-DS ganglion cell. This DS tip output model seems well suited for such a scheme since there is a directly correlatable component between the pre-synaptic signals. In the mature circuit on the right, the dashed amacrine cells have all of their connections weakened.

of a given branch is its proximal (somatic) end. However, as with retinal directional selectivity, the net result is that each dendritic branch functions as more than just a time–independent "point" integrator of inputs. Rather, the branches function as nonlinear "spatio"–temporal filters. We may also consider implications of trees of such filters, with respect to the somatic response to the cascading of branch filter characteristics. Finally, we note that this model allows for the efficient implementation of various filters which operate on the same input "bus", with the preferred sequence of each filter determined solely by the postsynaptic organization (see Figure 5.3).

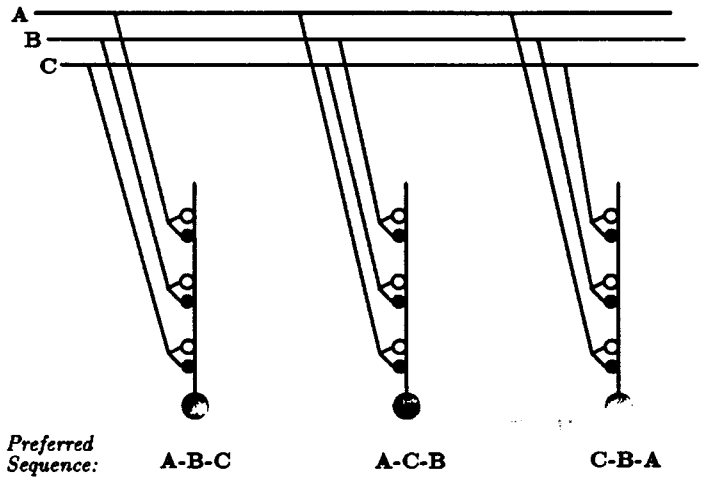

Figure 5.3: An afferent fiber tract could form synapses onto dendrites of different cells with various spatial ordering, relative to the soma of each cell, thus forming various non-linear spatio-temporal filters. In this cartoon the three target neurons would have different preferred temporal sequences of the signals A, B and C off the input bus.

In the more general case the coding of the inputs onto a dendrite depends, of course, on the cell. One possible candidate would be phonemes from an auditory input stream in which the temporal order of the phonems is unique for a given word.

5.7 So What Are Ganglion Cells For, Anyway?

The results of the work presented here suggest that the DS ganglion cell in turtle doesn't do very much in terms of the DS computation itself; rather, the ganglion cell's job seems to be to collect many instances of a specific computation - done by amacrine cells - in order to form a coherent, consistent receptive field. It may be that this sort of final "editing" of retinal processing is typical for the ganglion cell layer.

As we mentioned above, the conditions for DS dendritic waveforms are weak: therefore we suggest that not only may this mechanism be relevant outside the retina, but also that *some degree of DS may be the rule for IPL output rather than the exception.* As we mentioned in Section 4.1.1, if we assume that amacrine cells in general have outputs throughout their dendritic trees, then most of the outputs will be asymmetric with respect to the inputs that can effect them. The degree of input asymmetry for a given output may in turn be reflected in the degree of DS for that output. If this is the case, then we may surmise the following: a given species will demonstrate retinal DS if either *a)* the ganglion cells have the necessary machinery (e.g. Hebbian) to selectively collect DS IPL signals and/or *b)* motion or motion-simulating input onto the IPL is present during a critical plastic stage of development. This leads to the hypothesis that the existence of retinal DS for a species depends more on details of developmental mechanisms and timing for that species, rather than on any "special" biophysical mechanisms involved in the mature DS circuitry.

5.8 Implications for DS in the Visual Systems of Higher Species

As we mentioned in Chapter 2, DS responses in higher species tend to first emerge in visual cortex. Does the model presented here have any relevance for cortical DS? Certainly visual cortex has the retinotopic organization that makes this model arise in a simple way within retinal tissue. Similar biophysical mechanisms probably exist in cortex as well, as discussed above. Whether or not the synaptic organization necessary to recapitulate the retinal DS model exists in cortex remains to seen, but hopefully this model will generate testable predictions for DS-generating connectivity in visual cortex.

Appendix A

Isolation and Recording of Turtle Retina Allowing for Arbitrary Electrode Approach and Trans-Illumination of Retina

Isolated retina preparations have proved useful in many experimental protocols since developed by Ames and Nesbett for rabbit retina ([1]). These advantages include:

- Better clearance properties (useful in pharmacological studies).
- Avoidance of electrode shadowing of stimulus.
- Infra-red trans-illumination of the tissue which facilitates electrode placement and control.
- Visual observation during recording which allows for impalement of selected (e.g. stained) cells.

In 1989 Lipetz et. al. [45] described a new technique for the isolation of a functional turtle retina. While their technique apparently yields normal responses from cones and horizontal cells, it does not allow either direct electrode approach from the ganglion cell side, nor transmitted light microscopy. In this appendix we describe a modification of their technique,

which allows both physical and visual access to either side of the retina ([11]). In particular, in the majority of the dissections it is possible to locate the visual streak and use this as a location reference throughout the experiment. Because we initially used extracellular recordings to assess this preparation (with metal electrodes), and because intracellular protocols will be discussed in Appendix B, in this appendix we will confine recording results to conventional extracellular protocols.

A.1 Dissection Method

Prior to the dissection a small piece of filter paper is prepared and mounted in a holder (Figures A.1 and A.2). The arm of the holder is mounted on the head carriage of a dissecting microscope (with the optics removed), which serves as a useful platform for the dissection. After mounting, the paper holder is adjusted so that the filter paper is coplanar with the microscope stage.

With respect to the filter paper, we have had some success with both coffee maker filter paper (Mellita) and nitro-cellulose paper (Millipore, 0.45 μm pore size). Generally, the nitro-cellulose paper seems to have slightly more affinity for the retina, and it is a simple matter to melt small windows in this material with the heated end of glass tubing of the appropriate diameter.

Perfusate is taken from [5]: 93.5 mM NaCl, 2.6 mM KCl, 2 mM $MgCl_2$, 4 mM $CaCl_2$, 31.5 mM $NaHCO_3$, 10 mM glucose, 10 mM HEPES, bubbled with $95\%O_2/5\%CO_2$. In practice, 10× stock solutions, without $CaCl_2$ or glucose, were prepared ahead of time and stored in the refrigerator.

Turtles are dark-adapted in a light-tight box for at least 8 hours prior to an experiment. After adaptation the *entire* dissection procedure, including decapitation, is done using a head-mounted monocular infra-red (IR) viewer (Model 6100M, Electrophysics Corporation, Nutley, New Jersey). After decapitation and pithing the head is immediately mounted in a dissection holder, covered with foil to block out light, and put in the refrigerator (5°C).

After a variable amount of time (ranging from immediately to one day) the head and holder are unwrapped and one eye is enucleated. The head is then wrapped back in foil and returned to the refrigerator for possible dissection of the remaining eye later. The enucleated eye is placed on blotter paper and hemisected, and the posterior half laid face down on the paper to drain for about 20 seconds. The drained eyecup is then rinsed in the Ringer's solution for about one minute. The eyecup is then removed from

the Ringer's and the disc and streak are located. The cup is bisected on a non-porous surface (to avoid premature removal of the retina) along the perpendicular to the streak, narrowly skirting the disc. One half of the bisected cup is placed in a small dish of the Ringer's solution and put into the refrigerator for later use (up to 8 hours).

If the remaining half has the disk then another cut is made, parallel to the first, to remove the disc from the section. Further trimming may be done in order to make the section about 4mm wide. If necessary, the section is laid on its side on the non-porous surface in order to drain more vitreous. The section is then placed on blotter paper, and a scalpel is used to make two lateral cuts (perpendicular to the long axis) through the retina only, dividing the section in thirds. The section is then centered, retina side up, on a small ($\approx$ 3mm $\times$ 5mm $\times$ 1mm high, made of tape) support which is mounted on the XY stage of a dissection microscope. The lateral "ears" of the section are held down by two spring wire clips such that the middle third of the retina is elevated slightly by the support.

The filter paper retina carrier hole is then aligned in the XY plane, with the paper several mm above the tissue, so that the hole is centered on the middle third of the section. Monitoring from the side, the paper is then lowered using the dissection microscope's focus adjustment until the paper barely rests on the retina. The paper is then allowed to sit on the retina for about 20 to 40 seconds, and then the paper holder is lifted quickly by hand, taking the section of retina with it. The retina section is now attached by its ganglion cell surface to the underside of the filter paper. At this point the dissection is inspected and, if it is not satisfactory, adjusted with fine forceps in room light. In our experience, light exposure does no harm once the retina is isolated. The retina and filter paper is then placed under a nylon ring in the perfusion bath (flow $\approx$1ml/min). Recordings are begun after at least a one and half hour wait, but consistent light responses have been recorded within minutes of the dissection.

A.1.1 Importance of Low Light During Dissection

The key step to this technique is that of maintaining very low light levels during the dissection to prevent the interdigitation of the pigment epithelium with the photoreceptors prior to and during the actual isolation [17]. Other factors that may contribute to retinal adhesion to the pigment epithelium, including temperature or pH [70], were not evaluated. We have found that refrigeration schedules are not critical, and the material is relatively resistant

to anoxia, since we have obtained apparently reasonable light responses from both freshly killed animals and from heads that have been stored up to two full days under refrigeration.

A.2 Recording System for Superfusion and Transmitted-Light IR Microscopy

The perfusion system and stimulus/recording layout is set up to provide mixed stimulus and IR illumination from below, and recording and IR video monitoring from above, as shown in Figure A.3.

A.3 Stimulus Generation, Data Acquisition and Experiment Control

Light stimuli were generated on a Textronix 608 monitor with a P4 phosphor, controlled by a Picasso CRT Image Synthesizer (Innisfree, Cambridge, Massachusetts). All experiments described in this thesis used maximum contrast stimuli (full brightness from full off). The monitor image was collected by a 4 inch diameter convex lens and then mixed into the microscope IR illuminator path by a half-silvered mirror prior to the microscope condenser. The final image on the retina was demagnified by a factor of 40, and the intensity at retina was $\approx 25\mu W/cm^2$ (estimate).

Control of the Picasso and data acquisition was handled with an IBM Model AT Personal Computer, running under the Asyst system (Macmillan Software Company, New York, New York). Electrophysiological amplifier, window discriminator (World Precision Instruments), and Picasso phase outputs were both recorded on a PCM VCR recorder (Vetter), and digitized for on-line data analysis and storage. Off line data analysis was done with various standard computing resources.

A.4 Extracellular Recordings

In order to assess the viability of this preparation, extracellular recordings were done, presumably picking up spiking activity from ganglion cells (Dagan extracellular amplifier, Dagan Corporation, Minneapolis, Minnesota). Cells were located by advancing extracellular electrodes (2-5MΩ, parylene

coated tungsten electrodes, A-M Systems, Everett, Washington) under visual control onto the inner surface of the retina. Extracellular spikes (typically 50 - 200 μV) were obtained both in response to flashing spot stimuli (typically 400 μm diameter, centered on the electrode, 1hz) and spontaneously. Depending on the experiment, spikes were found both when the electrode tip contacted the surface of the retina, and sometimes only when the electrode was advanced (at a 45° angle to the surface) $\approx 50 - 200\mu$m beneath the surface. In the latter case, severe indentation of the surface was seen.

A.5 Properties of Ganglion Cells

A.5.1 ON, OFF, and ON/OFF Properties

Basic ON, OFF, and ON/OFF ganglion cell physiological types have been recorded in this preparation. Results from extracellular experiments on a group of 45 cells are shown in Table A.1. In these cells, the receptive field was mapped with a 1hz 200 by 200 μm spot, stepping over a 900 by 900 μm grid, and were classified according to the dominant response. Some cells showed a prominent ON or OFF response in the majority of their spot receptive field, but would show a clear reversal of type in restricted areas. These cells are listed in the table as "Variable".

Type	Number	Percentage
ON	8	18%
OFF	21	47%
ON/OFF	13	29%
VARIABLE	8	18%

Table A.1: Basic Ganglion Cell Types from Extracellular Recordings in the Isolated Intact Turtle Retina ($N = 45$)

A.5.2 Receptive Field Size and Location, Center Surround Organization

The distribution of receptive field sizes of the cohort of cells in Table A.1 is illustrated in Figure A.4. Field properties were mapped out as described above, and a Student T test was applied to the response at each grid point, selecting responses that were significantly above background at the 5 percent

confidence level. The total area of the grid covered by the selected points was then calculated, and the diameter of a circular field with the same area was derived.

Visualization of the retina during recording allows for immediate determination of the relation between soma location and the receptive field, relative to the visual streak. In our experiments we have consistently observed a bias in this relation which tends to put the receptive field center midway between the electrode tip and the streak.

Some cells showed a clear excitatory-center, inhibitory-surround response to spots of increasing diameter. These characteristics are discussed in detail in Appendix B.

A.6 Preservation of Photoreceptors

A major concern with the isolation procedure is the integrity of the fragile photoreceptor outer segments. Scanning electron micrographs of the photoreceptor surface is one way to evaluate this morphology [45]. In the micrographs shown in Figure A.5 the outer segments are clearly visible, and large areas of photoreceptors seem to have weathered the dissection rather well. We also saw extensive areas of damage, but we assume that the "good" areas are large enough for the electrophysiology.

A.7 Infra-Red Viewing of Preparation During Recording

An important advantage of this preparation is the ability to see the tissue during recording, especially for the whole-cell patch protocol described in the following appendix. An example IR video hardcopy of a retina during a whole-cell protocol is shown in Figure A.6.

A.8 Consistency of Method

This method has yielded preparations in which extracellular ganglion cell responses are quite readily obtained. In addition, there appears to be no obvious large-scale artifact in the mapped receptive fields that might be due to the dissection.

A.9 Stability and Longevity of Method

We have not encountered significant bleaching effects with the isolated preparation, despite the absence of pigment epithelium, possibly due to the low level of illumination. Vigorous responses to spots have been obtained from retinas after up to 14 hours of a protocol consisting of 200μm diameter flashing spots or moving gratings, presented at various locations over a 2×2mm retinal area for $\approx 80\%$ of the time, and large ($500 - 1000\mu$m diameter) stimuli for the remaining time. In addition, extracellular recordings from single cells have been maintained for up to 8 hours. This stability is especially useful when investigating the fine structure of the terrapin retina's complicated receptive fields.

A.10 Summary

We have demonstrated that fully isolated turtle retina is a viable preparation. The dissection technique that we describe is designed to be as robust as possible, and we believe that this preparation is amenable to a variety of extracellular, intracellular, pharmacological, and histological techniques.

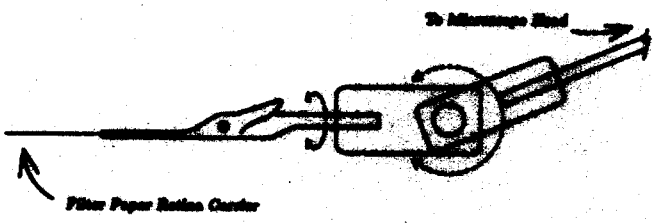

Figure A.1: Holder for filter paper retina carrier allows alignment of paper with dissecting microscope stage prior to dissection under IR. Modified alligator clip holds paper. Holder arm is attached to head of microscope for precision control of Z-axis movement.

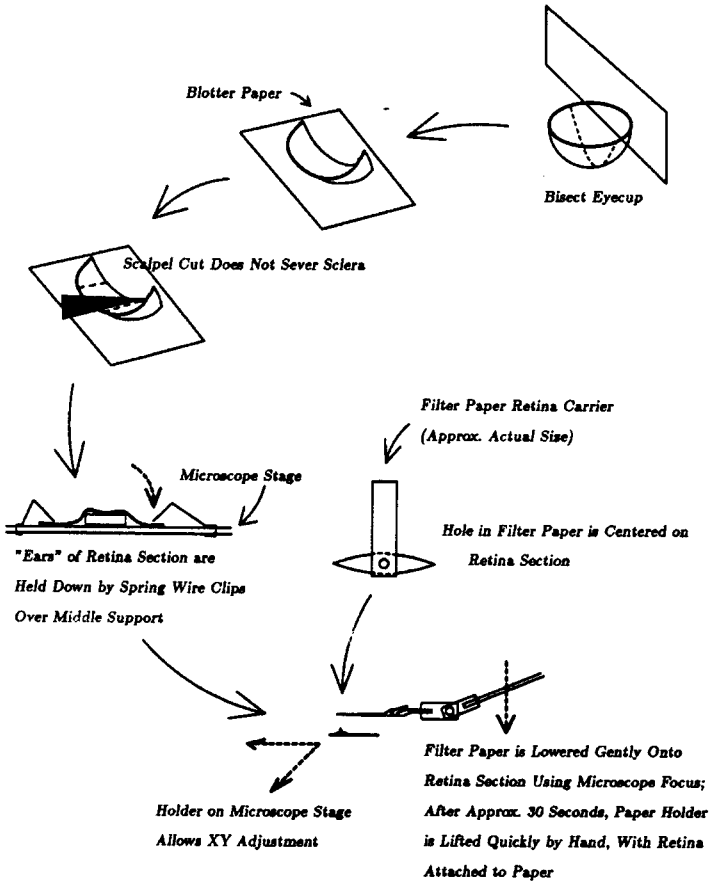

Figure A.2: Procedure for the dissection of intact isolated turtle retina. Inverted retina section is mounted on dissecting microscope stage for precision control of XY-axis movement. Microscope head optics are removed and visualization from above (for aligning paper with tissue) and from the side (for lowering of paper onto tissue) is only through IR goggle. Detached retina and paper are immediately mounted under nylon ring in perfusion bath (See Figure A.3).

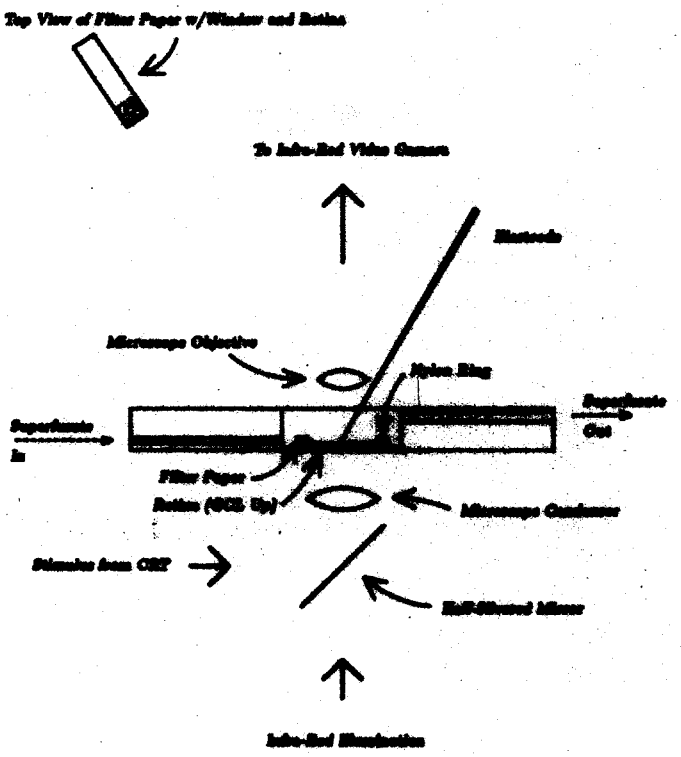

Figure A.3: Layout of tissue, bath, stimulus optics, infra-red illumination, and electrode during recordings from intact isolated retina.

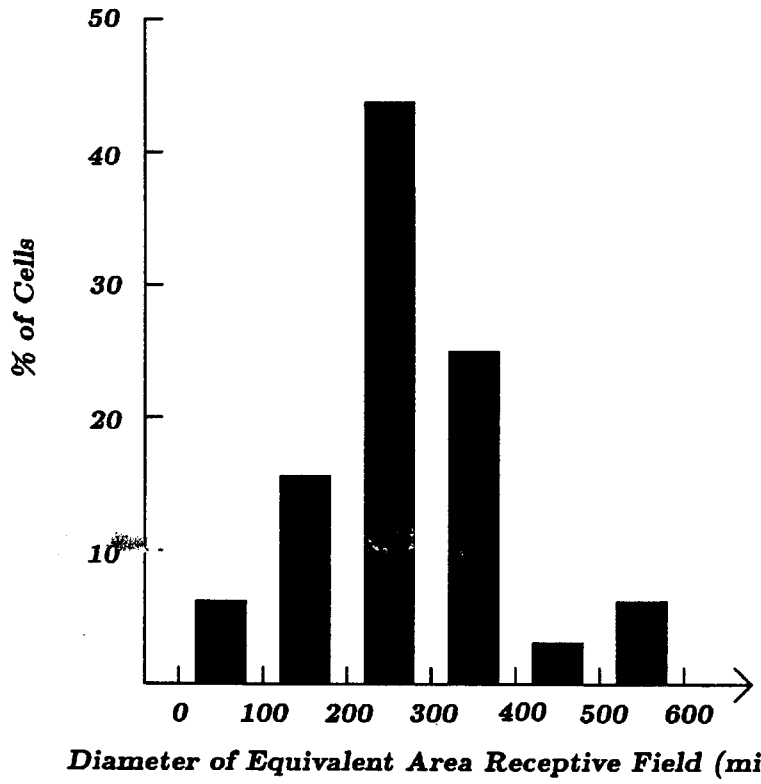

Figure A.4: Distribution of diameters of circles with equivalent areas of receptive fields for cells described in Table A.1 ($N = 45$).

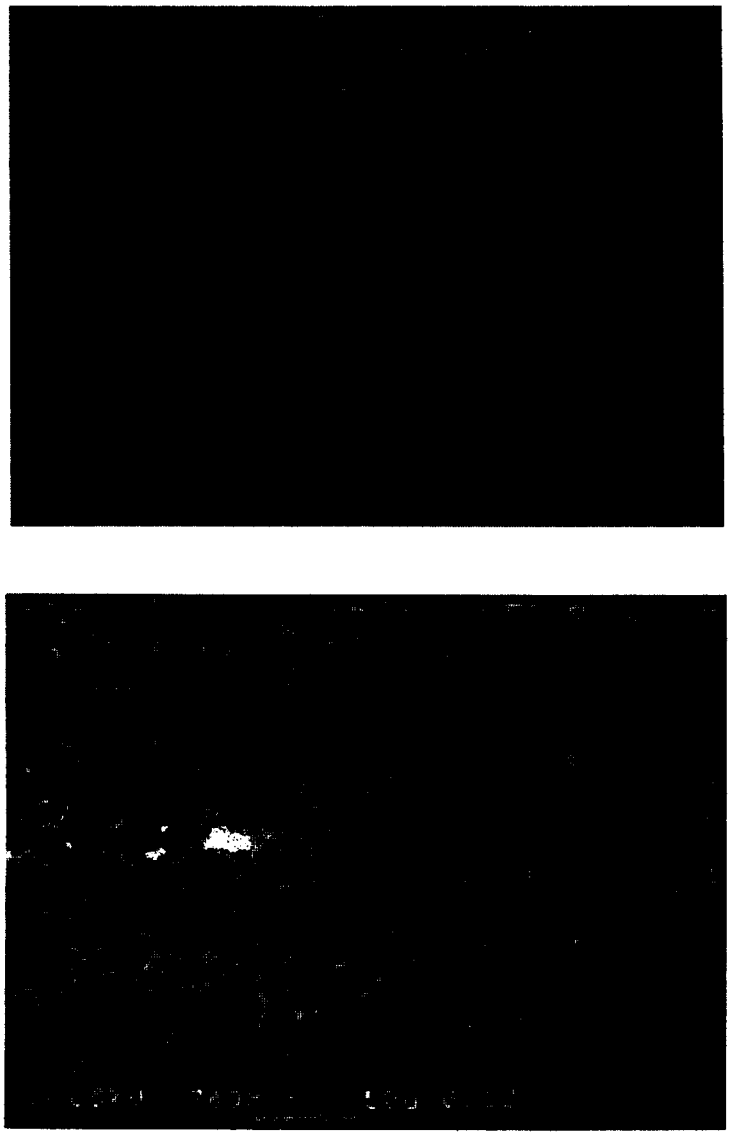

Figure A.5: Scanning electron micrographs of photoreceptor side of isolated intact turtle retina. Top: Large areas of photoreceptors do not show obvious damage after the dissection described in this appendix (magnification $\approx 350x$, zoom box $\approx 80 \times 50\mu$m). Bottom: Blow-up of the zoom box in top figure (magnification $\approx 1500x$), showing a tangle of intact photoreceptor outer segments.

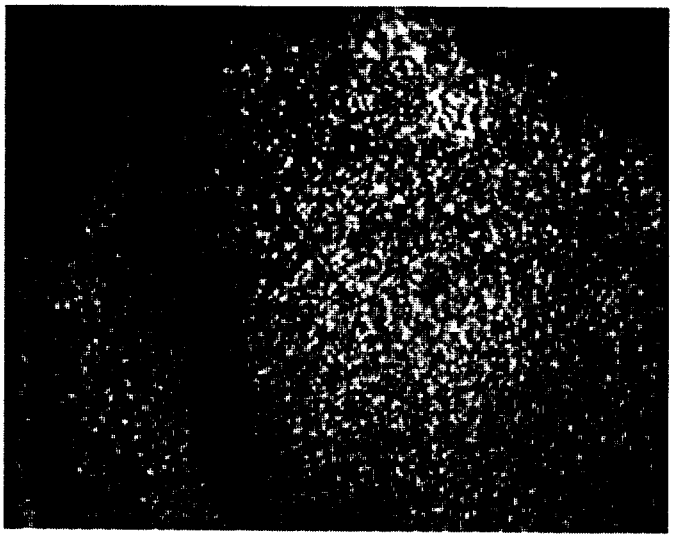

Figure A.6: Retina as seen during recording (Cell A67). This scanned image was taken from a video hardcopy of the IR video monitor (final magnification $80x$). The whole-cell patch electrode enters from the upper left corner, and the visual streak courses vertically on the left hand side, coming to within 250μm of the electrode tip. The receptive field of this cell was $\approx 300\mu$m in diameter, and was centered 100μm to the left and 200μm below the electrode tip position, between the soma and the streak. The stippling effect in the image is from ganglion cell and perhaps displaced amacrine cell somata .

Appendix B

Whole-Cell Patch Recordings in Isolated Intact Turtle Retina

In order to investigate the synaptic inputs to DS retinal ganglion cells we have developed a whole-cell patch technique in intact isolated turtle retina. This method allows the following:

- Initial extracellular determination of receptive field properties, with on-cell patch recordings.
- Intracellular recordings that are stable for typically > 2 hours, and that are quieter than conventional microelectrode recordings due to the low impedance of the whole-cell electrodes.
- Dialysis of the cell interior by the electrode solution allowing manipulation of the intracellular environment.

In this appendix we shall present the protocol used and basic properties of cells measured with the whole-cell patch.

B.1 Recording Method

We shall now describe the whole-cell patch protocol materials and methods.

B.1.1 Electrodes and Electrode Solutions

Whole-cell patch electrodes are made from Corning 7052 capillary glass, 1.65 mm O. D. 1.20 mm I. D. (A-M Systems, Everett, Washington) using a three pull sequence on a Flaming-Brown micropipette puller (Model P-80/PC, Sutter Instrument Corporation, San Rafael, California). A typical sequence is as follows:

Cycle	Heat	Pull	Velocity	Time
1	400	0	30	80
2	400	0	30	80
3	410	60	30	40

The electrodes have a steeply-tapering tip (diameter approximately 2 μm) and a resistance of approximately 4 $M\Omega$ when filled with the solutions to be described. We have not found it necessary to coat the electrodes nor otherwise treat them further other than a simple fire-polishing using a single (extra) heat cycle of the micropipette puller. This step consists of moving the tip of one electrode at a time into the heating element area, while the electrode is still mounted in the puller. The puller is then activated (Heat = 350, Time = 100) while holding the tip in this position. A typical electrode is shown in Figure B.1.

Intracelluar solutions are derived from the protocol of the first whole-cell patch recordings in intact vertebrate retina reported by Coleman and Miller [19]. Control solutions are composed of 90 mM KCH_3SO_4, 5 mM $NaCH_3SO_4$, 12 mM $MgCl_2$, 1 mM $CaCl_2$, 11 mM EGTA, 5 mM HEPES, 2 mM glucose, and 1 mM ATP, titrated with KOH to a pH of 7.4. For protocols which include the presumed blocking of $GABA_A$ responses of the recorded cell alone the control solution is used minus the ATP ([60]) and, occasionally, the $MgCl_2$. All the results presented in this thesis are from protocols using the control solution without ATP.

B.1.2 Electrode Manipulation

Electrodes are backfilled with a hypodermic needle and syringe, which is fitted with a 2μm in-line filter. Following the recommendation in [19], the

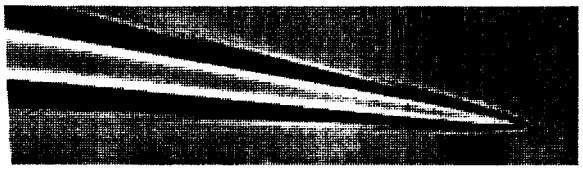

Figure B.1: Whole-cell patch electrode made with pull sequence in text (magnification 570×). $R_{electrode}$ = 4MΩ when filled with solution described in text. Tip diameter ≈ 2μm.

hypodermic needle is flushed with solution prior to filling an electrode. The filled electrode is then placed in a patch electrode holder (Model PC-S3, E.W. Wright, Guilford, Connecticut) which had a side port for pressure communication with the inside of the electrode. Tygon tubing (3/16" O. D. 3' length) connects the electrode holder to a 10cc syringe via a three-way valve, with one leg of the valve open to the atmosphere. This syringe is used to apply either pressure or vacuum to the inside of the electrode. The holder is mounted on a electrical micropositioner drive (Nanostepper Model, Scientific Precision Instruments, Neckargemünd, FRG). Once the electrode has been mounted in the holder, strong pressure (approximately 7cc of movement on the syringe) is applied. This pressure has three presumed functions; first, to force intracellular solution to the tip in order to finish filling the electrode, second, to cause an outflow to avoid tip clogging as the tip enters the bath solution, and third, to prevent the tip from getting fouled by either vitreous or extracellular components prior to being juxtaposed against a cell membrane.

After pressure is applied, the three-way valve is positioned to seal off the electrode from the other two outlets, and the electrode is rapidly advanced into the bath solution. The amplifier (Dagan Model 3900, Dagan Corporation, Minneapolis, Minnesota), is set to current clamp mode and adjusted to compensate for the the electrode series resistance and offset potential. Blocked electrodes or those whose resistance was not between 3-6MΩ are discarded. The electrode tip is then lowered onto the retina under video observation, with a 1 nA 40 Hz square-wave applied current. The angle between the electrode and the retina surface is ≈45 degrees. The electrode is

lowered in the Nanostepper continuous mode until contact with the vitreous is detected visually.

B.1.3 Electrode Solution Bleeding

After contact, electrode advancement is continued in the Nanostepper's "Defined Step" mode (3μm step, maximum adjustment of speed and current potentiometers, speed switch at 10x, 1ms delay) until either the electrode resistance increases suddenly or, more typically, a sudden "bleeding" of the tip solution into the tissue is observed on the monitor. At first the dramatic appearance of a large (roughly 100 – 200 μm diameter) stain was thought to be due to tip breakage, but subsequent inspection of the electrode showed that this was not the case. Apparently the bleeding occurs when the electrode tip leaves the extra-retinal space (including the dense vitreous) and enters the ganglion cell layer (GCL). It is possible that the resistance to flow of solution out of the electrode tip is reduced in the GCL, and that flow is also constrained within a very narrow layer. This may explain why an apparently very small amount of electrode solution could make such a large visual impression. In any event, *electrode bleeding has correlated strongly with achieving giga-seal and whole-cell access.*

B.1.4 Making the Seal

Immediately when the bleeding occurs the three-way valve is quickly moved to open communication between the electrode and the syringe. The goal here is to reduce the positive pressure significantly within the electrode (as evidenced by the subsequent outward movement of the syringe) without removing the pressure entirely. Reduction of pressure is often accompanied by an increase in the tip resistance, typically several MΩ. Occasionally the giga-seal forms spontaneously at this point. If not, the tip is slowly advanced (same Nanostepper settings as above, but speed switch set to 1x) until the tip resistance increases to approximately 10 - 20 MΩ. The three-way valve is then switched so that the inside of the electrode is exposed to atmospheric pressure. If a giga-seal does not form at this point on its own, slight suction is applied either by mouth or by switching the three-way valve to re-connect the syringe with the electrode and moving the syringe very slightly ($<<$1cc), until the giga-seal starts to form. When the giga-seal forms, as evidenced by the rapid increase in the tip resistance (tip voltage from the amplifier) the current clamp waveform is quickly shut off (0 current clamp mode). This

avoids large voltage excursions which can hinder seal formation or cause premature membrane rupture.

On-cell patch giga-seals are then allowed to stabilize for typically five to ten minutes before continuing. Typically seals start out at 1GΩ, and increase to 4 – 20GΩ. Seal resistance is checked periodically by 100–200 msec 10 pA pulses (see Figures B.2 and B.3). The stain from the earlier bleeding typically clears completely within five minutes. Also, the apparent "E_{rest}" in the on-cell patch mode can vary from -20 to +5mV, although between -5 and 0mV is most common. It is not known what causes these variations, but possible candidates include inconsistent electrode wire (Ag/AgCl) preparation.

B.1.5 On-Cell Patch Recordings Prior to Whole-Cell Access

In most protocols which resulted in successful whole-cell recordings of spiking cells, high signal to noise ratio extracellular recordings could be obtained when the on-cell patch giga-seal stabilized (Figure B.2). In fact, good extracellular recordings are almost diagnostic as far as the likelihood for successful whole-cell access.

When on-cell recordings were possible, receptive field spatial and DS properties were evaluated according to the protocols described in Section 3.2. As mentioned in this section, the success of these protocols was variable due to the varying quality and stability of the on-cell patch. Typical on-cell recording times ranged from 1 to 20 minutes.

B.1.6 Getting Whole-Cell Access

After on-cell patch recordings (if any), a 1 Hz flashing large spot stimulus was turned on and very weak suction was applied by mouth or with the syringe. Whole cell access was marked by either a fall in the tip potential and/or photoresponses (see Figures B.2 and B.3). If the cell was a ganglion cell spikes were often, but not always, seen as the membrane ruptured. Stable resting potentials and photoresponses were then recorded for times ranging from 30 minutes to over 4 hours.

B.1.7 Importance of Visualization of Tissue During Recording

In our experience visualization of the retina and electrode is vital to achieving whole-cell recordings. The recordings presented here were done at low

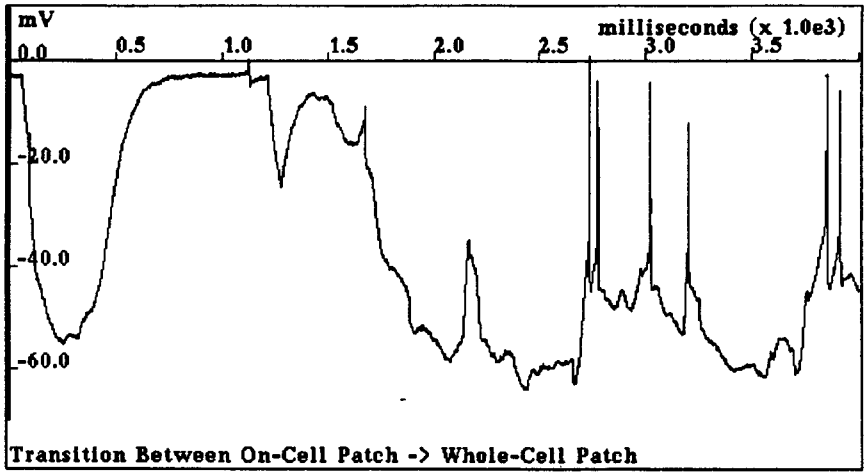

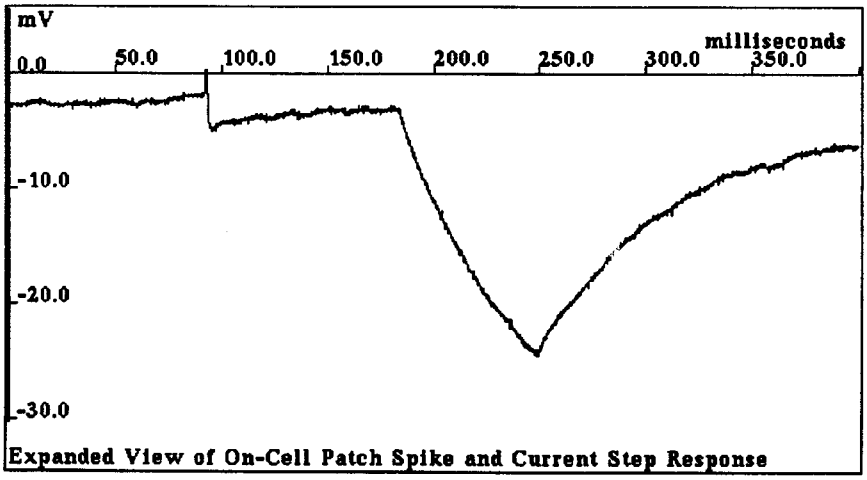

Figure B.2: Transition between on-cell patch and whole-cell patch. On-cell patch was monitored by hyperpolarizing current steps (10 pA, 70 msec), occurring here (top panel) at 1.2, 2.4, and 3.5 seconds. In the top panel, whole-cell access was indicated by drop in E_{rest}, light-evoked spikes, and a drop in R_{In}. Momentary drops in E_{rest}, for example as seen at the beginning of the trace, were typical when suction was applied to the electrode. After whole-cell access is achieved, bursts of spikes are seen in response to a flashing 1hz spot (ON/OFF transitions at 0, 500, 1000 ms, etc.). In the bottom panel the expansion of the trace in top panel (starting at the 1 second point of the this trace) shows a light-evoked on-cell patch spike, followed by the current step response. R_{seal} for this recording is about 5GΩ, and R_{In} is about 1GΩ.

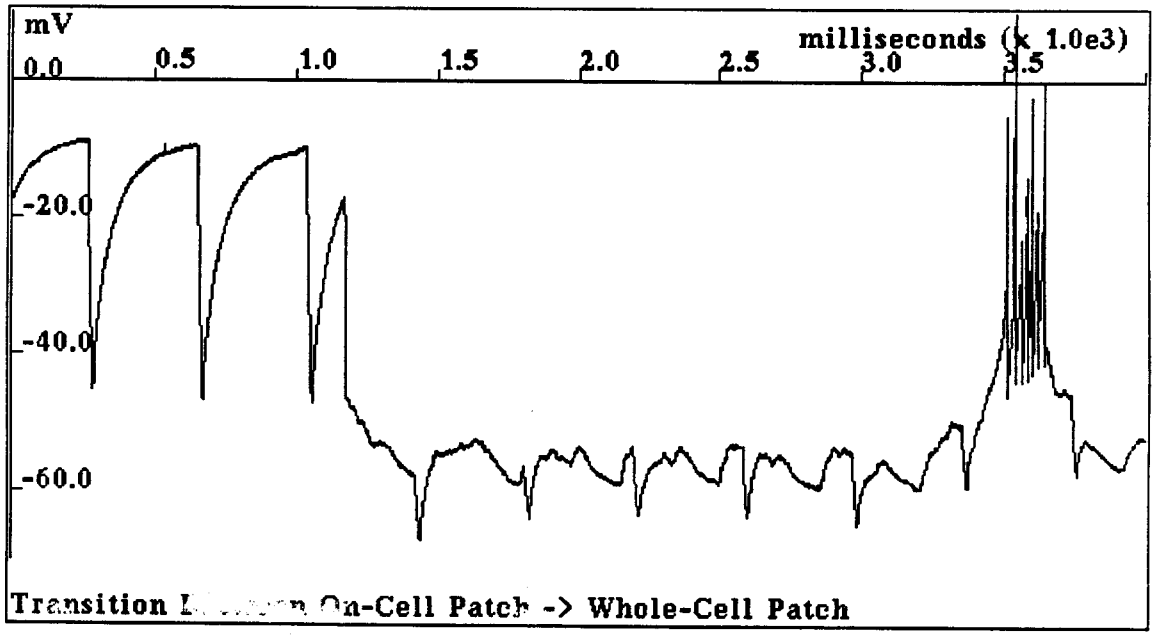

Figure B.3: The on-cell patch to whole-cell patch transition in this cell clearly shows the typically 4 to 10-fold drop in R_{In} seen with the transition (10 pA, 70 msec current steps). A flashing light stimulus at 1 hz throughout this recording fails to generate extracellular spikes, which is confirmed by the subthreshold light-evoked EPSPs seen after whole-cell access. The burst of spikes at 3400 ms is in response to a depolarizing current step. R_{seal} for this recording is about 8GΩ and R_{In} is about 1GΩ.

magnification ($\approx 80\times$), where individual somata were just at the limit of resolution (see Figure A.6). Thus, these recordings were done partially blind, in that there was no attempt to "stab" a specific cell. However, completely blind manipulation of the electrode (e.g. tip position monitored solely by tip resistance), has been much less successful, especially since the bleeding described earlier cannot be followed.

Also, the optics of our setup allow high-magnification ($> 500\times$) of sufficient quality to resolve specific somata with an adjacent electrode tip (see FigureB.4). It is likely that with minor improvements in the setup, it will be possible to record from specific cells, e.g. from previously–labelled cells.

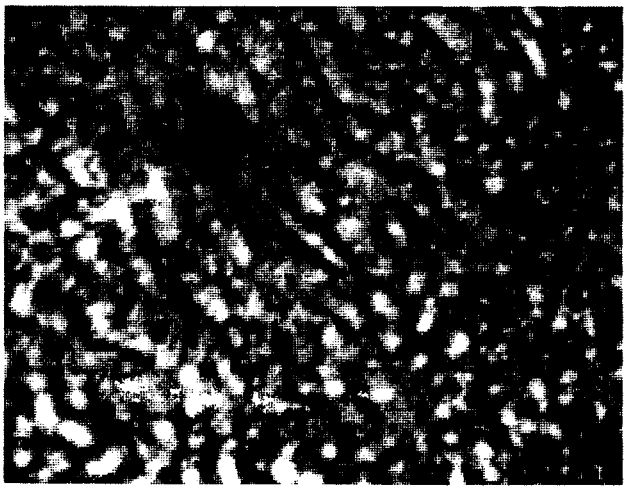

Figure B.4: Scanned infra-red video hardcopy image of intact isolated turtle retina at high resolution (magnification $\approx 800\times$) made during an experiment. Cell bodies are clearly visible with no staining. A whole-cell electrode tip is seen in the middle of the micrograph approaching a soma. The shank of the electrode extends from the upper left corner of the micrograph.

B.2 Whole-Cell Patch Recordings Show Both Light and Current-Evoked Spikes, Long Time Constants, and High Input Resistances

The whole-cell patch recordings show stable and vigorous action potentials in response to both flashing light stimuli and depolarizing current pulses, as shown in Figure B.5. This figure also demonstrates the typical long time constant (τ for the dashed current step response above is on the order of 50 milliseconds) and high input resistance (700 MΩ for this cell) of cells using the whole-cell technique.

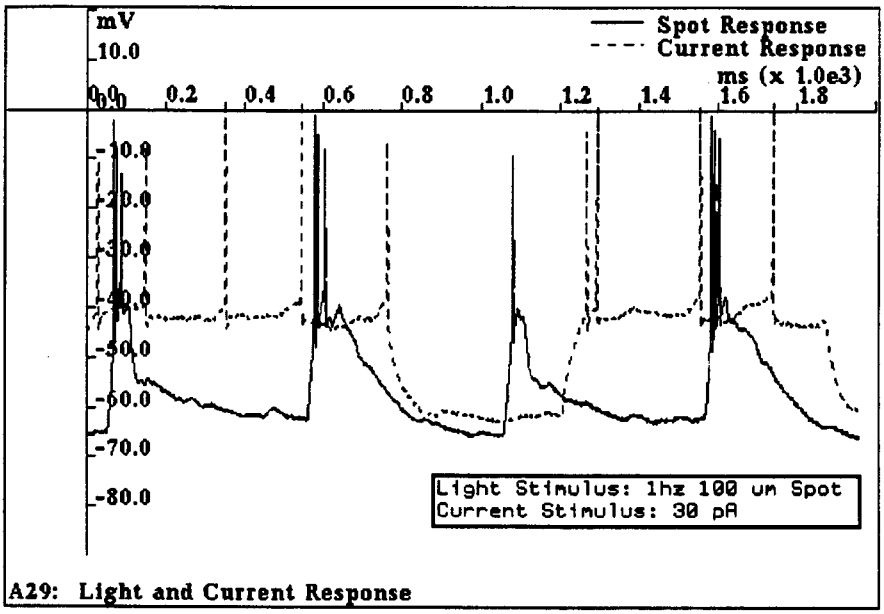

Figure B.5: Whole-cell patch recordings of an ON/OFF ganglion cell, showing responses to both flashing spot stimuli and depolarizing current pulses. On/off/on/off transitions of light spot are at 0, 500, 1000 and 1500 ms, respectively. On/off/on/off transitions of current pulse are at -100, 750, 1150 and 1900 ms, respectively. Non-uniform spike heights are partly due to the sampling rate of 1/ms.

We believe that the recordings presented here are likely to be from ganglion cells for two reasons: 1) the vigorous spike responses are more typical

of the classic ganglion cell response, rather than from amacrine cells, and 2) the electrode seal is established very soon after initial contact with the retinal surface (ganglion cell layer). However, it is still possible that some recordings are from spiking displaced amacrine cells.

B.3 Reduction of IPSPS Over Time With ATP-Less Whole-Cell Patch Electrode Solution

In most of the retinal cells that we have recorded from using the whole-cell technique, IPSPs are observed for large spots (typically $> 200\mu$m) for the first 10 to 30 minutes of the recordings. When ATP is not included in the electrode solution the IPSPs eventually disappear, often losing more than 50% of amplitude within a 30 second period. EPSPs, on the other hand, are much more stable, with many cells showing less than 10% attenuation of EPSPs over 1 to 2 hours. Figures B.6 through B.12 demonstrate the reduction of IPSPs to large spots over time.

B.3.1 Antagonistic Center/Surround is Maintained Despite Local Reduction of IPSPS

That the attenuation of inhibition using our technique is a *local* phenomenon is supported by the maintenance of an inhibitory surround in most cells. This is demonstrated in Figures B.10, B.11, and B.12, where the largest response continues to be from a sub-maximal spot, despite lack of IPSPs. These results also point out that antagonistic center/surround properties are derived from interactions both pre and post-synaptic to the ganglion cell, and is, in some cases, purely post-synaptic.

B.4 Measurement of Passive Parameters with Whole-Cell Patch Recordings

Data from 59 cells recorded under whole-cell conditions were pooled to estimate R_{In}, τ_0, and E_{rest}. The protocol used was a 10 trial average of the response under current clamp to a 10 pA square wave (no DC offset). Linear regression on the logarithm of this response was used to derive τ_0. An example response is shown in Figure B.13.

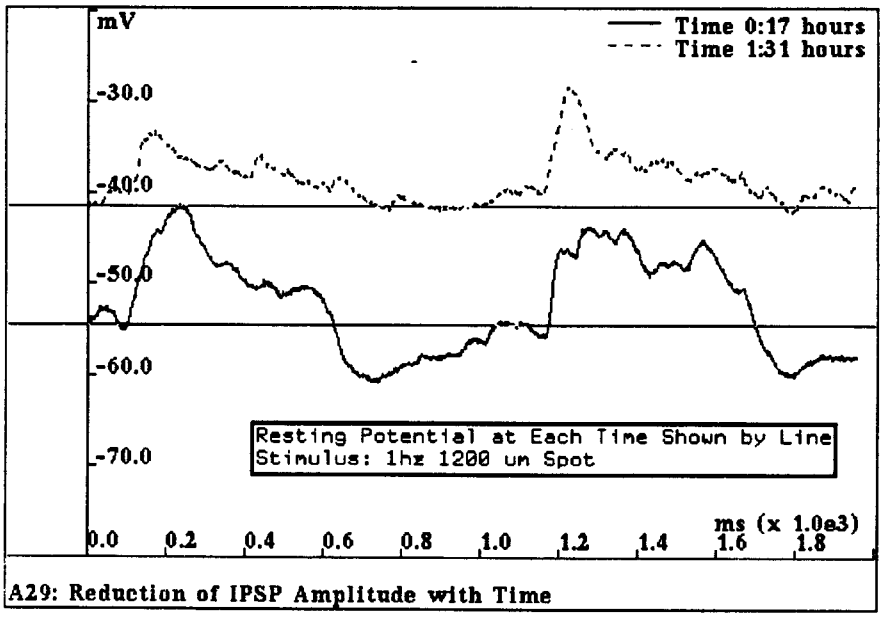

Figure B.6: Light responses of ON ganglion cell (A29) to 1200 μm diameter spot at times noted, relative to start of whole-cell access. These traces are averages of 4 trials. On/off/on/off transitions of light spot are at 0, 500, 1000 and 1500 ms, respectively. Recording at 17 minutes is subthreshold for spikes, and spikes were lost in this cell after 30 minutes. In this particular cell, the resting potential depolarized over time, but it was more typical to see a drop in E_{rest} during the recording. IPSPs relative to E_{rest} are seen at light OFF in the earlier recording, but this negative phase is lost in the later recording. Note that the rise in E_{rest} for this cell would be expected to *amplify* any IPSP.

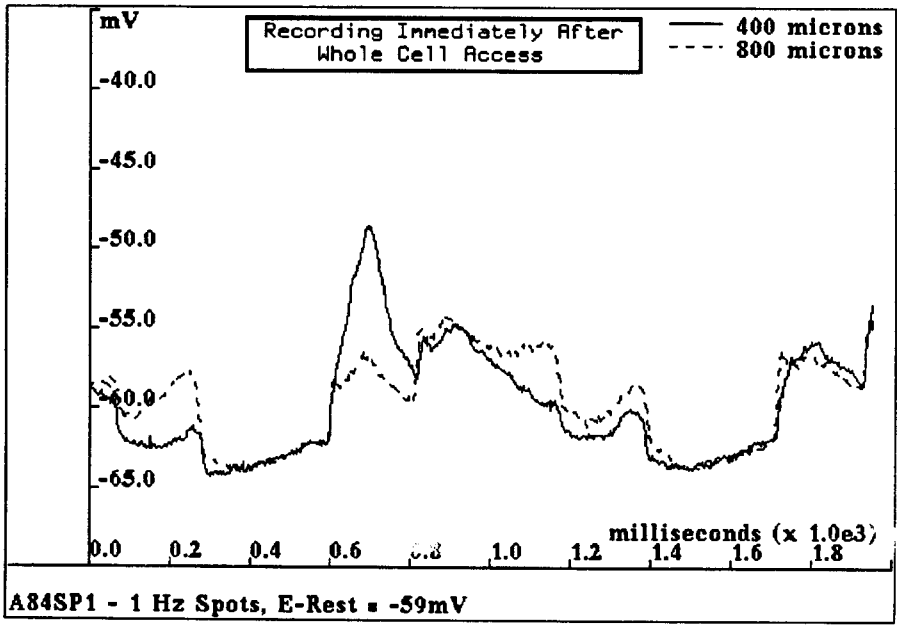

Figure B.7: Responses of ganglion cell A84 to 400 and 800 μm diameter spot at start of whole-cell access (average of 4 trials). On/off/on/off transitions of light spot are at 0, 500, 1000 and 1500 ms, respectively. Stimuli are subthreshold for spikes. Here the cell shows a center/surround OFF response, with a complicated (negative) ON response.

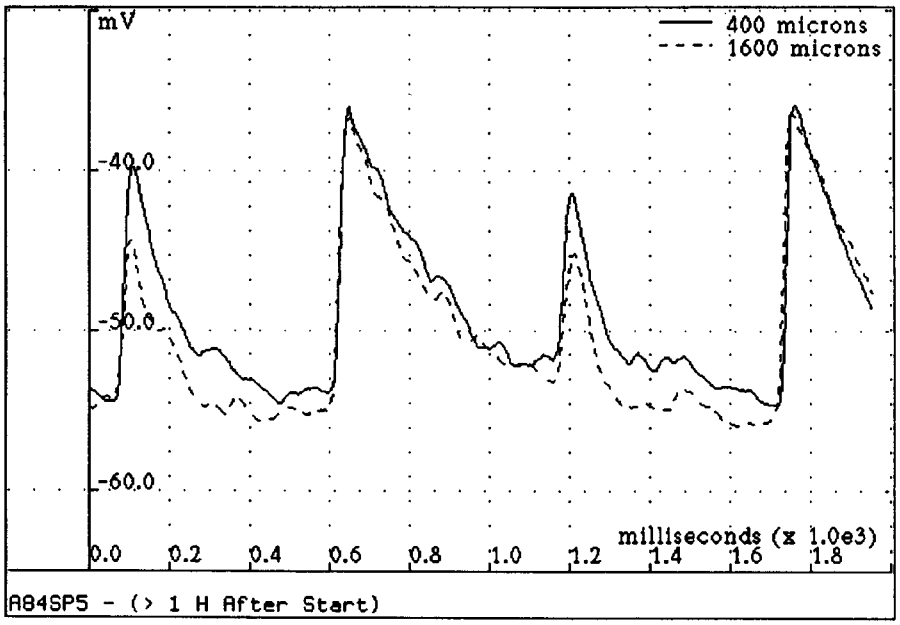

Figure B.8: Response of cell A8 , taken more than one hour after start of whole-cell access (average of 4 trials). E_{rest} = -55 mV. This cell now show an ON/OFF response, and each edge response is simpler than the initial recording. These responses suggests that inhibitory input to the cell has been blocked, uncovering an underlying excitatory ON/OFF input. Actual blockage of inhibitory synaptic channels is further supported by the slight rise in E_{rest} ($\approx$ 5mV), although, as mentioned earlier, it was more typical to see a drop in E_{rest} over time. Note also the loss of antagonistic center/surround properties in this particular cell. As noted in the text and in Figures B.10 to B.12, in many cells a loss of IPSPs was seen over time with nonetheless maintenance of center/surround properties. As before, on/off/on/off transitions of light spot are at 0, 500, 1000 and 1500 ms, respectively.

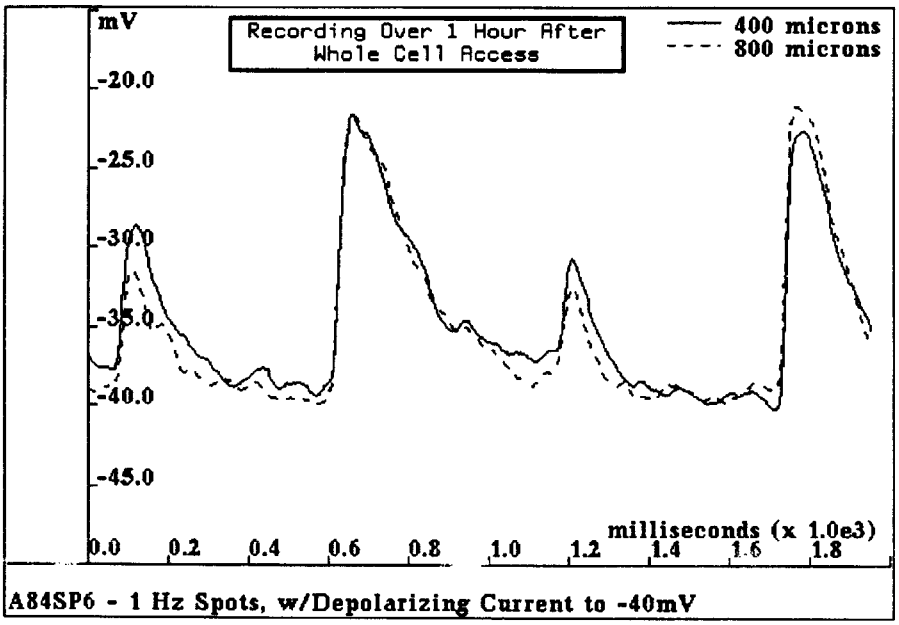

Figure B.9: Response of cell A84 taken immediately after that in Figure B.8, with addition of depolarizing current (to -40 mV) in order to unmask any "silent" IPSPs (average of 4 trials). No negative phase is observed, confirming the blockage of inhibitory input over time.

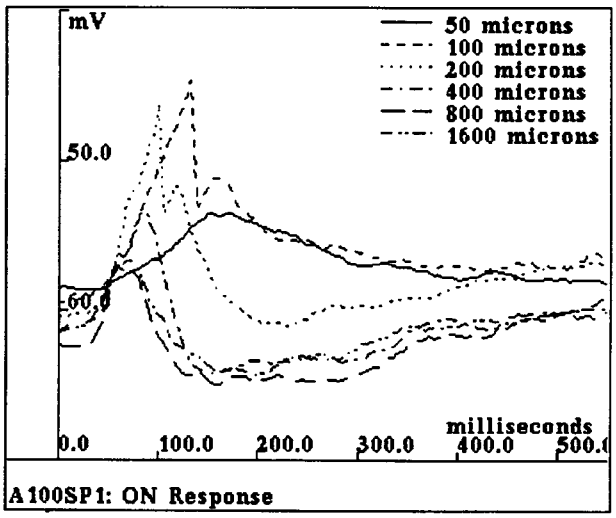

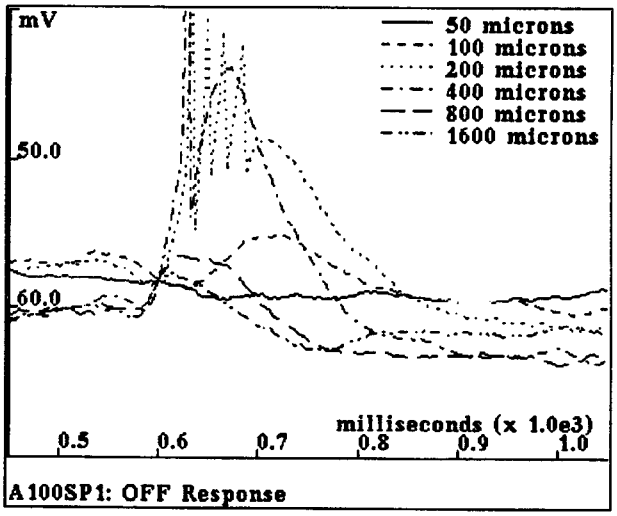

Figure B.10: ON and OFF responses of ganglion cell A100, 3 minutes after start of whole-cell access, to 1 hz 50 to 1600 μm diameter spots (average of 2 trials). E_{rest} = -59 mV. On and off transitions of light are at 0 and 500 ms, respectively. This cell shows a strong OFF component, with a weaker ON component, each of which is strongest for the 100-200 μm spots. An IPSP to both ON and OFF transitions is seen for the larger spots.

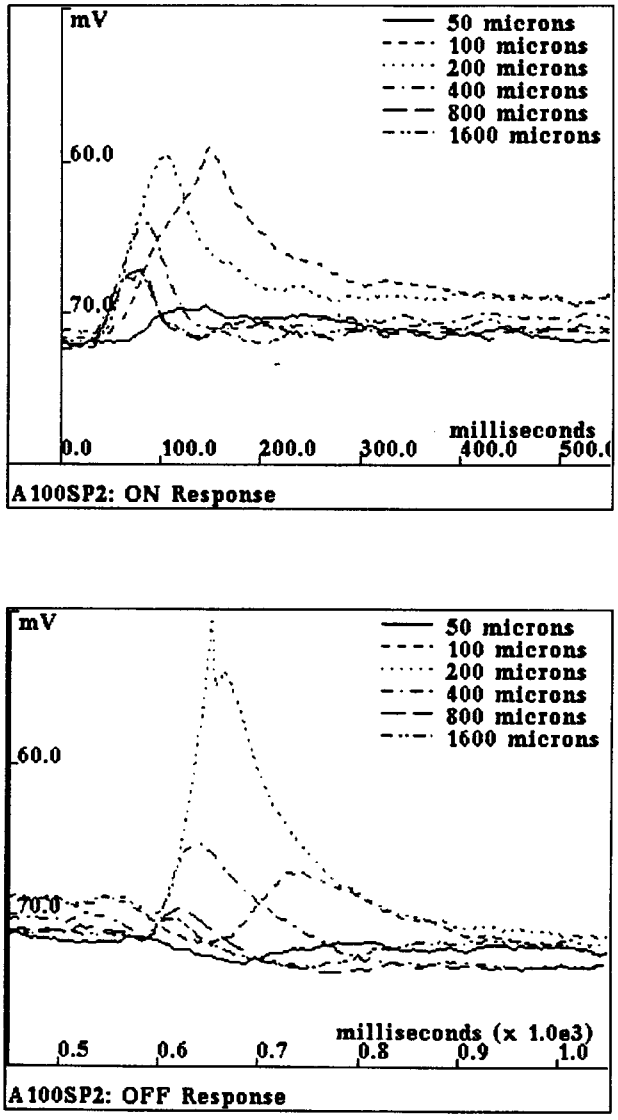

Figure B.11: Responses of cell A100 under same conditions as Figure B.10, 31 minutes after start of whole-cell access. The antagonistic center/surround behavior is maintained, but only slight IPSPs to the larger spots are seen. However, the resting potential has dropped by about 10 mV (E_{rest} = -72 mV), which may hide the relatively small IPSPs seen in Figure B.10.

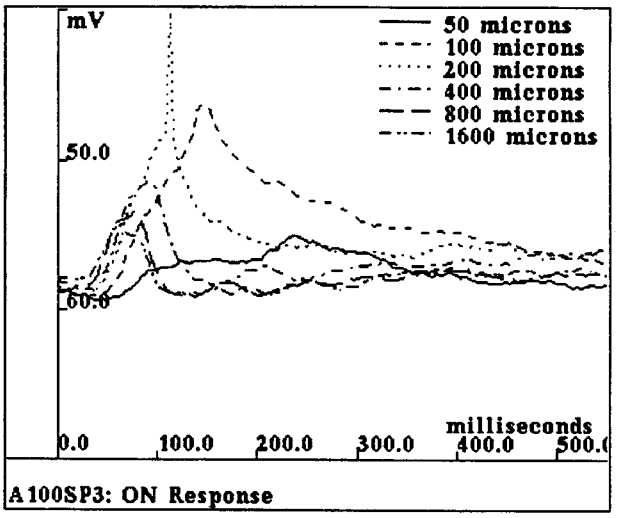

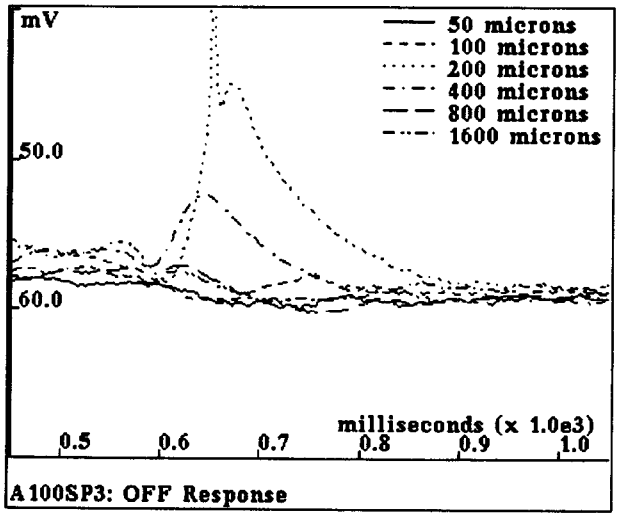

Figure B.12: Responses of cell A100 under same conditions as the previous two figures, but with a depolarizing holding current (to -58 mV) in order to "unmask" any hidden IPSPs of Figure B.11. However, the IPSP phase seen in Figure B.10 is not observed here, suggesting that IPSPs have been blocked. The fact that an antagonistic center/surround characteristic remains suggests that the inhibition of the inhibition is local to the recorded cell. Note the spike-induced fast-afterhyperpolarization in the OFF response to the 200μm spot, suggesting that voltage-dependent re/hyperpolarizing mechanisms are preserved.

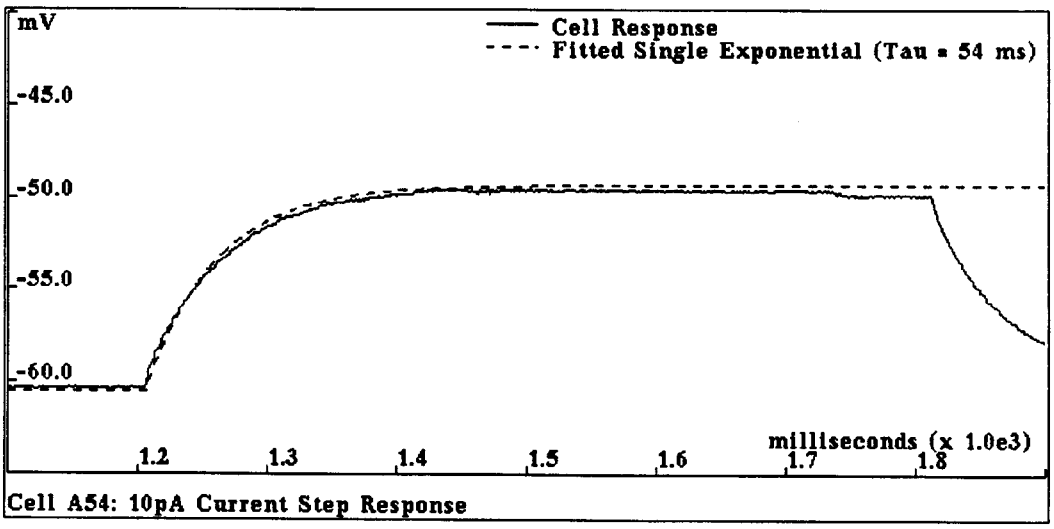

Figure B.13: Example current clamp record of response to 10 pA square wave (average of 10 trials). E_{rest} = -55 mV. The results in this section are derived from similar responses of 59 cells.

B.4.1 Estimates of R_{In} and τ_0

We have found that the whole-cell patch technique with turtle retinal ganglion cells gives relatively high values of R_{In} (mean = 0.87GΩ) and τ_0 (mean = 56 milliseconds). The distributions of these parameters are shown in Figures B.14 and B.15.

These values are consistent with reports in other neurons using the whole-cell patch technique. For example, Coleman and Miller ([19]) give mean values of R_{In} = 1.5GΩ and τ_0 = 68 ms. Likewise, in the salamander retinal slice preparation, Lukasiewicz and Werblin ([46]) report mean values of R_{In} = 2.9GΩ and τ_0 = 41.3 ms. Similar values have been reported from non-retinal neurons as well.

If we assume that the specific capacitance C_m = 1.0μF/cm^2, then the measured τ_0 of 56 milliseconds implies a specific resistivity of R_m = 56KΩcm^2. This value is consistent with estimates from at least two modelling studies (cerebellar Purkinje cells [58], R_m > 45KΩcm^2; hippocampal pyramidal cells [9], $R_m \approx$ 40KΩcm^2) which derived R_m by various and independent methods.

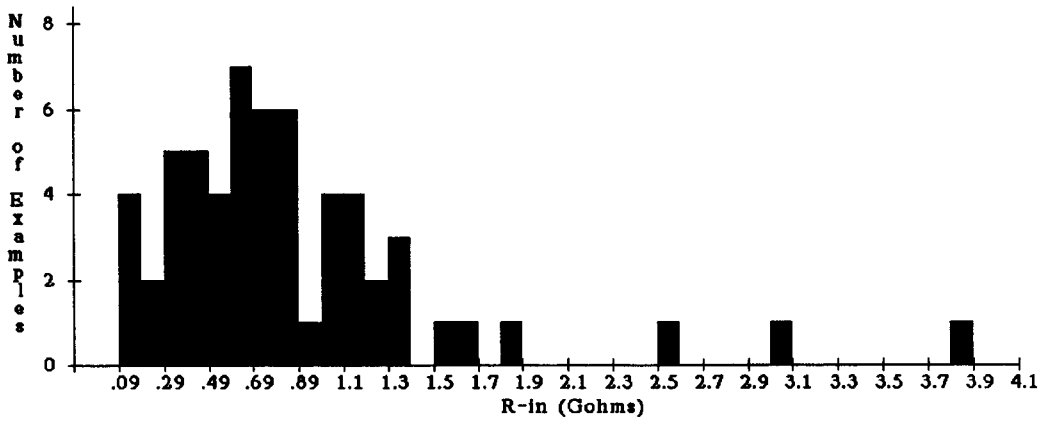

Figure B.14: Distribution of R_{In} values for a series of 59 cells. The mean value for $R_{In} = 0.87\text{G}\Omega$ (SEM = 0.09).

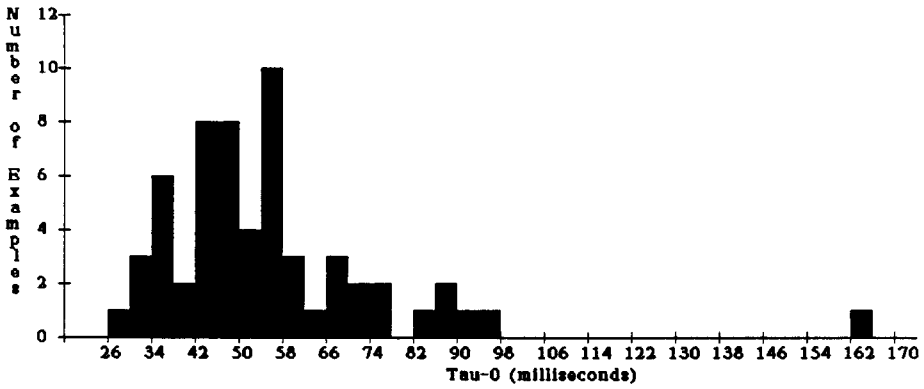

Figure B.15: Distribution of τ_0 values for the same 59 cells shown in Figure B.14. The mean value of $\tau_0 = 56$ milliseconds (SEM = 3).

B.4.2 Effect of Non-Linear Membrane on R_{In} and τ_0

Given the fairly large voltage excursion (typically 10 mV) and long time constant of the step responses, and that the responses had both a hyperpolarizing and depolarizing component (relative to the resting potential), it is likely that non-linear conductances participated in shaping the responses. Since many rectifying channels tend to activate in this voltage range (particularly for depolarizations), it is possible that this protocol underestimated both R_{In} and τ_0.

B.4.3 Effect of Electrode Seal on R_{In} and τ_0

In addition, given the the high values for both R_{In} and τ_0 it is useful to consider the contribution of the giga-seal (between the electrode and the extracellular space) on these parameters. A rough estimate would be to assume a measured value of $R_{In} = 1\text{G}\Omega$ and consider a lower bound of $R_{seal} = 2\text{G}\Omega$. For this value of R_{seal}, half of the input conductance ($1/R_{In}$) would be due to electrode leak, and thus the true $R_{In} = 2\text{G}\Omega$. Likewise, τ_0 under these conditions would be underestimated by a factor of 2. In practice, $R_{seal} > 5\text{G}\Omega$, but this value is of course measured prior to whole-cell access, and it is possible that the seal is partly compromised by the whole-cell access. In summary, these factors may also contribute to an underestimation of both R_{In} and τ_0.

B.4.4 Estimation of E_{rest}

After IPSP attenuation (see Section B.4.5), the resting potential tended to be stable for the remainder of the recording. For the set of 59 cells just presented, the mean value for E_{rest} was -56 mV. The distribution of E_{rest} values in these cells is shown in Figure B.16.

B.4.5 Correlations Between Passive Parameters

As shown in Figures B.17, B.18 and B.19, there was only a slight positive pair-wise correlation between R_{In}, τ_0 and E_{rest}. One possible mechanism contributing to these correlations involves the state of the inhibitory synaptic channels. Typically, the attenuation of IPSPs during whole-cell access was accompanied by a drop in E_{rest} by $\approx$ 10 to 15 mV. In a few cells, R_{In} also dropped as the IPSPs disappeared by approximately 50%. These preliminary observations suggest that blockage of IPSPs may be caused by

tonic *activation* of the associated synaptic channels, when there is no ATP in the electrode solution.

B.5 Staining of Recorded Cells

We have also done trials of whole-cell recording with Lucifer Yellow in the electrode solution (not shown). Preliminary results indicate that this staining method works well in our turtle preparation.

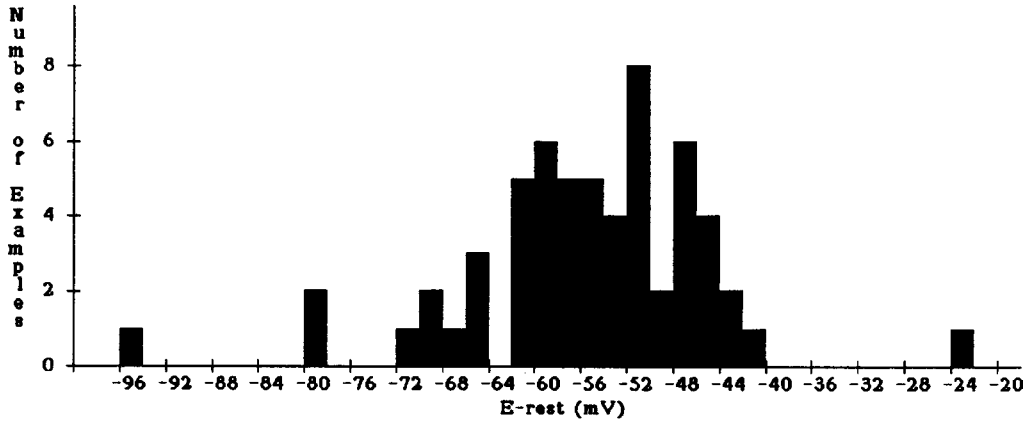

Figure B.16: Distribution of E_{rest} values for the same 59 cells shown in Figure B.14. The mean value of $E_{rest} = -56$ mV (SEM = 1).

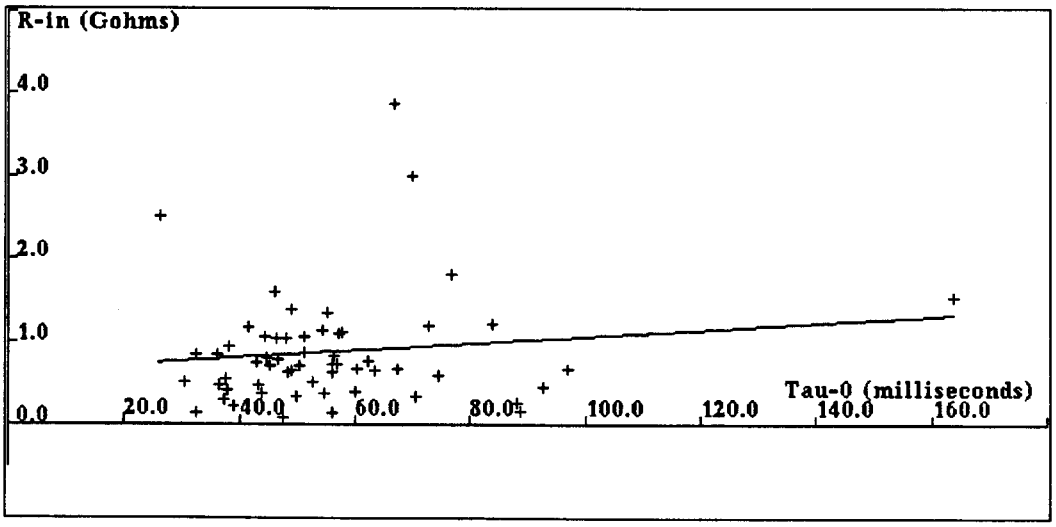

Figure B.17: Scatter plot of R_{In} and τ_0 values for the 59 cells shown in Figure B.14. Solid line is least-squares linear fit (correlation coefficient $r = 0.13$).

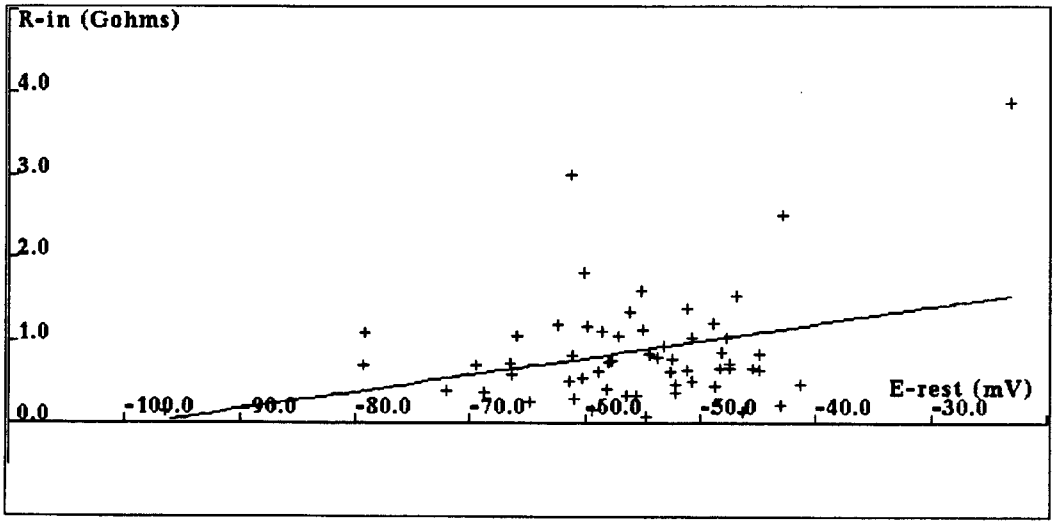

Figure B.18: Scatter plot of R_{In} and E_{rest} values for the 59 cells shown in Figure B.14. Solid line is least-squares linear fit (correlation coefficient $r = 0.33$).

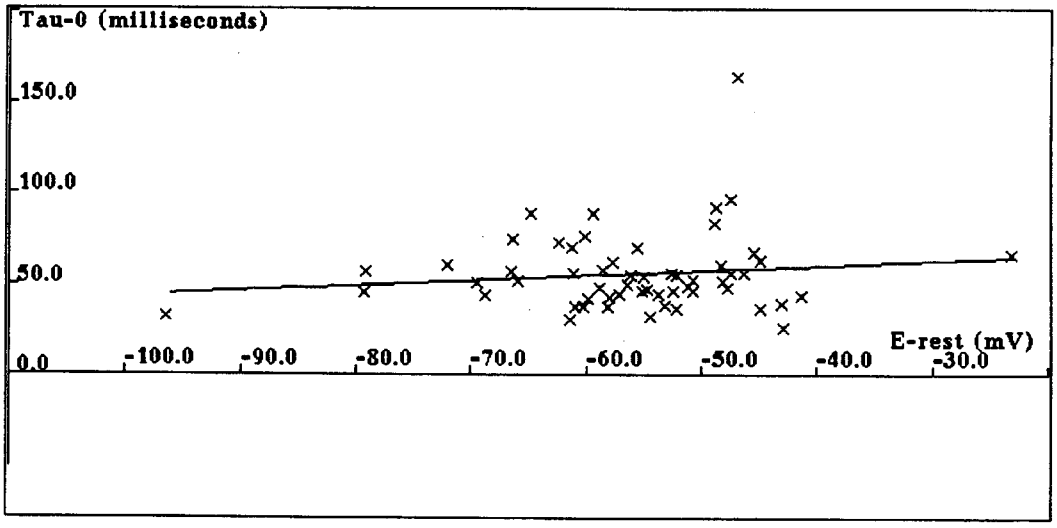

Figure B.19: Scatter plot of τ_0 and E_{rest} values for the 59 cells shown in Figure B.14. Solid line is least-squares linear fit (correlation coefficient $r = 0.14$).

Appendix C

The SURF-HIPPO Neuron Simulator

C.1 Introduction

The SURF-HIPPO Neuron Simulator is a circuit simulation package for investigating morphometricly and biophysically detailed models of single neurons and small networks of neurons (Figure C.1). SURF-HIPPO is based in part on the SURF circuit simulator, written by Don Webber, VLSI CAD Group at the University of California at Berkeley. SURF was written in both Common LISP and *LISP, and SURF-HIPPO retains this option (the *LISP version for the Connection Machine (CM2) is under development).

SURF-HIPPO allows ready construction of multiple cells from various file formats (including the format used by the simulator package NEURON, written by Hines, see below), which can describe complicated dendritic trees in 3-space with distributed non-linearities and synaptic contacts between cells. The retention of XYZ coordinates for each circuit node may be exploited, for example, by simulations which use spatially-coded input, or with multiple cell simulations that have contacts between cells defined by spatial proximity (Figure C.2). Stationary and moving two dimensional light input (for retinal simulations) is also provided. Multi-compartment intracellular calcium accumulation is provided for modelling calcium-dependent processes (e.g. Ca^{++}-dependent K^{+} channels).

This chapter provides an overview of SURF-HIPPO. Complete documentation is included with the program code.

C.2 Numerical Methods

The serial version of SURF-HIPPO uses a numerical technique adapted from that of Hines ([37]) with some changes, including adaptive time steps. *LISP simulations use the relaxation-based methods exclusively. At present, all simulations are done with the direct (serial) methods.

Briefly, the key contribution of the Hines algorithm is an elegant ordering of tree circuit topologies – clearly relevant for neurons – that results in a tri-diagonal circuit matrix. The resulting matrix equation may then be solved in $O(n)$ time, as opposed to the $O(n^2)$ time for a general matrix. Hines also proposed that the solving of voltage-dependent Hodgkin-Huxley channel particle states may be done out of the loop (i.e. at times interleaved between the node voltage time steps), since there is an inherent time delay between a given node voltage and the state of any channel particles controlled by that node. This explicit solution of the particle states simplifies and speeds up the overall circuit simulation.

C.3 Channel Models

All voltage-dependent channels are described with a modified Hodgkin-Huxley model ([10]). An advantage of this formulation is that channel particle parameters are consistent and may be related to specific biophysical mechanisms.

C.4 System Versions

One version of SURF-HIPPO, complete with extensive user interface (menus, 3-D graphics of dendritic trees, automatic plotting) runs in the Symbolics LISP Machine environment. Another (with a user interface currently under development) runs in the Sun environment (under Austin Kyoto Common Lisp (AKCL)). SURF-HIPPO is not "public domain" in the sense that it is not supported, but inquiries are welcome.

C.5 SURF-HIPPO Basics

Functions which describe circuits may be written in a variety of different ways, allowing for a flexible and relatively general input base for circuit descriptions. The simplest method is by calling the appropriate sequence

of "create-segment" functions. A more sophisticated method of constructing (complicated) cell geometries is with the "create-tree" function, which takes a list of tree node parameters and generates the "create-segment" calls automatically.

Another method of entering cell descriptions is by tracing the histology directly on the screen, using SURF-HIPPO's Dynamic Neuron Builder (Figure C.3).

Finally, as mentioned above, SURF-HIPPO can read cell description files in the format used for Hines's NEURON program.

C.6 Representation of Circuit Structure

Symbolically, circuits are composed of a set of object instances, of which there are several different types: nodes, segments, somata, channels, synapses, current sources, particles, concentration integrators, etc. There are many different interrelationships between objects in a hierarchical fashion, e.g. an instance of a channel object references an instance of a node object (corresponding to the electrical circuit node that it is attached to), an instance of a segment or soma object that it is a part of, instances of particle and/or concentration particle objects that determine the channel's conductance, and, indirectly, instances of particle nodes which correspond to the particles' states.

The structure organization for a typical circuit element is as follows:

```
;Segment name is same a distal node name. Segments are added from soma out.
(defstruct (segment :conc-name)
  (name "" :type string)
;                              g-axial
;Proximal node        Prox o---/\/\/\-----+---o Distal
;Distal node                              |
;                                   memb-elements
;                                        |
;                                       Gnd
  (node-1 nil :type node)
  (node-2 nil :type node)
  (cell nil :type cell)
;For retinal cells: 1 to 5 for dendrites in the inner
;plexiform layer. NIL if not in IPL.
  (ipl-stratum nil      :type integer)
```

```
;microns
  (length zero :type long-float)
  (diameter zero :type long-float)
;Elevation angle relative to proximal branch orientation.
  (theta zero           :type long-float)
;Azimuth angle relative to proximal branch orientation.
  (phi  zero            :type long-float)
  (core-seg nil :type core-segment)
  (model nil :type model-instance)
;microsiemens
  (g-axial zero :type long-float)
  (g-leak zero :type long-float)
;millivolts
  (v-leak -70.0 :type long-float)
;nanofarads
  (capacitance zero :type long-float)
;Concentration integrator
  (conc-int nil)
;If this segment is connected to a Hines node, then this is the
;index for that node.
  (branch-node-index nil))
```

Simulation of circuits is in terms of their nodes, which include the actual electrical nodes (corresponding to somata and segments) as well as elements whose states are both dependent on other nodes and in turn control either branch elements of the circuit or other (non-voltage) nodes. This latter class of elements include the following:

Element Type	"Voltage" =	Dependent On	Controls
V-dep particles	Prob. of open state	Membrane voltage	$g_{channel}$
Ca^{++}-dep particles	Prob. of open state	$[Ca^{++}]$ Integrator	$g_{channel}$
$[Ca^{++}]$ Integrator	$[Ca^{++}]$	I_{Ca}	Ca^{++}-dep particles

The "voltages" of the circuit nodes correspond to the state variables of the circuit. Note that branch elements (resistors, channels, capacitances, synapses) do not represent the state variables per se; their values are computed in terms of the appropriate node "voltages".

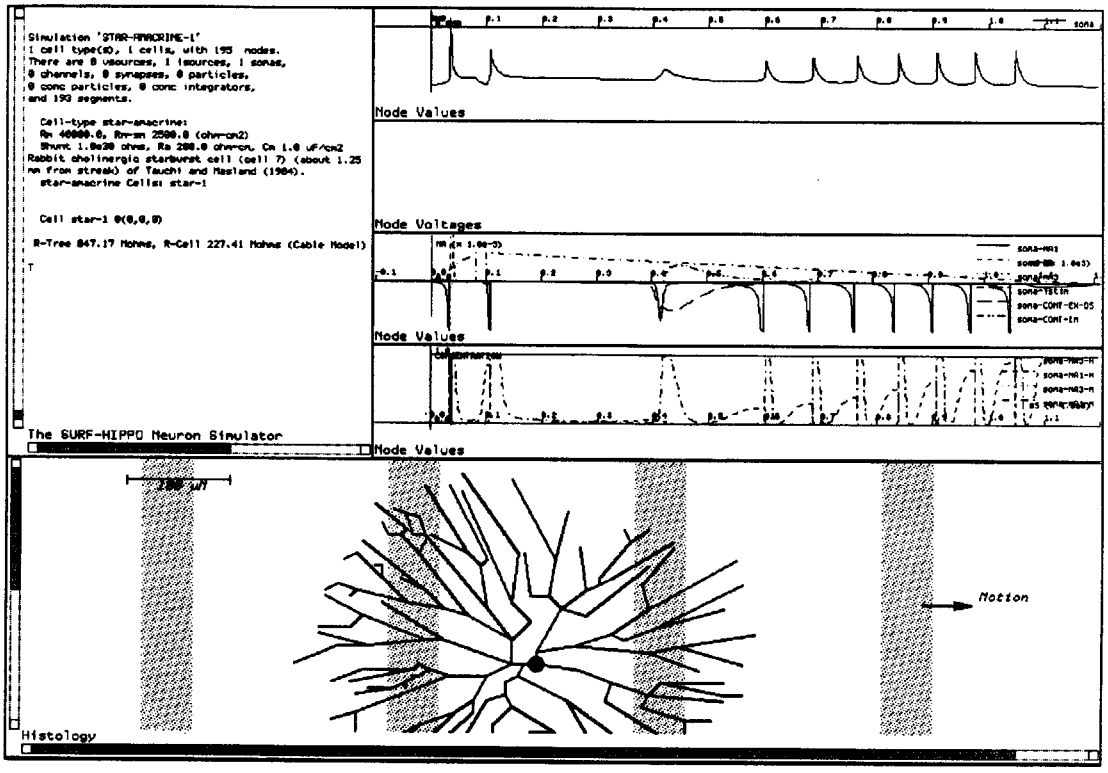

Figure C.1: An example SURF-HIPPO simulation. Various windows on the screen show node voltages, membrane currents, channel particle states, and cell histology with stimulus.

Figure C.2: Cell descriptions entered into SURF-HIPPO include 3-dimensional node coordinates, useful for spatially-coded input or for establishing spatially-dependent relationships between multiple cells. In this figure the simulated star amacrine cell from Figure C.1 is shown at a viewing angle of 2° relative to the retinal plane.

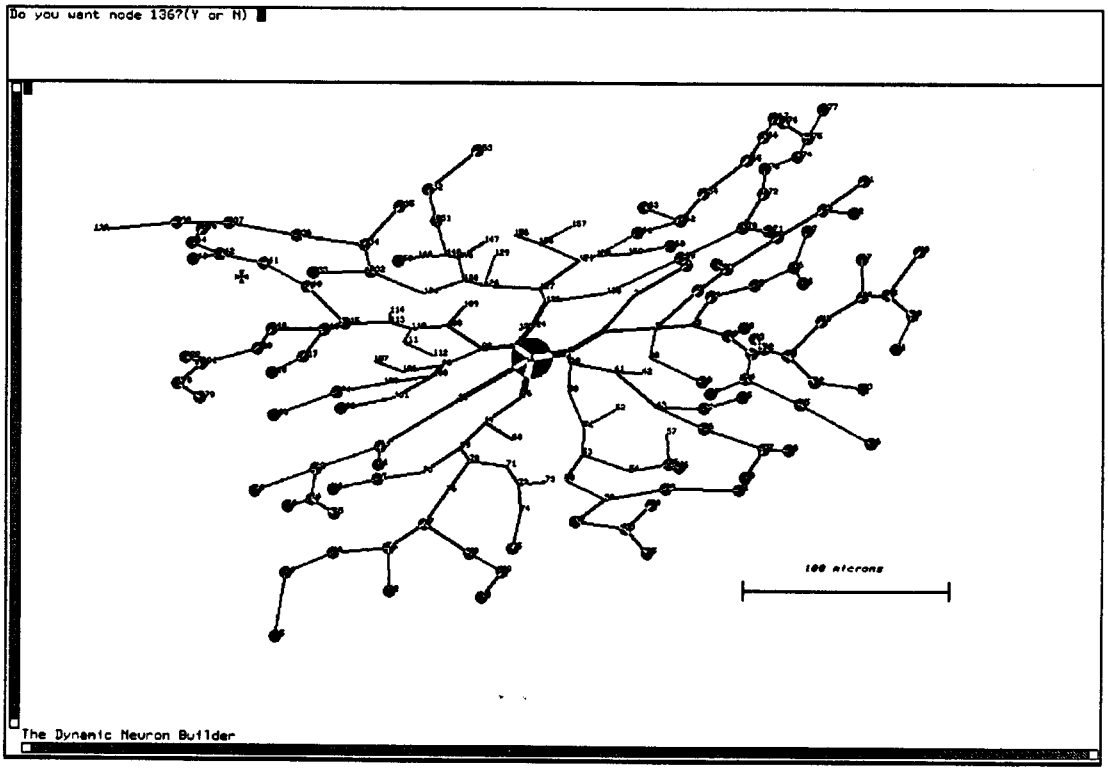

Figure C.3: The Dynamic Neuron Builder allows the entering of a cell geometry directly on the screen, using the mouse. For example, in this figure the histology of a putative DS turtle retina ganglion cell ([38]) from Kolb (type G20 [42]) was xeroxed onto a transparency, which was then taped to the computer screen and traced with the mouse. The Dynamic Neuron Builder also allows the inclusion of various synaptic arrangements, specified by menu commands. In this figure, excitatory synapses (filled circles) were automatically added in an annulus centered on the soma (160 μm I.D., 400μm O.D.).

Bibliography

[1] A. Ames III and F.B. Nesbett. Intracellular and extracellular compartments of mammalian central nervous tissue. *J. Physiology, London*, 184:215–238, 1966.

[2] F.R. Amthor and N.M. Grzywacz. The time course of inhibition and velocity independence of direction selectivity in the rabbit retina. *Investigative Opthalmology and Visual Science*, 29(4):225, 1988.

[3] F.R. Amthor and N.M. Grzywacz. Nonlinearity of the inhibition in underlying retinal directional selectivity. *Visual Neuroscience*, 6:95–104, 1991.

[4] F.R. Amthor, C.W. Oyster, and E.S. Takahashi. Morphology of on-off direction-selective ganglion cells in the rabbit retina. *Brain Research*, 298:187–190, 1984.

[5] M. Ariel and AR. Adolph. Neurotransmitter inputs to directionally sensitive turtle retinal ganglion cells. *J Neurophysiol*, 54(5):1123–43, nov 1985.

[6] M. Ariel and N.W. Daw. Pharmacological analysis of directionally sensitive rabbit retinal ganglion cells. *J. of Physiology*, 324:161–185, 1982.

[7] H.B. Barlow and R.M. Hill. Selective sensitivity to direction of movement in ganglion cells of the rabbit retina. *Science*, 139:412–414, 1963.

[8] H.B. Barlow and W.R. Levick. The mechanism of directionally selective units in rabbit's retina. *J. Physiol.*, 178:477–504, 1965.

[9] L. Borg-Graham. Modelling the somatic electrical behavior of hippocampal pyramidal neurons. Master's thesis, Massachusetts Institute

of Technology, 1987. Also appears as MIT AI Laboratory Technical Report 1161 (1989).

[10] L. Borg-Graham. Modelling the non-linear conductances of excitable membranes. In J. Chad and H. Wheal, editors, *Cellular Neurobiology: A Practical Approach*, chapter 13, pages 247–275. IRL/Oxford University Press, 1991.

[11] L. Borg-Graham and N. M. Grzywacz. An isolated turtle retina preparation allowing direct approach to ganglion cells and photoreceptors, and transmitted–light microscopy. *Investigative Opthalmology and Visual Science*, 31(4:1039), 1990. ARVO Annual Meeting Abstract.

[12] L. Borg-Graham and N.M. Grzywacz. A model of the directional selectivity in retina: Transformations by neurons singly and in concert. In T. McKenna, J. Davis, and S.F. Zornetzer, editors, *Single Neuron Computation*. Academic Press, 1991.

[13] L. Borg-Graham and N.M. Grzywacz. Whole-cell patch recordings analysis of the input onto turtle directionally selective (ds) ganglion cells. *Investigative Opthalmology and Visual Science*, 32(4:2067), 1991. ARVO Annual Meeting Abstract.

[14] C. Brandon. Cholinergic neurons in the rabbit retina: Dendritic branching and ultrastructural connectivity. *Brain Research*, 426:119–130, 1987.

[15] T. H. Brown, E. W. Kairiss, and C. L. Keenan. Hebbian synapses: biophysical mechanisms and algorithms. In W. M. Cowan, E. M. Shooter, C. F. Stevens, and R. F. Thompson, editors, *Annual Review of Neuroscience*, pages 475–511. Annual Reviews Incorporated, 1990. Vol.13.

[16] H.H. Bülthoff and I. Bülthoff. Gaba antagonist inverts movement and object detection in flies. *Brain Res.*, 407:152–158, 1987.

[17] B. Burnside and A.M. Laties. Actin filaments in apical projections of the primate pigmented epithelial cell. *Investigative Opthalmology and Visual Science*, 15(570), 1976.

[18] J.H. Caldwell, N.W. Daw, and H.J. Wyatt. Effects of picrotoxin and strychnine on rabbit retinal ganglion cells: lateral interactions for cells with more complex receptive fields. *J. of Physiology*, 276:277–298, 1978.

[19] P. A. Coleman and R. F. Miller. Measurement of passive membrane properties with whole-cell recording from neurons in the intact amphibian retina. *J. Neurophysiology*, 61(1), jan 1989.

[20] M. H. Criswell. *Cellular mechanism of movement detection and directionality in the turtle retina.* PhD thesis, Indiana University, 1987.

[21] F.M. DeMonasterio. Properties of ganglion cells with atypical receptive-field organization in retina of macaques. *J. of Neurophys.*, 41(6):1435–1449, 1978.

[22] R.D. DeVoe and P.L. Carras. Directional selectivity and synaptic potentials of identified turtle retinal ganglion cells. *Society of Neuroscience Abstracts*, 17(549.11), 1991.

[23] R.D. DeVoe, P.L. Carras, M.H. Criswell, and R.G. Guy. Not by ganglion cells alone: directional selectivity is widespread in identified cells of the turtle retina. In R. Weiler and N.N. Osborne, editors, *Neurobiology of the Inner Retina*, pages 235–246, Berlin Heidelberg, 1989. Springer–Verlag.

[24] J.E. Dowling. *The retina, an approachable part of the brain.* Harvard University Press, Cambridge, 1987.

[25] E.V. Famiglietti. On and off pathways through amacrine cells in mammalian retina: the synaptic connection of starburst amacrine cells. *Vision Res*, 23:1265–1279, 1983.

[26] E.V. Famiglietti. 'Starburst' amacrine cells and cholinergic neurons: Mirror–symmetric on and off amacrine cells of rabbit retina. *Brain Res.*, 261:138–144, 1983.

[27] J.E. Fulbrook and A.M. Granda. Velocity–sensitive retinal ganglion cells in turtle. In preparation.

[28] A.M. Granda and J.E. Fulbrook. Classification of turtle retinal ganglion cells. *Journal of Neurophysiology*, 62(3):723–737, 1989.

[29] N.M. Grzywacz and F.R. Amthor. A computationally robust anatomical model for retinal directional selectivity. In D.S. Touretzky, editor, *Advances in Neural Information Processing Systems, Vol. 1*, pages 477–484. Morgan Kaufman, 1989.

[30] N.M. Grzywacz and F.R. Amthor. Facilitation in on–off directionally selective ganglion cells of the rabbit retina. *Neurosci. Abst.*, 15:969, 1989.

[31] N.M. Grzywacz and F.R. Amthor. Independent on and off computations of retinal directional selectivity in rabbit. *Neurosci. Abst.*, 17:344, 1991.

[32] N.M. Grzywacz and C. Koch. Functional properties of models for direction selectivity in the retina. *Synapse*, 1:417–434, 1987.

[33] B. Hassenstein and W.E. Reichardt. Functional structure of a mechanism of perception of optical movement. In *Proceedings 1st International Congress Cybernetics Namar*, pages 797–801, 1956.

[34] K. Hausen. Monocular and binocular computation of motion in the lobula plate of the fly. *Verh. Dtsch. Zool. Ges.*, 74:49–70, 1981.

[35] D. O. Hebb. *The Organization of Behavior.* Willey, New York, 1949.

[36] B. Hille. *Ionic Channels of Excitable Membranes.* Sinauer Associates, Sunderland, Massachusetts, 1984.

[37] M. Hines. Efficient computation of branched nerve equations. *Int. J. Bio-Medical Computing*, 15:69–76, 1984.

[38] RJ. Jensen and RD. DeVoe. Comparisons of directionally selective with other ganglion cells of the turtle retina: intracellular recording and staining. *J Comp Neurol*, 217(3):271–87, jul 1 1983.

[39] C. Koch, T. Poggio, , and V. Torre. Computations in the vertebrate retina: gain enhancement, differentiation, and motion discrimination. CBIP paper 019, MIT, sep 1986.

[40] C. Koch, T. Poggio, and V. Torre. Retinal ganglion cells: a functional interpretation of dendritic morphology. *Phil. Trans. R. Soc. Lond.*, 298:227–264, 1982.

[41] C. Koch, T. Poggio, and V. Torre. Nonlinear interactions in a dendritic tree: Localization, timing, and role in information processing. *Proc. Natl. Acad. Sci.*, 80:2799–2802, 1983.

[42] H. Kolb. The morphology of the bipolar cells, amacrine cells and ganglion cells in the retina of the turtle pseudemys scripta elegans. *Philos Trans R Soc Lond [Biol]*, 298(1092):355–93, sep 13 1982.

[43] D.M. Linn and S.C. Massey. Gaba inhibits ach release from the rabbit retina: A direct effect or bipolar cell feedback? *Society of Neuroscience Abstracts*, 16(297.10):713, 1990.

[44] L.E. Lipetz and R.M. Hill. Discrimination characteristics of turtle's retinal ganglion cells. *Experientia*, 26:373–374, 1970.

[45] L.E. Lipetz, R.A. Normann, I. Perlman, and J.P. Chandler. A technique for reliable preparation of intact functional isolated retina of the turtle. *Investigative Opthalmology and Visual Science*, 30(3), 1989. ARVO Annual Meeting Abstract.

[46] P. Lukasiewicz and F. Werblin. A slowly inactivating potassium current truncates spike activity in ganglion cells of the tiger salamander. *J. Neurosci.*, 8(12):4470–4481, dec 1988.

[47] P. L. Marchiafava. The responses on retinal ganglion cells to stationary and moving visual stimuli. *Vision Research*, 19:1203=1211, 1979.

[48] R. H. Masland, J. W. Mills, and C. Cassidy. The function of acetylcholine in the rabbit retina. *Proc. R. Soc. Lond.*, 223:121–139, 1984.

[49] H.R. Maturana. Functional organization of the pigeon retina. In *22nd Intern. Congr. Physiol. Sci.*, pages 170–178, Leiden, 1962.

[50] H.R. Maturana, J.Y. Lettvin, W.S. McCulloch, and W.H. Pitts. Anatomy and physiology of vision in the frog (*rana pipiens*). *J. Gen. Physiol.*, 43 (Suppl. 2):129–171, 1960.

[51] M. Meister, R.O.L. Wong, D. A. Baylor, and C.J. Shatz. Synchronous bursting activity in ganglion cells of the developing mammalian retina. *Investigative Opthalmology and Visual Science*, 31(4:569), 1990. ARVO Annual Meeting Abstract.

[52] R. B.J̃r. Norgren and M.Ñ. Lehman. Retrograde transneuronal transport of herpes simplex virus in the retina after injection in the superior colliculus, hypothalamus and optic chiasm. *Brain Research (NETHERLANDS)*, 479(2):374–378, 1989.

[53] P. O'Donnell, C. Koch, and T. Poggio. Demonstrating the nonlinear interaction between excitation and inhibition in dendritic trees using computer-generated color graphics: a film. *Society of Neuroscience Abstracts*, 11(142), 1985.

[54] H. Ögmen. On the mechanisms underlying directional selectivity. *Neural Computation*, 1991.

[55] T. Poggio and W.E. Reichardt. Considerations on models of movement detection. *Kybernetik*, 13:223–227, 1973.

[56] W. Rall. Theoretical significance of dendritic tress for neuronal input–output relations. In R.F. Reiss, editor, *Neural Theory and Modelling*, pages 73–79. Stanford University Press, 1964.

[57] P.H. Schiller and J.G. Malpeli. Properties and tectal projections of monkey retinal ganglion cells. *J. Neurophys.*, 40(2):428–445, 1977.

[58] D. P. Shelton. Membrane resistivity estimated for the Purkinje neuron by means of a passive computer model. *Neuroscience*, 14(1):111–131, 1985.

[59] R.D. Smith, N.M. Grzywacz, and L. Borg-Graham. Picrotoxin's effect on contrast dependence of turtle retinal directional selectivity. *Investigative Opthalmology and Visual Science*, 32(4:2913), 1991. ARVO Annual Meeting Abstract.

[60] A. Stelzer, A. R. Kay, and R. K. S. Wong. Gaba-a-receptor function in hippocampal cells is maintained by phosphorylation factors. *Science*, 241:339–341, 1988.

[61] J.F. Storm. Potassium currents in hippocampal pyramidal cells. In J. Storm-Mathisen, J. Zimmer, and O.P. Ottersen, editors, *Progress in Brain Research*, volume 83, pages 161–187. Elsevier Science Publishers B. V. (Biomedical Division), 1990.

[62] M. Tauchi and R.H. Masland. The shape and arrangement of the cholinergic neurons in the rabbit retina. *Proc. R. Soc. London, B*, 223:101–119, 1984.

[63] V. Torre and T. Poggio. A synaptic mechanism possibly underlying directional selectivity to motion. *Proc. R. Soc. Lond.*, 202:409–416, 1978.

[64] D. Vaney. The mosaic of amacrine cells in the mammalian retina. In N. Osborne and G. Chader, editors, *Progress in Retinal Research*, volume 9, pages 49–100. Pergamon Press, 1990.

[65] D.I. Vaney. "coronate" amacrine cells in the rabbit retina have the "starburst" dendritic morphology. *Proc. R. Soc. London, B,*, 220:501–508, 1984.

[66] D.I. Vaney, Collin S.P., and Young H.M. Dendritic relationships between cholinergic amacrine cells and direction–selective retinal ganglion cells. In R. Weiler and N.N. Osborne, editors, *Neurobiology of the Inner Retina*, pages 157–168. Springer–Verlag, 1989.

[67] S. Watanabe and M. Murakami. Synaptic mechanisms of directional selectivity in ganglion cells of frog retina as revealed by intracellular recordings. *Jap. J. of Physiology*, 34:497–511, 1984.

[68] F.S. Werblin, G. Maguire, and P. Lukasiewicz. Amacrine-bipolar cell interactions mediate change detection in the retina of the tiger salamander. In R. Weiler and N.N. Osborne, editors, *Neurobiology of the Inner Retina*, pages 401–411, Berlin Heidelberg, 1989. Springer–Verlag.

[69] H. J. Wyatt and N. W. Daw. Directionally sensitive ganglion cells in the rabbit retina: specificity for stimulus direction, size, and speed. *J. Neurophysiol.*, 38:613–626, 1975.

[70] Y.H. Yoon and M.F. Marmor. Effects on retinal adhesion of temperature, cyclic amp, cytochalasin, and enzymes. *Investigative Opthalmology and Visual Science*, 29(6), 1988.

This blank page was inserted to preserve pagination.

CS-TR Scanning Project
Document Control Form

Date : 5/18/95

Report # AI-TR-1350

Each of the following should be identified by a checkmark:
Originating Department:

☒ Artificial Intellegence Laboratory (AI)
☐ Laboratory for Computer Science (LCS)

Document Type:

☒ Technical Report (TR) ☐ Technical Memo (TM)
☐ Other:_____

Document Information

Number of pages: 151 (158-IMAGES)
Not to include DOD forms, printer instructions, etc... original pages only.

Originals are:
☒ Single-sided or
☐ Double-sided

Intended to be printed as :
☐ Single-sided or
☒ Double-sided

Print type:
☐ Typewriter ☐ Offset Press ☒ Laser Print
☐ InkJet Printer ☐ Unknown ☐ Other:_____

Check each if included with document:

☒ DOD Form (2) ☐ Funding Agent Form ☒ Cover Page
☐ Spine ☐ Printers Notes ☐ Photo negatives
☐ Other: _____

Page Data:

Blank Pages (by page number): FOLLOWING PAGES TITLE, 2, 3

Photographs/Tonal Material (by page number): 46, 48, 51, 54, 111, 112, 115, 120

Other (note description/page number):

Description :	Page Number:
IMAGE MAP	(1-2)
UNN'ED TITLE & BLANK PAGES	(3-6)
PAGES #'ED 2 BLANK, 3 BLANK	
PAGES #'ED 4-148	(7-151)
SCAN CONTROL, COVER, DOD (2)	(152-155)
TRGTS	(156-158)

Scanning Agent Signoff:

Date Received: 5/18/95 Date Scanned: 5/22/95 Date Returned: 5/ /95

Scanning Agent Signature: Michael N. Cook

REPORT DOCUMENTATION PAGE

Form Approved
OMB No. 0704-0188

1. AGENCY USE ONLY (Leave blank)	2. REPORT DATE	3. REPORT TYPE AND DATES COVERED
	January 1992	technical report

4. TITLE AND SUBTITLE

On Directional Selectivity in Vertebrate Retina: An Experimental and Computational Study

5. FUNDING NUMBERS

N00014-85-K-0124
BNS-8809528
IRI-8719394

6. AUTHOR(S)

Lyle J. Borg-Graham

7. PERFORMING ORGANIZATION NAME(S) AND ADDRESS(ES)

Artificial Intelligence Laboratory
545 Technology Square
Cambridge, Massachusetts 02139

8. PERFORMING ORGANIZATION REPORT NUMBER

AI-TR 1350

9. SPONSORING/MONITORING AGENCY NAME(S) AND ADDRESS(ES)

Office of Naval Research
Information Systems
Arlington, Virginia 22217

10. SPONSORING/MONITORING AGENCY REPORT NUMBER

AD-A253493

11. SUPPLEMENTARY NOTES

None

12a. DISTRIBUTION/AVAILABILITY STATEMENT

Distribution of this document is unlimited

12b. DISTRIBUTION CODE

13. ABSTRACT *(Maximum 200 words)*

The retina is a good candidate for exploring the relationship between neural computation and circuit, in particular given its physically *peripheral* location and its physiologically *central* status. One example of a spatial-temporal computation in the retina is directional selectivity. This computation may rely on interactions within the dendritic tree which are incrementally more complex than the basic "point integration" and fire neuronal response.

In this Thesis I use experimental and theoretical techniques to characterize the direction selectivity circuit in vertebrate retina. For the experimental side I have developed *a)* an isolated intact turtle retina

(continued on back)

14. SUBJECT TERMS (key words)
computational neuroscience
retina electrophysiology
neural modelling

15. NUMBER OF PAGES
148

16. PRICE CODE

17. SECURITY CLASSIFICATION OF REPORT	18. SECURITY CLASSIFICATION OF THIS PAGE	19. SECURITY CLASSIFICATION OF ABSTRACT	20. LIMITATION OF ABSTRACT
UNCLASSIFIED	UNCLASSIFIED	UNCLASSIFIED	UNCLASSIFIED

Block 13 continued:

preparation and *b)* a whole-cell patch recording protocol of directionally selective ganglion cells, the combination of which is well-suited for characterizing complicated retinal receptive fields. I will show evidence that when the inhibitory synaptic input is markedly reduced the excitatory input to directionally selective ganglion cells in turtle is itself directionally selective. This reduction was accomplished by *a)* voltage clamping to the reversal potential of inhibitory currents and *b)* by removing ATP from the electrodes which, in turn, blocks the inhibitory input over time.

This finding implies that the necessary and sufficient conditions for the computation of directional selectivity occurs pre-synaptic to the ganglion cell. For the theoretical side of the Thesis, and consistent with the above constraint, I present a model for the direction selective circuit that relies on directionally selective distal outputs from functionally independent oriented amacrine cell dendrites. I postulate that these dendrite cables receive symmetric, evenly distributed, but temporally distinct excitatory and inhibitory inputs along their length. Performance of the model (tested with a biophysically and morphometricly detailed neuron simulator program, SURF-HIPPO) is consistent with the data, and generates testable predictions.

I shall also discuss how this model may work in a developmental context and, finally, implications for more general non-linear spatio-temporal filtering within dendritic trees.

Scanning Agent Identification Target

Scanning of this document was supported in part by the **Corporation for National Research Initiatives,** using funds from the **Advanced Research Projects Agency** of the **United states Government** under Grant: **MDA972-92-J1029.**

The scanning agent for this project was the **Document Services** department of the **M.I.T Libraries.** Technical support for this project was also provided by the **M.I.T. Laboratory for Computer Sciences.**